István Halvax, BSc

Deformation gradient and magnetic fabric in the Pohorje-Pluton (Slovenia)

MASTERARBEIT

zur Erlangung des akademischen Grades

Master of Science

Masterstudium Erdwissenschaften

eingereicht an der

Technischen Universität Graz

Betreuer

Univ.-Prof. Mag. Dr. Walter Kurz

und Ao.Univ.-Prof. Dr.phil. Harald Fritz

Institute of Earth Sciences Graz

Graz, 04. 2014

EIDESSTATTLICHE ERKLÄRUNG

AFFIDAVIT

Ich erkläre an Eides statt, dass ich die vorliegende Arbeit selbstständig verfasst, andere als die angegebenen Quellen/Hilfsmittel nicht benutzt, und die den benutzten Quellen wörtlich und inhaltlich entnommenen Stellen als solche kenntlich gemacht habe. Das in TUGRAZonline hochgeladene Textdokument ist mit der vorliegenden Masterarbeit identisch.

I declare that I have authored this thesis independently, that I have not used other than the declared sources/resources, and that I have explicitly indicated all material which has been quoted either literally or by content from the sources used. The text document uploaded to TUGRAZonline is identical to the present master‘s thesis.

Datum / Date

Unterschrift / Signature

Acknowledgement

First of all, I thank my supervisors Prof. Mag. Dr. Walter Kurz and Prof. Dr. Harald Fritz. Both of them were very supportive and professional during my development at university and especially during the research and composition of this thesis. They helped me through times with loss of understanding and gave me the right impulses and motivation without taking away my own thoughts and ways.

Special thanks also to my supervising professor in geophysics, Dr.Robert Scholger. I could not have unravelled the nature of magnetic fabrics without his didactic and patient manner.

My biggest thanks deserve my family, who always supported me in every possible way. Especially in stressed and tired times they find the words to help me on my feet again.

Also thanks to my great classmates for good times in lectures, field trips and off-campus when a breath of air was needed and of course for the great and fun time. I specially thank Sara, Cyrill, Klaus, Peter, Valentin and all my colleges at my workstation for constructive discussions and other help.

Last but not least thanks also to all my lectors and the laboratory staff.

Thank you all …

30.04.2014,Graz

_____

István Halvax

Summary

The Pohorje tonalite intrusion west of Maribor (northern Slovenia) was studied by microstructural and susceptibility analysis. The investigations reveal the deformation condition, strain geometry and kinematics during and subsequent to the intrusion of pluton. The gradient of the magmatic and tectonic deformation in the study area highlights several stages since the emplacement in the early Miocene (18.1Ma).

The cooling pluton was exhumed rapidly with early flattening and W-E- directed normal faulting of the covering host rocks. The host rock fabrics suggest a contact metamorphism in an aureole of several tens of meters. During the late stage of the exhumation NW-SE- shearing associated with fluid penetration led to a fabric overprint in both the tonalite body and the host rock. Late NW-SE extension is characterized by brittle normal faulting with cataclastic deformation within the tonalite.

Zusammenfassung

Die geologische Entwicklung des Pohorje (Bachern) Tonalit westlich von Marburg (Nordslowenien) wurde mittels mikrostrukturellen und Suszeptibilitäts- Analysen untersucht. Die Ergebnisse geben Aufschluss über den Deformationsgradienten, den Spannungsverhältnissen und der Kinematik während und nach der Intrusion des Magmenkörpers. Die wesentlichen Verformungsschritte seit der Intrusion im Frühen Miozän (18.1Ma) wurden mittels des magmatischen und tektonischen Deformationsgradienten segregiert und beschrieben.

Demzufolge wurde der Intrusivkörper nach der Kristallisation schnell exhumiert und koaxial deformiert. Die überlagernden Gesteinseinheiten wurden in westliche bzw. östliche Richtung abgeschoben. Die Intrusion weißt eine Aureole mit einer konkakt-methamorphen Überprägung des Umgebungsgesteines in mehreren Zehner Meter auf. In der späten Exhumationsphase wurde sowohl der Intrusivkörper als auch das Umgebungsgestein in NW-SE Richtung geschert und durch das Eindringen von Fluid alteriert. In einer späten NW-SE Extension unter spröden Bedingungen kam es zu zahlreichen Abschiebungen und einer Kataklase des Tonalit.

Index

1. Introduction

The research area is situated in the Pohorje Mountains (Fig. 1), which are located west of the city Maribor (Marburg) in Slovenia. The mountain range is bordered to the north by the river of Drava and the sedimentary basin of the Ribnica Trough, which fills the valley south of the Drava River. The Pohorje Mountain Range has generally gentle slopes with a maximum elevation of 1543 meters above sea level. The pluton is extending over an area of about 1000 km^2 between 46°25' and 46°32' North and 15°13' and 15°38' East.

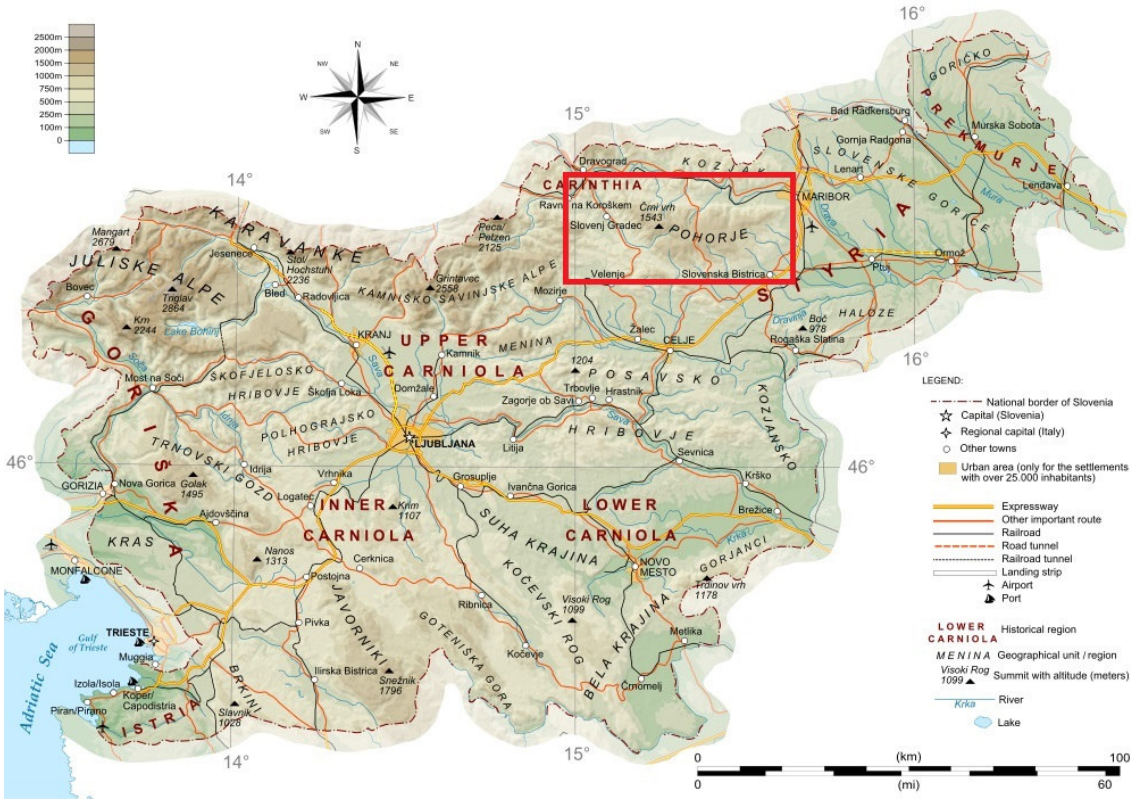

Fig. 1 Geographic Overview; The Pohorje Mountain Range is located in the north east part of Slovenia marked by the red square. *(http://en.wikipedia.org/wiki/File:General_map_of_slovenia.svg, 2014)*

The sampling was preceded along four profiles across the Mountain Range. All four profiles course from north to south and follow forest roads. The easternmost profile starts north of the town Slovenska Bistrica and follows the road northwards along Partizanska bolnica Jesen to Ruše. The central-east one follows the road starting just

north of the market town Oplotnica passing by Koča na Pesku and ends in Lovrenc na Pohorju. The central-west one is starting on the northern side of the mountain range at the southern end of the village Ribnica na Pohorju and reaches up to the cottage Ribniška koča. The westernmost Profile follows the road from Vulenica southwards to the cable car station of Partizanski Dom (see Fig. 2). The two middle profiles were investigated with a great focus whereas the two outer profiles had the purpose to find correlations.

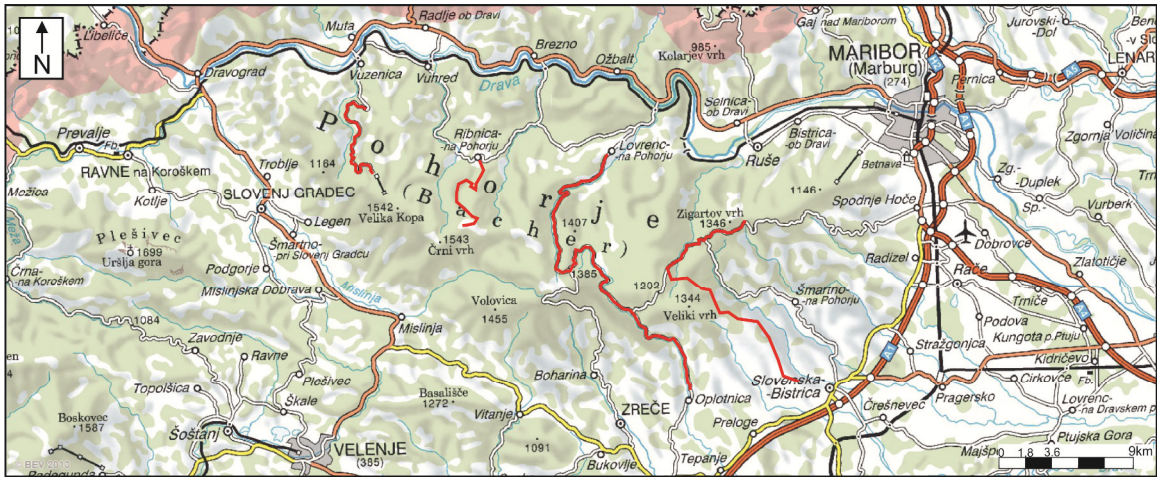

Fig. 2 Overview map of the Pohorje Range. The four work profiles are marked in red. *(http://www.austrianmap.at/amap/index.php?SKN=1&XPX=637&YPX=492, 2014)*

1.1. Statement

The aim of this thesis is the reconstruction of the Pohorje pluton's emplacement history, in particular the transition between the magmatic flow fabric to ductile and to brittle deformation structures within the Pohorje calc-alcaline igneous complex of Slovenia, and to establish the relative timing of magmatic and tectonic events. To determine these processes, the pluton, the contact metamorphic areola and the host rocks of the pluton were investigated with structural geological methods. In addition, the pluton was investigated using geophysical methods, in particular the anisotropy of the magnetic susceptibility (AMS). The laboratory work includes analyses of thin sections, the use of optical microscopy to determine rock petrography and micro-fabric analysis (rheology and kinematics). Furthermore, the thin sections were used to

determine the lattice preferred orientation (LPO) of quartz c-axes. The analysis of magnetic susceptibility was also processed from oriented geological rock samples. The statements concluding from susceptibility analysis are reinforced by magnetic mineral determination via Curie temperature measurement.

2. Geological setting

The majority of the Pohorje mountain range is built-up of igneous rocks of tonalitic to granodioritic composition. The shape of the pluton has been described by different authors either a laccolith or a batholith *(Fodor, et al., 2008)* and extends from WNW to ESE. In addition, dacitic dikes and flows are breaking throw the surrounding units of low grade metamorphic rocks in the western part of the range. These low grade metamorphic rocks are assemblages of Upper Cretaceous carbonates, Permo-Skythian and early Palaeozoic metasediments. The pluton itself intruded into a medium to high grade metamorphic host rocks. These units are mainly paragneiss, mica schist, phyllite and amphibolite.

Numerous plutonic bodies appear along the Periadriatic Lineament within the Alps, but extend also along the Sava-Vadar Zone of the Dinarides and Hellenides *(Pamić, et al., 2002)*. The Periadriatic Lineament is a dextral strike slip fault zone, which can be followed from the Ligurian sea approaching NE to the south-western end of the Tauern window and continuing in ESE direction. South of the Pohorje igneous complex it finally fades into the Donat Fault. Both Periadriatic Lineament and the Donat Fault are displaced by the NW-SE striking Pöls-Lavanttal (Labot) Fault Zone. This displacement occurred in late Miocene/Pliocene times *(Kázmér, et al., 1996)* and is the consequence of the counter clockwise rotation of crustal blocks in the eastern part of the Eastern Alps *(Wölfler, et al., 2011)*.

The Periadriatic Lineament is separating the Southern Alpine units from the Austroalpine *(Bauer, 1980)*. In contrast to the Austroalpine, the Southern Alpine is characterized by south vergence and are by far less overprinted during the evolution of Alpine metamorphism.

Along the Periadriatic Lineament numerous calc-alkaline plutonic bodies and dikes intruded into upper parts of the earth crust. The majority of these dikes are found in vicinity to larger plutons *(Exner, 1976)*. The plutons occur in four different magmatic associations: (1) Eocene granitiods; (2) Oligocene granitoids including tonalities; (3) Oligocene shoshonite and calc-alkaline volcanics with lamprophyres; (4) Egerian-

Eggenburgian (Chattian) calc-alkaline volcanics and granitoids *(Pamić, et al., 2002)*. Referring to the radiometric ages from Pamic et al. *(2002)* the magmatic activities vary roughly between 55Ma and 29Ma in general. While plutons along the Periadriatic lineament have ages clustering around 30 Ma *(e.g. Rosenberg)* recent studies show that the easternmost intrusion along the Periadriatic lineament – the Pohorje pluton – has a mean intrusion age of 18.11 ±0.74 Ma *(Márton, et al., 2006)*.

2.1. Regional tectonic framework

2.1.1. Fault Systems of the Eastern Alps

The Periadriatic Lineament is the major fault within the Alpine Orogeny and has a long precursor history. It shows in general a dextral displacement associated with a counter clockwise rotation of the Adriatic plate. The individual segments of the Periadriatic Lineament and the related faults show a diachronous activity with successive younger fault activity towards the east (Wölfler et al., *2011)*. Hence, the oldest fault-related sedimentary basin is of Oligocene age in the Lower Inn Valley and the youngest are the Gorenjska, Barje, Savinja and Velenje basins with late Miocene to Pliocene ages in Slovenia. Since the Oligocene the Alps underwent an East orientated escape tectonics, together with exhumation of the Tauern window, which explains this additive shift towards the East. This can also be seen in the progradation of conjugated fault systems within the Alps. The Inntal fault, dated to early Miocene *(Ortner, et al., 2006)*, was originally a thrust fault dipping to the south. The westward dipping Brenner normal fault was linked with the sinistral displacement of the Inntal fault. As a consequence the western Tauern Window exhumed initially. South of the tectonic window this displacement unveils in the so called DAV (Defereggen-Antholz-Vals fault system). In a second stage, during the Early Miocene the easternmost margin of the Tauern window exhumed by normal faulting along the Katschberg fault. The conjugated strike slip faults SEMP (Salzach-Ennstal-Mariazell-Puchberg fault) to the north and the Mölltal fault in the south mobilized the future Gurktal Block towards the east. In a third stage, the sinistral shear was transferred to the Mur-Mürz fault system and dextral shear to the the Pöls Lavanttal lineament. *(Wölfler et al. 2011)* During this time the Periadriatic

Lineament extended more and more towards the east. Wölfler et al. showed in their publication the fault activities in the Eastern Alps *(Fault Activity by Wölfler et al., Table 11, p.78)* The cluster of the fault activity is around 30 Ma in the Eastern Alps and somewhat younger within the Tauern window. Similar age of fault activity is also shown by Müller et al. (2000). Only at the very eastern faults the activity is significantly younger. The fault activity of the Periadriatic Lineament east of the Lavanttal Fault is dated 24-17.5 Ma and 17.5-16.5 Ma *(Fodor, et al., 1998)*. Together with the Pöls-Lavantal fault a horse tail-like geometry developed in the area of the Pohorje Range and principally exposed the pluton. Fault activity of the Pöls-Lavantal fault system is dated 21-12Ma *(Kuhlemann, et al., 2003).*

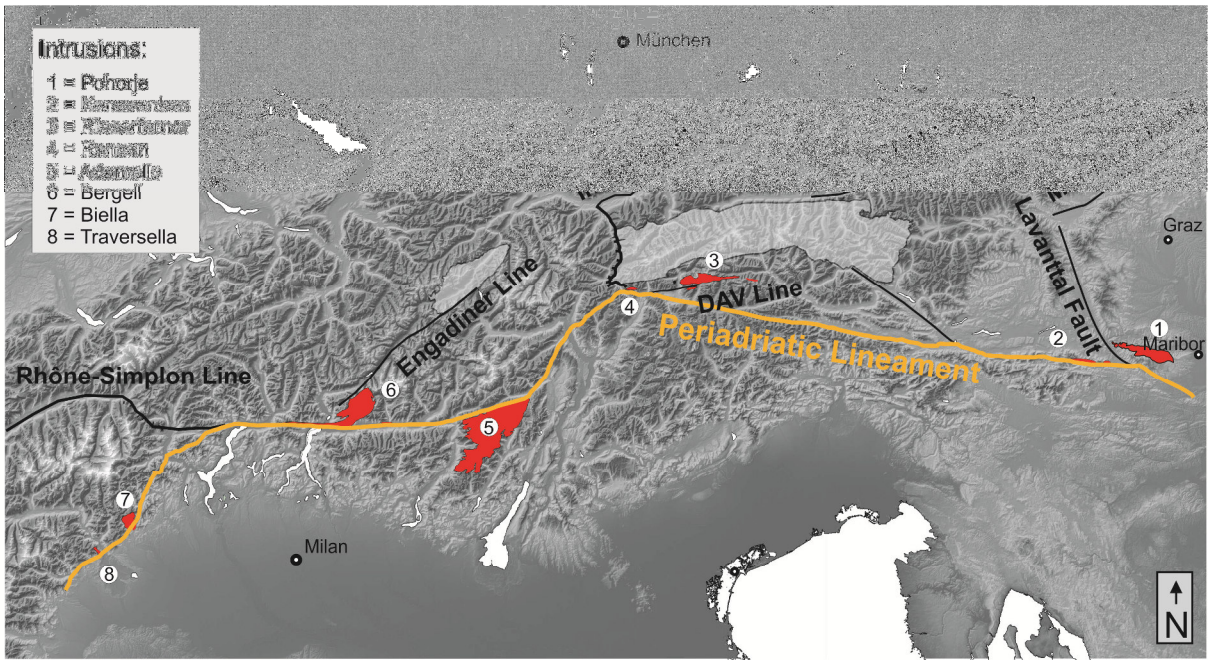

Fig. 3 Periadriatic Lineament (orange) and main fault systems in the Central and Eastern Alps (black). The major intrusions (1 to 8) are (listed from East to West) Pohorje, Eisenkappel (or Karawanken), Rieserferner, Rensen, Adamello, Bergell, Biella and Traversella. *(http://alpengeologie.org/, 2013)*

2.1.2. Associated Plutons along the Periadriatic Lineament

Two different kinds of plutonic bodies can be found along the Periadriatic Lineament. These two groups differ in their age. The first group of igneous intrusions emplaced during Permian times. These show generally a higher content of K, Rb, Sr and Ti

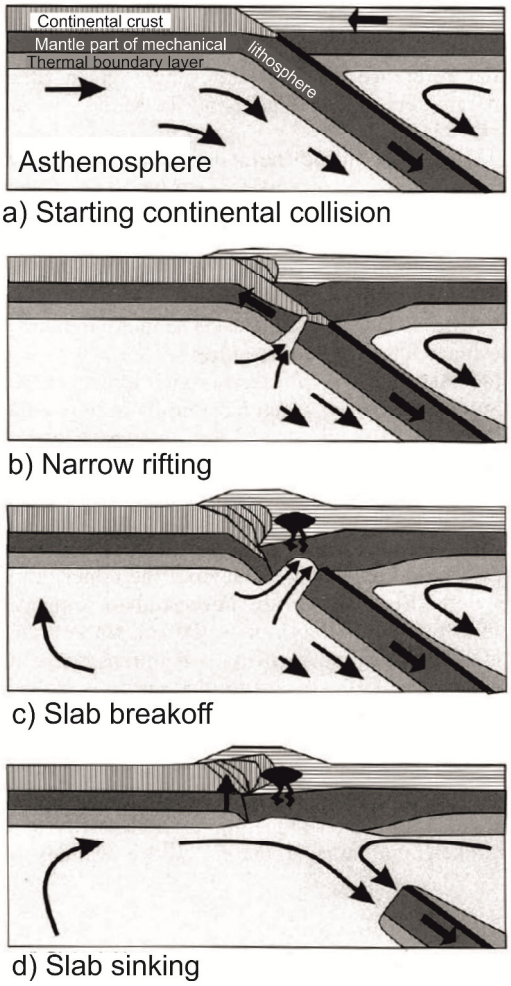

Fig. 4 : Schematic illustration of the slab breakoff of the Adriatic plate and subsequent magmatisms along the Periadriatic fault by *Davies and von Blanckenburg, 1995*.

(Gratzer & Koller, 1993). The second, younger group is associated with the collision of the Adriatic indenter with the European plate. Gratzer and Koller interpreted the pre-Alpine plutonic bodies to have their source in a molten oceanic crust *(1993)*. Examples for these Permian to Triassic plutons are the Iffinger, Brixener, Kreuzberg, Mt. Sabion, Cima d'Asta or the Eisenkappel complexes. The complexes of Alpine age can be found over the whole length of the 1700 km long fault system formed by the Periadriatic-, the Sava- and the Vardar line. Their source is considered to be generated along the African-European suture. These igneous complexes are suggested to have their source in the asthenosphere. Davies and von Blanckenburg *(1995)* suggest slab breakoff as mechanisms where a slab window allowed hot astenospheric material to rise. The increased temperatures in the upper plate led to anatexis and hence to magmatism (Fig. 4). These younger igneous complexes intruded along the Lineament in Oligocene times. The Adamello, Bergell, Biella, Pohorje, Rensen, Rieserferner, the tonalitegneiss of Eisenkappel and the Zagorje are all plutons of this group. Further, the granitoid plutons along the Periadriatic Lineament are accompanied by numerous acidic to mafic dykes *(Pamić, et al., 2002).*The Pohorje pluton, considered here, was emplaced significantly later in Miocene times.

2.1.2.1. Alpine Intrusions

The Adamello plutonic body is of Tonalitic – Granodioritic composition and is located at the junction of the Tonale fault and the S Guidicarie fault in Italy (Fig. 3). The age of the body is dated between 40 Ma in the northern corner and 32 Ma in the southern part *(Pamić, et al., 2002)*. The batholith experienced a late to post-magmatic deformation with cataclasites and pseudotachylytes, related to displacement along the Tonale fault *(Pennacchioni, et al., 2006)*. The deformation in the contact aureole of the intrusion is described as syn-magmatic *(Stipp, et al., 2002)*.

The Bergell tonalite (Fig. 3) is outcropping between the southern termination of the Engadine fault and the Tonale fault, north-east of Lake Como (Italy). Westwards of the main intrusion a tail-like appendix intruded into a mylonitic shear zone of the Insubric Line *(Rosenberg & Stünitz, 2003)* (here mentioned as Tonale fault). With the cooling of the Bergell tonalite a gradual transition from magmatic flow to solid-state deformation can be detected *(Berger & Stünitz, 1996)*. The crystallization of the tonalite is dated at 32-30 Ma *(von Blanckenburg, et al., 1992)*.

Both the Biella and the Traversella plutons (both located nearby the homonymous towns) intruded north-west of the Periadriatic Lineament around 30 Ma *(Borsi, et al., 1973)*. In different areas of the Biella massif the petrology varies between granitic to more mafic syenitic and monzonitic rocks. The Traversella intrusion is described as monzodiorites to gabbros. The analyses of Hrouda and Lanza *(1989)* show that both plutonic bodies are unaffected by deformation.

The Rieserferner pluton is located west of the Tauferer valley near the village of Hopfgarten. The age of the crystallization is 27 ± 3Ma *(Exner, 1976)*. The igneous complex consists of three asymmetric dome structures and has in general a tonalitic to granodioritic composition. In contrast to the other complexes, the Rieserferner is not located along the Peradriatic Lineament, but along the DAV. The pluton is placed in a pull-apart structure and is sheared in the eastern parts into the DAV fault *(Steeken, et al., 2000)*.

The Rensen Pluton is cropping out within the Austroalpine west of the Altfaßtal and Valstal in South Tyrol (Italy). The petrology of the body shows tonalite in the northern rim, the so called “tonalitic rim facies”, and granodioritic-tonalitic in the southern main part of the pluton *(Krenn, et al., 2003)*. The crystallization took place in Oligocene times - 30Ma *(Bellieni, et al., 1991)*. Located south of the Tauern Window and north of the DAV, the -magmatic evolution of the Rensen is likely linked with activity of the DAV.

The tonalite-gneiss along the Pulstertal and Lesachtal fault are like the already mentioned intrusions calkalkaline series and of Oligocene age *(Sprenger, 1996)*. The magmatism occurred as dykes as well as intrusives and appears with sharp boundaries to the neibouring rocks *(Pfiffner, 2009)*.

The tonalite-gneiss in the region of Eisenkappel, Carinthia, has due to radiometric Rb-Sr measurements on biotite a crystallization age of 29 ± 6 Ma. The intrusion is outcropping in form of a lamella and shows a strong contact-metamorphic impact on the surrounding rock, whereas the contact is distinct. *(Scharbert, 1975)*

2.1.3. Units of the Upper Austroalpine: Medium to high grade Metamorphic Units of the Koralm-crystalline and low grade Metamorph Units of the Gurktaler Nappe

The medium grade metamorphic units, now exposed north-east and south-east of the Pohorje pluton, are considered as part of the Koralm-crystalline, a crystalline-nappe within the Koralpe-Wölz nappe system. The Koralpe-Wölz nappe system consists, starting from the tectonically upper units, of the Plankogel and the Radenthein Crystalline, underlain by the Koralm and Saualm Crystalline and by the Wölz, Rappold and Grobgneis Crystalline *(Gasser, et al., 2009)*. The Austroalpine nappe system was first described by Tollmann *(1977)*. Its subdivision was redesigned by Schmid et al. *(2004)*. In contrast to Tollmanns’s classification into Lower, Middle and Upper Austroalpine, Schmid et al. abandoned the term Middle Austroalpine and subdivides the Austroalpine into Lower Austroalpine and Upper Austroalpine *(Schmid, et al.,*

2004). Recently, both models are used for the characterization of numerous regional geological settings. In this work neither the Middle Austroalpine Units used by Tollmann, nor the Lower Austroalpine units will be described in detail since both terms are used to subdivide the Alpine Nappe stack. In this work post stacking history is considered and thus the differences in terminology have no immediate context with this thesis.

The Upper Austroalpine units comprise four nappe systems. The lowermost nappe is the Silvretta-Seckau nappe system consisting of biotite-plagioclase gneisses and mica schists, hornblende gneisses, amphibolites, orthogneisses and locally occurring migmatites and ultramafic complexes. This nappe system can be observed in the region south of Schladming, Rottenmann, Seckauer Tauern and in the Troiseck-Floning Zug (all in Styria, Austria) *(Gasser, et al., 2009)*. The Silvretta-Seckau nappe system is overlain by the Koralpe-Wölz nappe system. It is built up exclusively by pre-Mesozoic rocks and represents an extruding metamorphic wedge *(Schmid, et al., 2004)*. This nappe system is a series of basement units and contains High-Pressure metamorphic rock associations with eclogite, and MORB-type gabbro with Permian protolith ages. The rocks often show a Barrow-type metamorphic overprint *(Schmid, et al., 2004)* and are mainly micaschists, paragneisses, pegmatites and orthogneisses, locally marbles, amphibolites and the already mentioned eclogites.

The High-Grade metamorphic character of this nappe system is, according to Schmid et al. *(2004)*, related to the subduction of the Meliata-Hallstatt Ocean and the subsequent collision of the Austroalpine units and the southalpine units *(Neubauer, et al., 1999)*.

The higher nappe complex of the Upper Austroalpine is the Ötztal-Bundschuh nappe. The nappe is overprinted by minor Eoalpine metamorphism and shows an increasing metamorphic grade towards the base of the nappe.

The tectonically highest nappe within the Upper Austroalpine is the Drauzug-Gurktal nappe system. It comprises the Grazer Paläozoikum, the Gurktal nappe and the Steinach nappe. All of them are low grade metamorphic nappes and can be correlated to the units south of the SAM (southern border of Alpine metamorphism described by Hoinkes et al. *(1999)). (Schuster, et al., 2004)*

2.1.4. High-grade metamorphic garnet-peridotite rocks

In the south-western region of the mountain range high-grade metamorphic rocks are described by Janák et al. *(2006)* as ultrahigh-pressure metamorphics with 900 °C and 4 GPa. It is suggested, that this metamorphism is a result of subduction of continental crust during the Cretaceous orogeny. The exhumation took place in two stages, with a main stage during Late Cretaceous times and a final stage in the Miocene *(Janák, et al., 2006)*. Miller and Konzett referred that the garnet-peridotite rock were suggested to be UHP-rocks by indirect evidence. The unambiguous evidence by the existence of coesite and/or diamond is not yet discovered in the southern Pohorje region *(Miller & Konzett, 2005)*.

2.1.5. The *Ribnica-Selnica* sedimentary basin

The Ribnica-Selnica sedimentary trough is located north of the Pohorje range and extends W-E immediately north of the pluton. It is bordered in the western part of the range by the volcanic body and in the eastern part by the high grade units of the Upper Austroalpine. The sediments within this basin are classified as basal conglomerates, marine sandstones, siltstones and marls. The trough also brings evidence that the dacitic body has to be significantly younger than the intrusive rocks. Vitrinite reflectance and fission track data has shown a thermal overprint in Early Miocene sediments. *(Sachsenhofer, et al., 1998)*

2.2. Petrological and chemical Characterization of the Pohorje Pluton

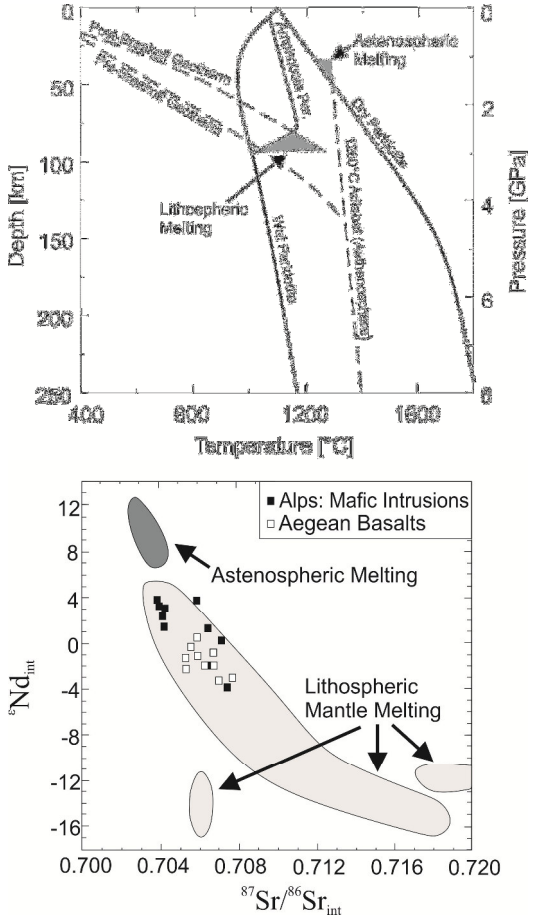

Fig. 5 Nd/Sr ratio of intrusive complexes with asthenospheric and lithospheric origin *(after Davies & von Blanckenburg, 1995)*

The Intrusive Igneous Complexes along the Periadriatic Lineament (see Chapter 2.1.2) have a general composition of tonalite, accompanied by granodiorite and rare diorite. They also can be associated with many acidic to mafic dykes *(Pamić, et al., 2002)*. The Alpine mafic rocks that formed during the late Alpine evolution (with intrusion ages cluster around 29-33 Ma) are related to Lithospheric Mantle Melting instead of Asthenospheric Melting. Davies and von Blanckenburg *(1995)* suggest that the slab breakoff of the down-going plate took place too deep to allow melting of the asthenosphere. The origin of the magma is described by them as a product of metasomatised and hydrated layers heated up by the upwelling heat resulting from the slab breakoff. That makes the parental rocks of the igneous complexes of lithospheric origin. This is also confirmed by the Nd/Sr ratio (Fig. 5). Several diagrams regarding the petrochemestry of the Pohorje pluton were made in the course of the research of Pamić and Palinkaš *(2000)*. To be mentioned are the K_2O wt% versus SiO_2 wt% and the CaO wt% versus Feo_{tot} wt% plots. The former one classifies the Pohorje as High-K calc-alkaline intrusion and latter show the expected data for I-type granites. The Pohorje Pluton consists of a mineral assemblage of amphibole, biotite, plagioclase, K-feldspar, quartz and accessories. The quartz-alkaline-plagioclase ratio of the Pohorje indicates tonalitic composition. The body was just slightly tectonized and, referring to Márton et al. *(2006)*, the tonalite was later modified by K-metasomatism to a granodiorite. Thermo-barometry of Fodor et al. *(2008)* shows different crystallization

depths for the western and the eastern part of the intrusion. They calculated 3 to 4 kbar (8-11 km) and 750 to 770 °C for the western and 6 to 7 kbar (16-19 km) and 760 to 820° C for the eastern half of the body. These calculations are based on ablation-inductive coupled plasma-mass spectrometry U-Pb analyses on oscillatory-zoned zircons.

3. Structural and Petrological Data

3.1. Petrography

Within the scope of this thesis no focus on petrological research was made, since there exist several works on petrology of the Pohorje mountain range e.g. Pamić & Palinkaš *(2000)*. The tonalite is arranged in three groups. The arrangement is not a macroscopic feature, but a feature of mineralization, microfabric and deformation mechanism. Also the host rock is graded in three different groups. Here a gradient can be detected of sericitization and the deformation mechanism. While closer to the intrusion the host rock is a gneiss with distance it is a micaschist. The seventh group described is of magmatic appearance.

Tonalite I:

Main constitutes within thin sections of this group (Table 4, p.75) are plagioclase and quartz, subordinarily biotite and K-feldspar. Further to be mentioned, is the presents of myrmecite (Fig. 7d) and the replacement of chlorite after biotite (sometimes into chlorite with abnormally blue interference colours). The plagioclase and the biotite are idiomorphic to hypidiomorphic, while the few K-feldspars and quartz seen in the thin sections are in general xenomorphic. Plagioclase often forms twins - the majority of them are formed by deformation with a very thin lamella width, but twins are also present as growth twins *(Passchier & Trouw, 2005)*. The plagioclase tends to have oscillatory zoning, in which the composition anorthite to albite ratio is varying. Also is dissolution together with quartz in form of myrmecites within the thin sections. The distribution of quartz is clearly affected by the larger plagioclase, therefore to be found in the interspace between these large crystals. Quartz crystals vary inequigranular to seriate in their grain size and have interlobate grain shapes. Biotite has grown along grain boundaries of feldspar and quartz. According to Bowen's fractional crystallization model this happens at a late stage of intrusion crystallization. The orientation of the mica evaluated and presented in Fig. 6. The K-feldspar within this group is rare. Similar to the plagioclase also the K-feldspar form large crystals. Orthoclase generally forms

Karlsbad-types of twins. Accessory minerals like zircon, rutil and apatit as well as oxides are rare but present.

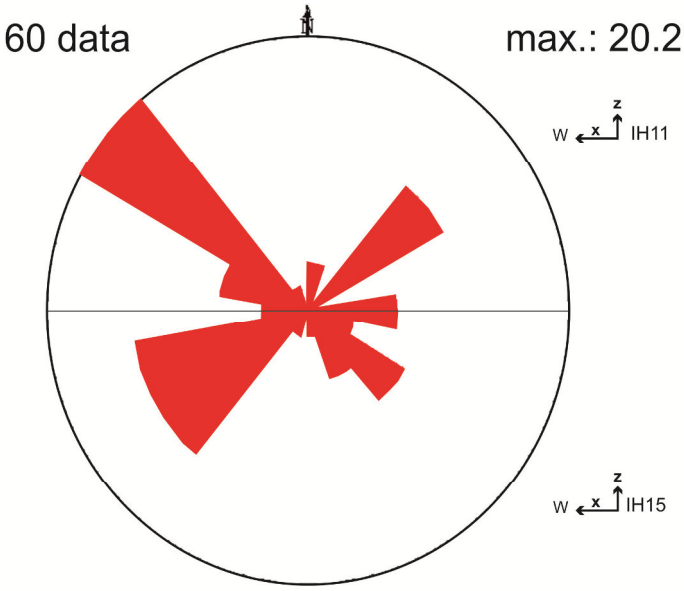

Fig. 6 Evaluation of the mica orientation within tonalite I. The upper hemisphere of the plot is representing the mica orientations in IH11, the lower hemisphere IH15. Both samples show a strong tendency of a NW-SE respectively NE-SW preferred orientation.

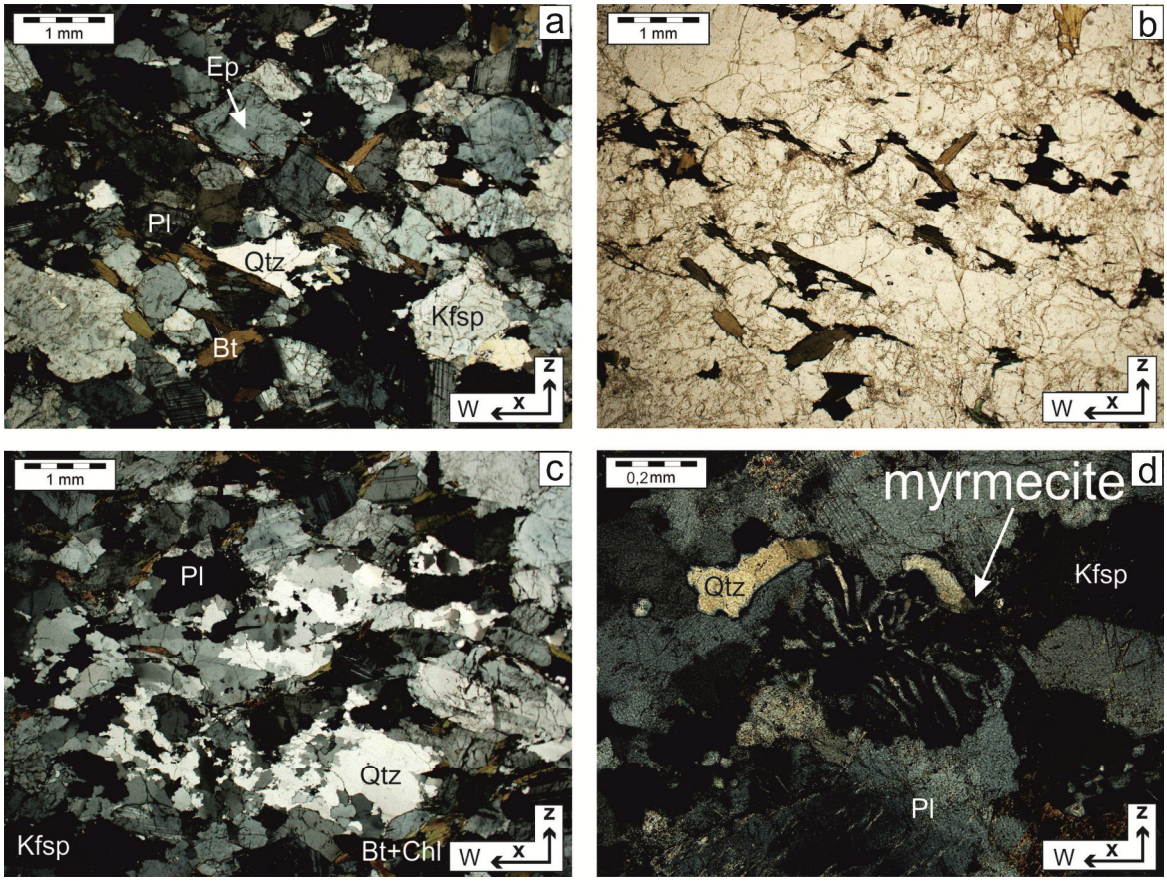

Fig. 7(a) (polarized) and (b) (unpolarised) photograph are showing IH11. The orientation of mica within these samples is significant (c) IH11: visualizing the large feldspar grains and the quartz dynamically recrystallized with GBM and SGR. (d) IH15: myrmecite worms in a plagioclase. The quartz within this section is mainly recrystallized by GBM.

Tonalite II:

The main minerals in this group (Table 5, p.75) are, like in the group tonalite I, quartz and plagioclase with somewhat more quartz compared to plagioclase. Minor components are biotite, K-feldspar and garnet. Other minerals are chlorite, epidote and clino-zoisite. Accessory minerals like zircon, rutil and titanit as well as oxides are rare but present. The feldspars form large hypidiomorphic minerals and are not well orientated. The plagioclase has growth and deformation twins. Also visible is oscillatory growth and the segregation to myrmecites. Orthoclase tends to form twins after Karlsbader law. Sericitic alteration of feldspar is often defined by the oscillatory zones (Fig. 8d). Quartz has inequigranular to seriate and interlobate grain boundaries, also is tonalite II cataclastic due to brittle deformation. The long axes of quartz grains are subparallel to the foliation. The phyllosilicates, biotite and chlorite, are also arranges subparallel to the foliation and starting to form a weak schistosity. In general in contrast to tonalite I a foliation of tonalite II is distinct (Fig. 8a&b).

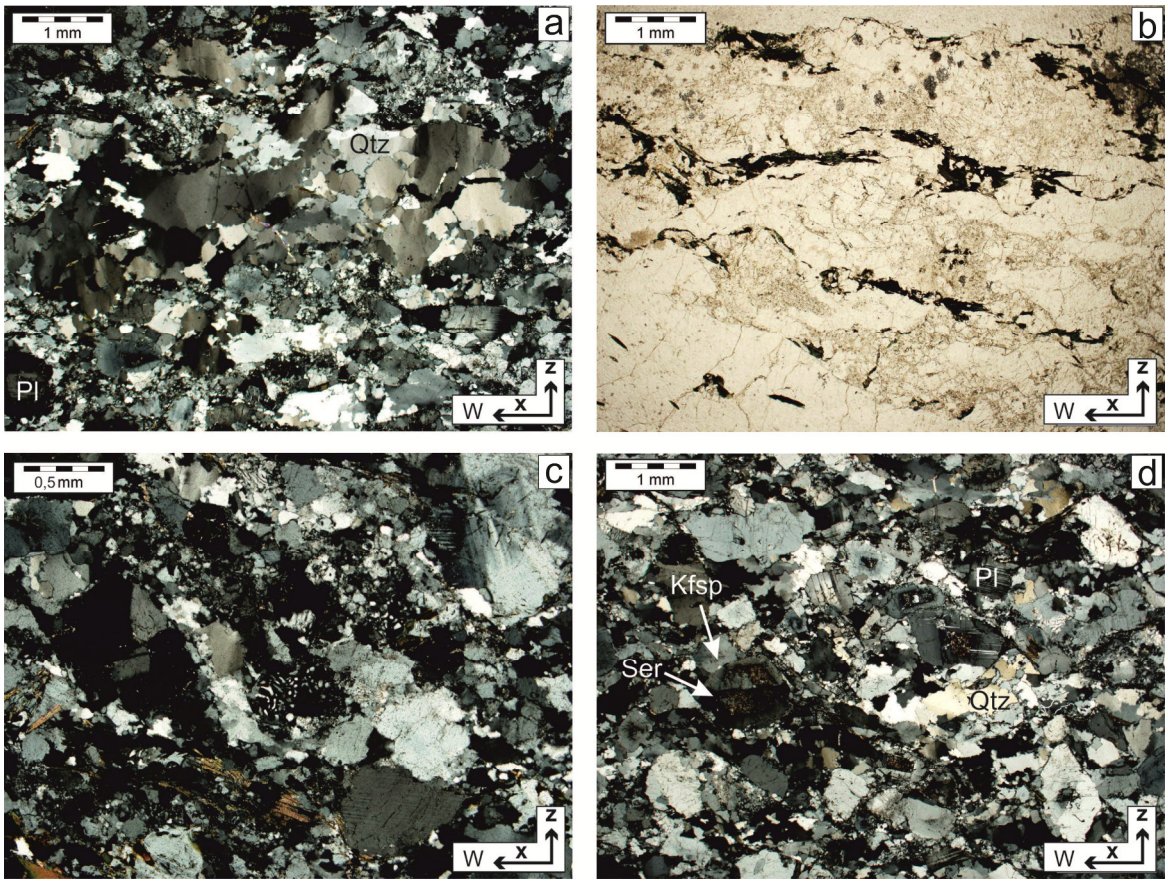

Fig. 8 (a) IH04 - BLG and SGR quartz recrystallization. (b) unpolarised photo with foliated mica. (c) magmatic fabric with myrmecite in the centre of the picture. (d) feldspar sericitic alteration within certain oscillatory horizons.

Tonalite III:

The tonalite III (Table 6, p.76) is characterized by its distinct cataclastic texture and microfaults. Especially the quartz is highly affected by brittle behaviour. The main components are quartz and plagioclase, side components are K-feldspar and phyllosilicates. Feldspar, dominantly plagioclase, has usually hypidiomorphic grain boundaries. The deformation twins of the plagioclase have a tendency of being subparallel to the foliation, growth twins and myrmecites are uncommon. Zonal plagioclase growth and orthoclase twins are also present. The thin sections contain certain domains of quartz sub-grains (Fig. 9c&d). Besides of them, the quartz is in a cataclastic matrix with undefinable minerals (Qtz+Pl+Kfsp). Phyllosilicates are biotite, with alteration to chlorite and often sericite. Compared with tonalite I and tonalite II the amount of oxides is significantly higher. These oxides are either in form of veins or as large grains. Accessories found in this group are zircon, rutil and titanite. Garnet is not found within this group.

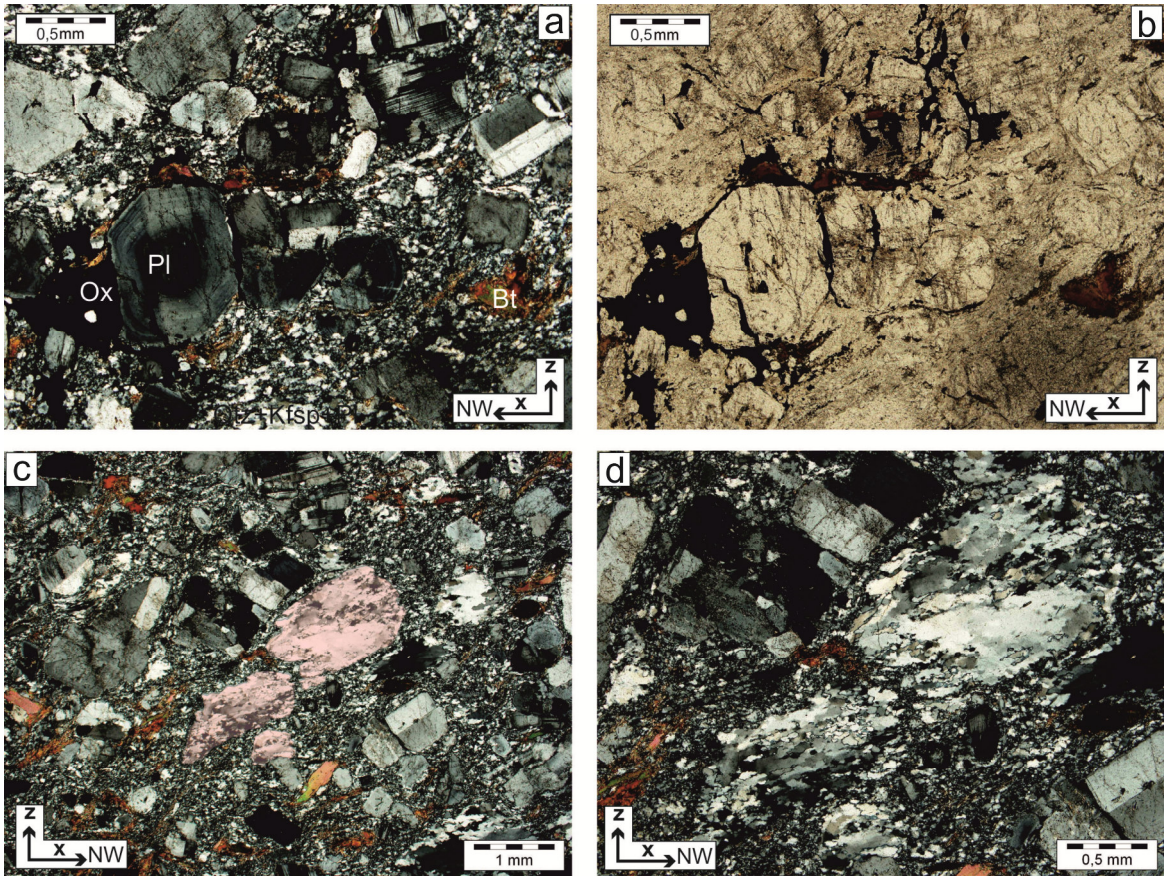

Fig. 9 All four photographs are showing IH25. (a) and (b) large feldspars with frequent twins subparallel to the foliation and oxide minerals. The matrix of this group is strongly catclastic. (c) quartz domain highlighted in pink. (d) quartz domain enlarged with 10x magnification.

Host rock I

According to macroscopic observation this group (Table 7, p.76) is gneiss to mica schist (see p.28). On microscopic scale the following features can be determined: The only primary minerals that are not secondarily altered are quartz and garnet. Feldspar and phyllosilicates are almost completely altered (Fig. 10). Quartz crystals vary strongly in their size and are usually xenomorphic, sometimes hypidiomorphic. Quartz grains are elongated subparallel to the schistosity representin in parts an axial plane foliation of small folds. The few relicts of primary phyllosilicates are biotite and muscovite and have elongated grain shapes. The main secondary alteration product of biotite and muscovite is sericite. In addition to that, chlorite is also present in the thin sections - most commonly around fragments of garnet.

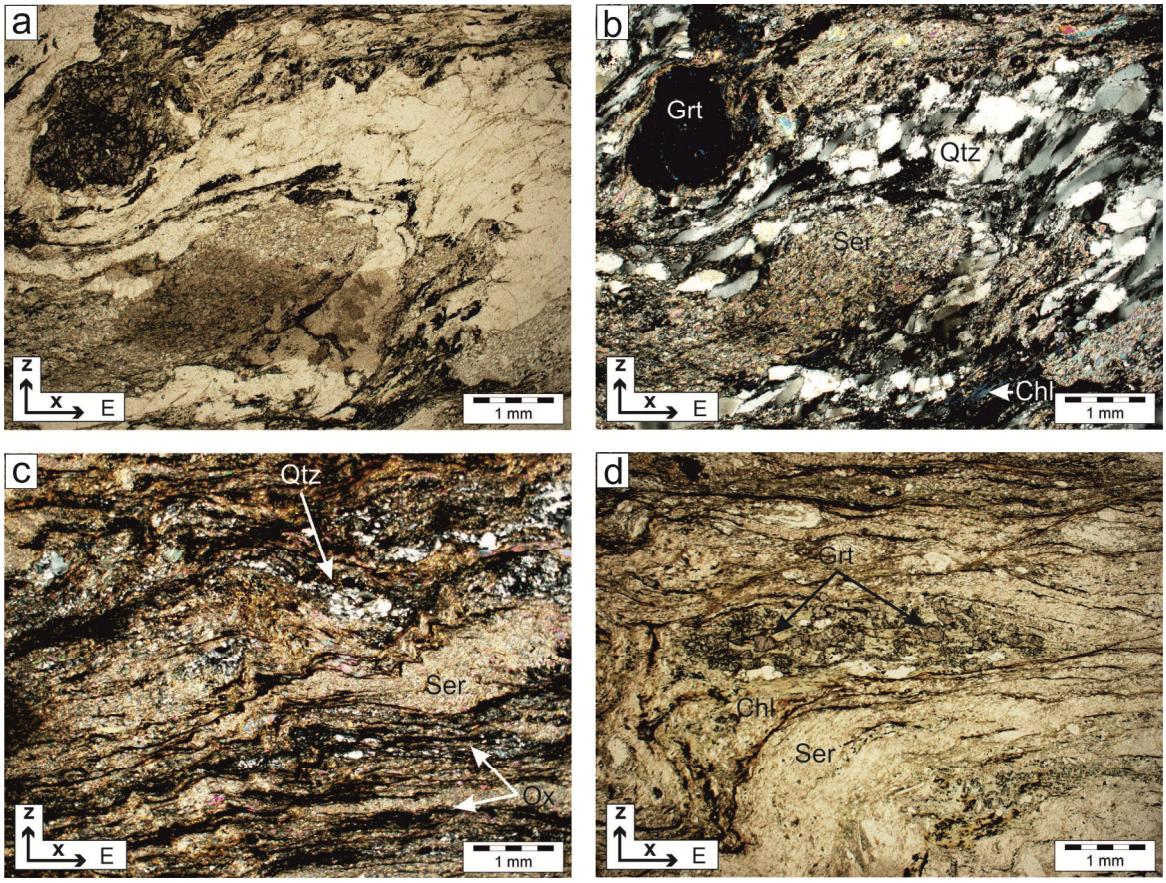

Fig. 10 IH18 unpolarised (a) and polarised (b). The quartz is elongated and especially affected by SGR. (c) and (d) strong sericitization of Host Rock I (IH20).

Host rock II

These rocks (Table 8, p.76) are similar to host rock I but show a stronger sericitization. The thin sections are dominated by a matrix mixed together of strongly disaggregated and altered quartz, feldspar and mica. The few remaining minerals are often xenomorphic. In some domains with quartzite composition the mineral structure is still sustained. Plagioclase and K-feldspar are infrequently in such condition. Garnet is common in host rock II, but usually fragmented and diverted subparallel to the cleavage (Fig. 11c&d). In the shade of these fragments mica recrystallization is usual. Oxides are dragging trough fine micro-fault lines. The alteration of phyllosilicates to chlorite is rare within this group. The difference to Host Rock I is discussed in chapter 3.3.1.

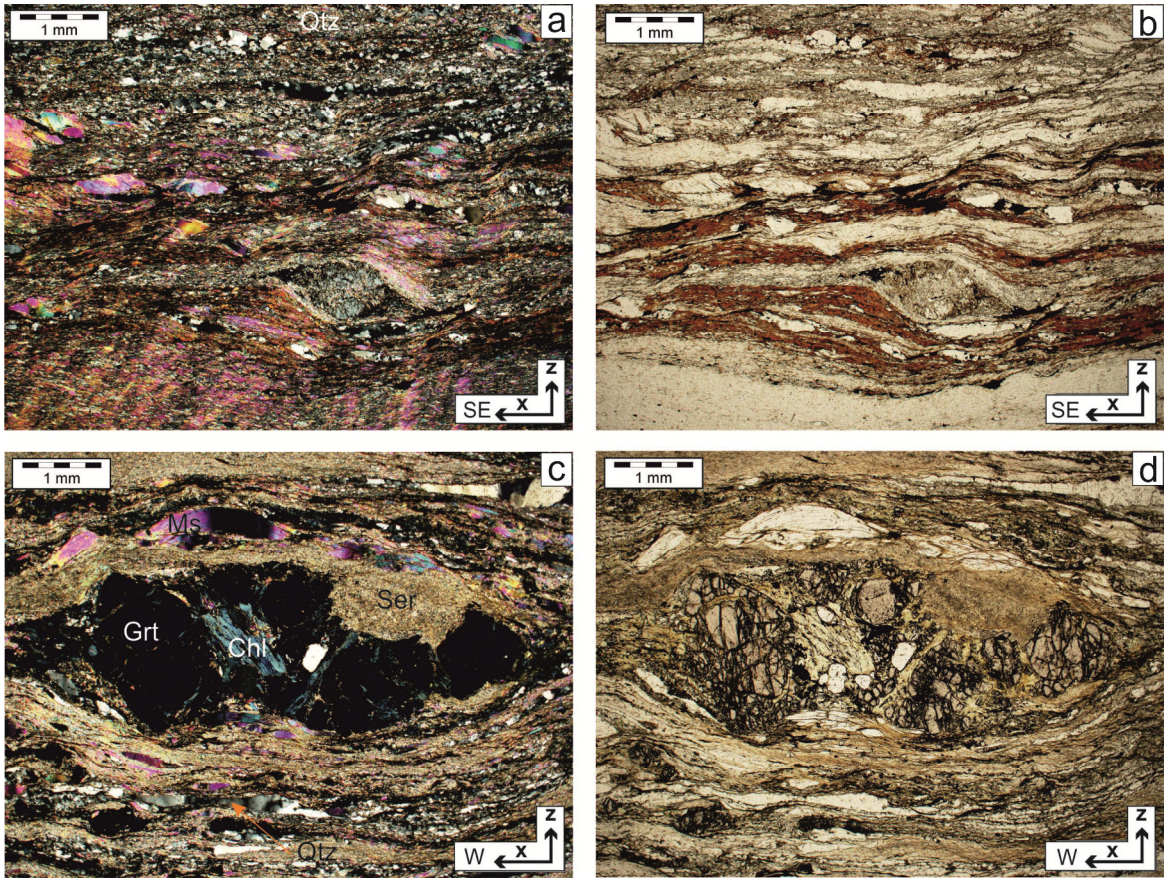

Fig. 11 rock samples of Host Rock II – top IH49 and bottom IH79 – are highly sericitic and sheared. (a) polarized and (b) unpolarised photo of relictic feldspar with an asymmetric shape indicating displacement top NW. (c) polarized and (d) unpolarised photo of mosaic-fragmented garnet porphyroclast with a secondary chlorite alteration – shearing top W.

Host rock III

These mica schists (Table 9, p.77) differ from host rock I and II by its weaker developed sericitic alteration. The main components are quartz, feldspar (typically more K-feldspar), garnet and phyllosilicates in form of biotite, muscovite and some alteration to chlorite. Quartz is often concentrated within bands, with seriate grain boundaries. The grain shape is generally interlobate. Biotite and muscovite is hypidiomorphic and elongated and either in layers or in the shade of rigid minerals such as garnet. Oxides are common within host rock III and are dragging trough fine micro-fault lines (Fig. 12a&b).

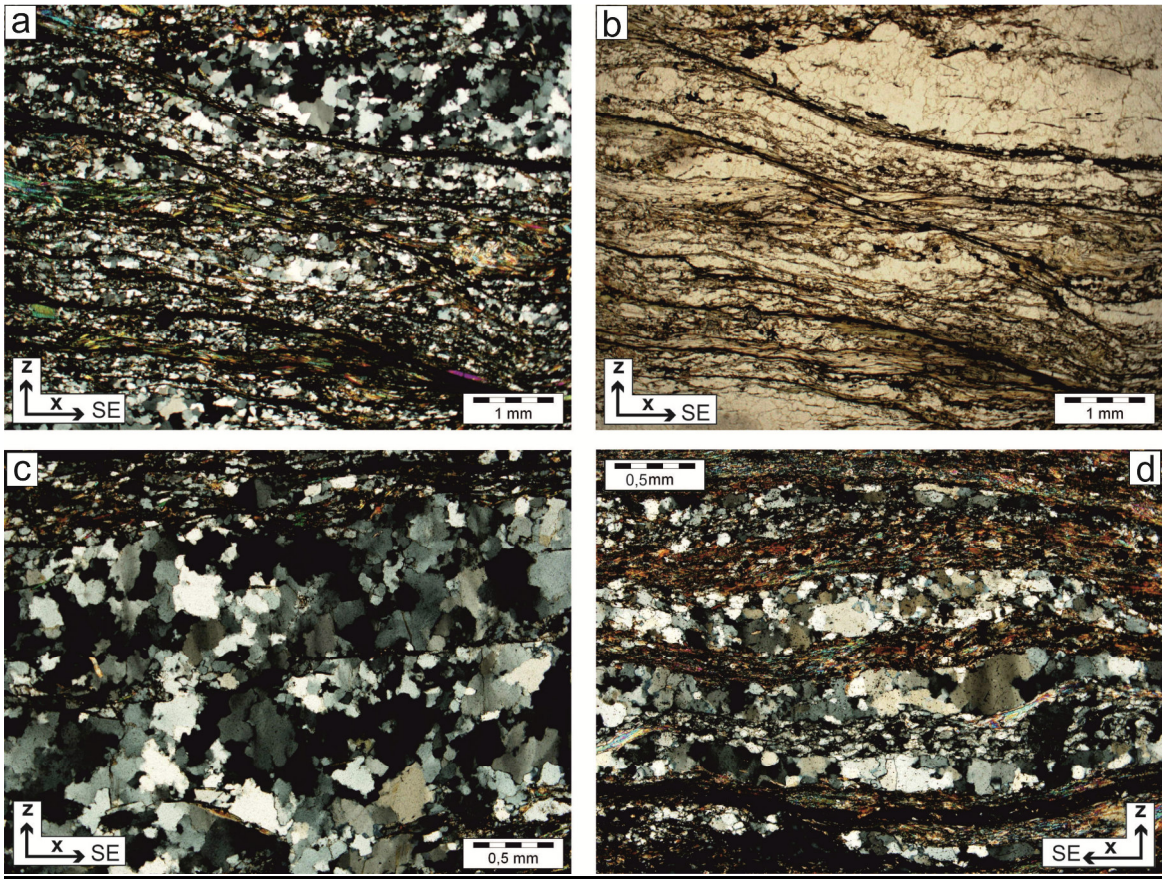

Fig. 12 (a) and (b): IH80 – microfaults and shear bands with oxide mineralization. (c) 10x magnification and (d) 2x magnification of bulging dominated quartz deformation.

Migmatite

Except quartz and few relictic K-feldspars every mineral is grained in a fine mixture of cataclastic and sericitic domains. The migmatization is easily identified in the field (Table 10, p.77), but due to strong deformation hardly recognizeable in thin sections. The grain shape of quartz appears usually elongated. Recrystallization mechanisms are variable. They vary from GMB to BLG within the irregularly shaped quartz layers (ptygmatic folds). The quartz within the eastwards dipping extensional faults is not overprinted by dynamic recrystallization.

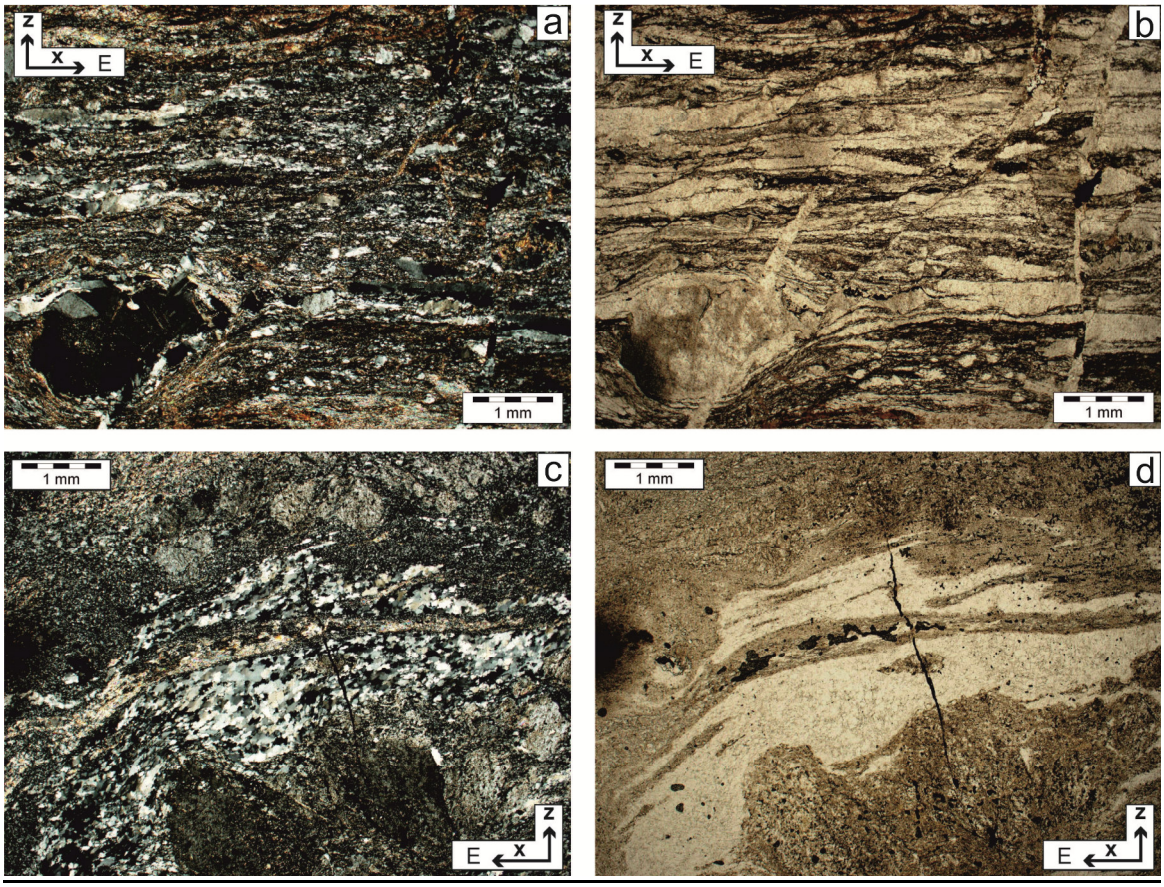

Fig. 13 (a) polarized and (b) unpolarised: quartz layers interchanging with a sericitic and cataclastic matrix and a relictic K-feldspar. Eastwards dipping extensional veins are cutting through the fabric. (c) polarized and (d) unpolarised: ptygmatic quartz layer

3.2. Geological field investigation

The main body of the pluton is apparently undeformed and preserved magmatic mineralogy and fabrics. Exceptions are brittle structures such as fault and joint systems. Two different joints and faults are distinguished, chlorite decorated joints and faults and those who do not show hints of mineralisation

3.2.1. Tonalite:

The topography of the tonalite body has steep sidewalls on both the northern and the southern side and a flat centre part with gentle slopes and well eroded. Therefore, outcrops are rare in the centre. Usually the rock body is covered abundantly with soil. Outcrops are easier found on the rim of the intrusion. The Tonalite appears here very solid and in case of weathering the alteration horizon does not penetrate the rock deeply (2-3 cm). Shear bands are formed usually in thick (0.5–1.5 meter) blocks and just rarely dissembled in smaller parts (Fig. 15).

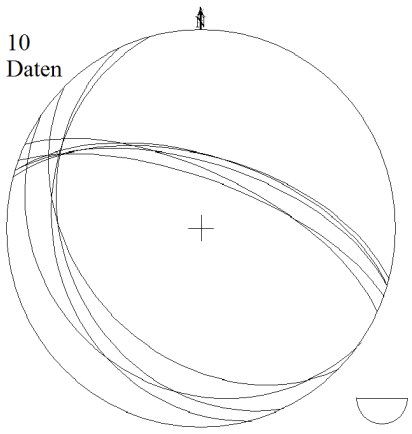

Fig. 14 The plot is a Lambert projection (equal-area projection) on the lower hemisphere of orientation data from the orthogonal fault system shown in **Fig. 15**.

Fig. 15 : A) Road outcrop 6 km uphill of Lovrenc na Pohorju along the dirt road towards the south. The outcrop is showing orthogonal fault systems with multiple normal faults facing NE and conjugated planes facing SW. B) Demonstration of the relative movement of the blocks to each other.

The outcrop in Fig. 16 (next page) is located 46°31.067'N and 015°15.314'E on the Ribnica na Pohorju profile. The first part of the outcrop (coming from Ribnca na Pohorju) is fractured into plains dipping NE. The transition into section (B) is abrupt. Here the rock has three distinct planes (JS1, JS2 and JS3). Section (C) is barely fractured. The fractures in this area are most likely due to previous road construction. In the middle section (see Fig. 16, section D) a fault zone is crossing though the outcrop. The rock in this area is strongly fractioned into specimens with 10-50 cm diameter. The outcrop is very representative since it shows several features already discussed.

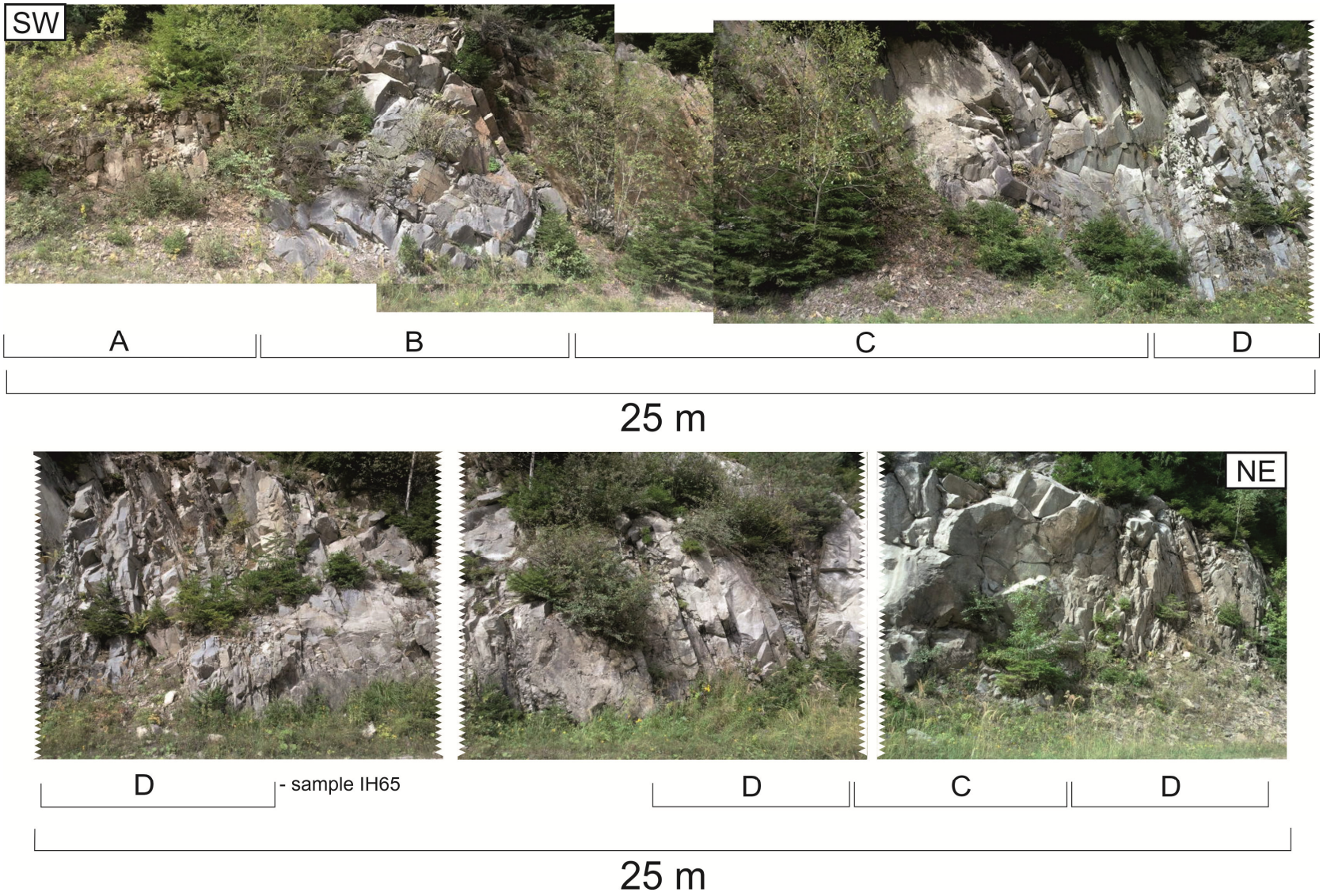

Fig. 16 picture of an outcrop on the profile south of Ribnica na Pohorju. Outcrop can be subdivided in different sections (A-D); (A) cataclastic section with joint sets parallel to JS2 (B) rock fractures parallel to JS1, JS2 and JS3. (C) barely fractured rock (D) fault zone with strong fractioning

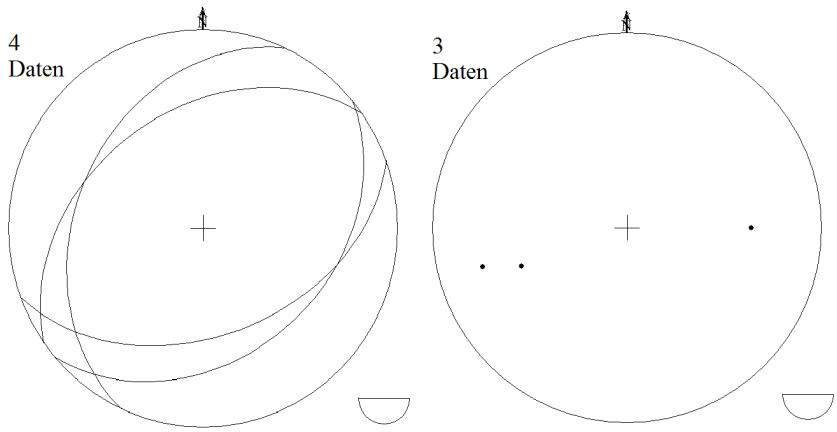

Fig. 17 left: Lambert projection (equal-area projection) of tonalite 1 samples (according to the classification described in chapter 4.1). right: stereographic projection (globular projection) of tonalite I sample. Both projections are on the lower hemisphere.

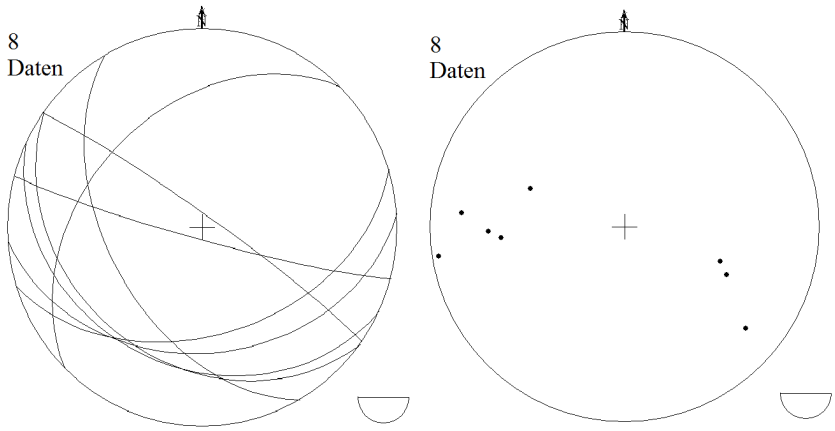

Fig. 18 left: Lambert projection (equal-area projection) of tonalite I1 samples (according to the classification described in chapter 4.1). right: stereographic projection (globular projection) of tonalite II sample. Both projections are on the lower hemisphere.

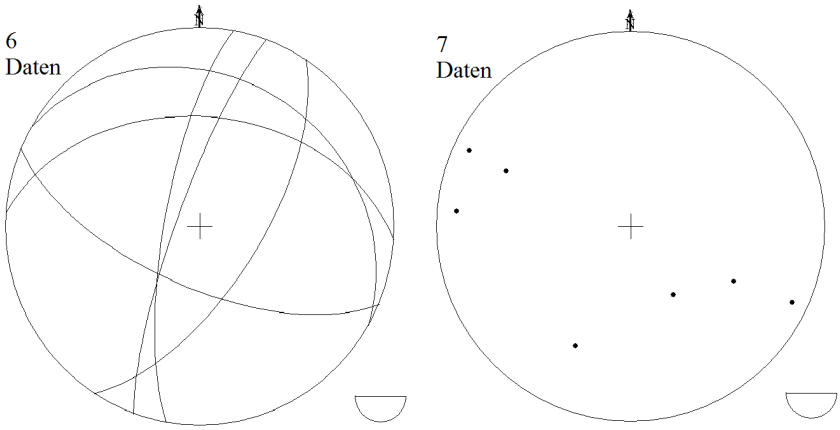

Fig. 19 left: Lambert projection (equal-area projection) of tonalite II1 samples (according to the classification described in chapter 4.1). right: stereographic projection (globular projection) of tonalite III sample. Both projections are on the lower hemisphere.

As expected structural features in the plutonic body are rare in the centre areas of the mountain range and are mainly found on the steep sides of the Pohorje. On the southern side two structural features are frequent. These are for ones, conjugated shear joints named JS1, JS2 and JS3 (Fig. 20) and secondly, secondary chlorite mineralization (Fig. 21). The chlorite mineralization is located in a set of joints dipping in an intermediate to high angle towards north-east. The chlorite mineralization on these joint planes does not show a preferred orientation. This joint set is equal in orientation with the JS2, represented in (Fig. 20), tough not to seen as equal since not all joints of JS2 show a chlorite mineralization.

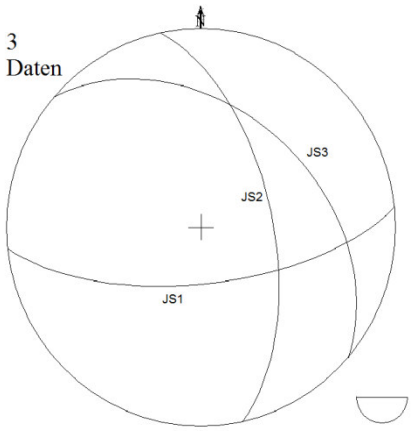

Fig. 20 showing the statistic mean of the three conjugated shear joint sets (JS1, JS2 and JS3) on the southern boundary of the Pohorje mountain range. The intersection between JS2 and JS3 is in a low angle whereas the other two intersections are almost 90 degrees. The plot is a Lambert projection (equal-area projection) on the lower hemisphere. A plot of every JS1, JS2 and JS3 plains is added to the appendix.

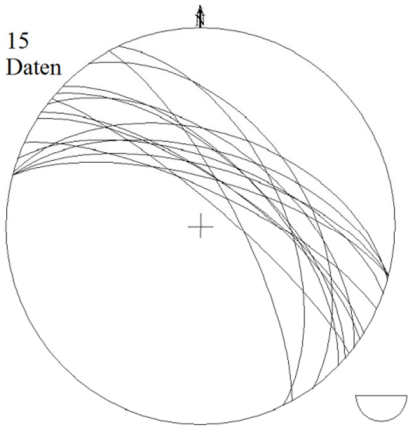

Fig. 21 Lambert projection (equal-area projection) on the lower hemisphere representing the orientation of joint set where secondary chlorite mineralization appears.

Also along the northern boundary of the Pohorje mountain range three sets of joints are frequently present (Fig. 22). Different to the southern side of the range the three joint sets are in the greatest possible extent equiangular. Other megascopic structures on the northern boundary of the range are north-south orientated fault zones, which can be also detected as depressions in the morphology of the range. The graben south of Ribnica na Pohorju marks also one of these faults with a dextral displacement. The contact between the host rock and the tonalite on the western side of this fault is about 10 meters further south as on the eastern side. The outcrop shown in Fig. 23 reveals “Riedel”-planes roofing the direction of displacement.

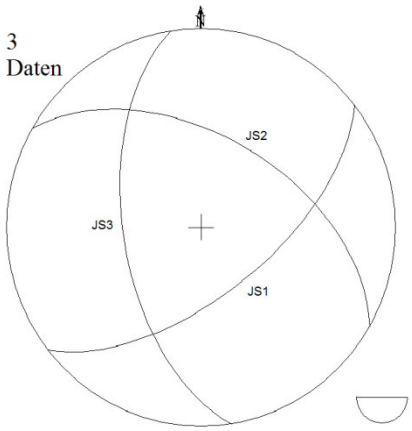

Fig. 22 showing the statistic mean of the three conjugated joint sets (JS1, JS2 and JS3) on the northern boundary of the PMR. The intersections of the three planes are equiangular. The plot is a Lambert projection (equal-area projection) on the lower hemisphere. A plot of every JS1, JS2 and JS3 plains is added to the appendix.

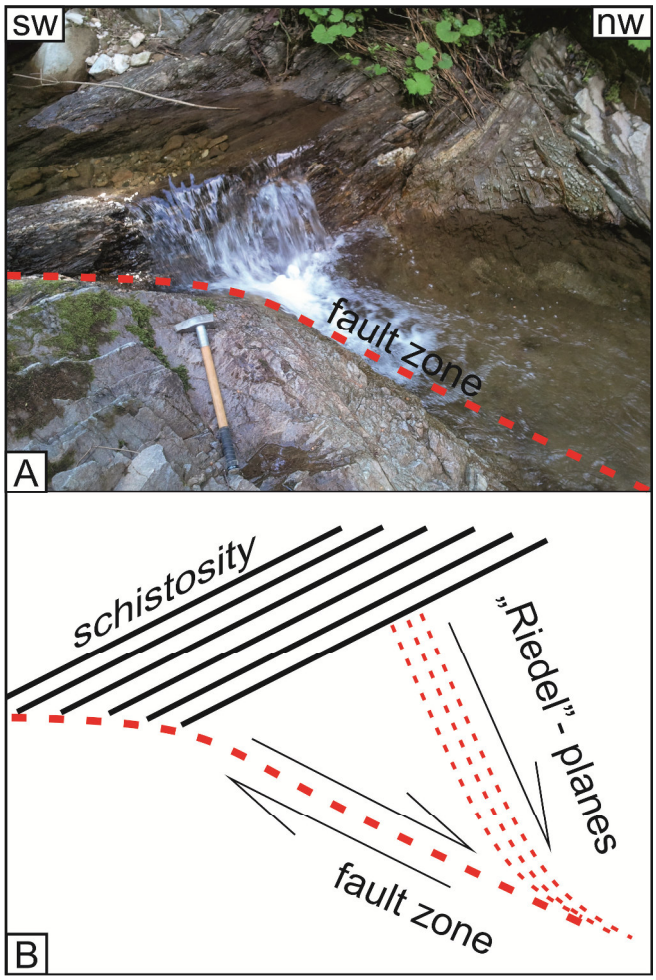

Fig. 23 A) showing the dextral offset along the fault zone in the graben south of Ribnica na Pohorju. The rock east of the fault (lower part in the picture) is tonalite. West of the fault the host rock is in-situ (upper part in the picture). The gneiss (host rock) has a schistosity dipping NW-SE. B) The graphic is pointing out the "Riedel"-planes at this outcrop. These planes are breaking through the gneiss W-E dipping and bending into the direction of the fault as closer they get to it.

3.2.2. Host rock:

The host rock around the intrusion is as described in chapter 2.1.3 mica-schist or gneiss. In striking distance from the intrusion it is gneiss that can be compared with the "Stainzer Plattengneis" found at the eastern side of the Koralpe in Styria. In general, the gneiss is compact and hard with a visible schistosity. With distance from the pluton contact the rock also appears with a strong schistosity and a weaker cohesion between the (mica-) layers and therefor classified as a micaschist. This graduation suggests a contact areola of the intrusion. Such gradient can also be seen in the sericitization described in chapter 3.1 (host rock I to III). In the contact area of the dacite extrusion the host rock is mainly phyllite. In course of the field work a serpentinite lens (IH16/17) in the south-eastern corner of the intrusion (100meter uphill of the town border of Visole) and an amphibolite lens (IH77) south of the town of Lovrenc na Pohorju was mapped and analysed under the microscope. These lenses and the foliation of the host rock are older than the intrusion. Hence it can be learned from them just little concerning the intrusion history.

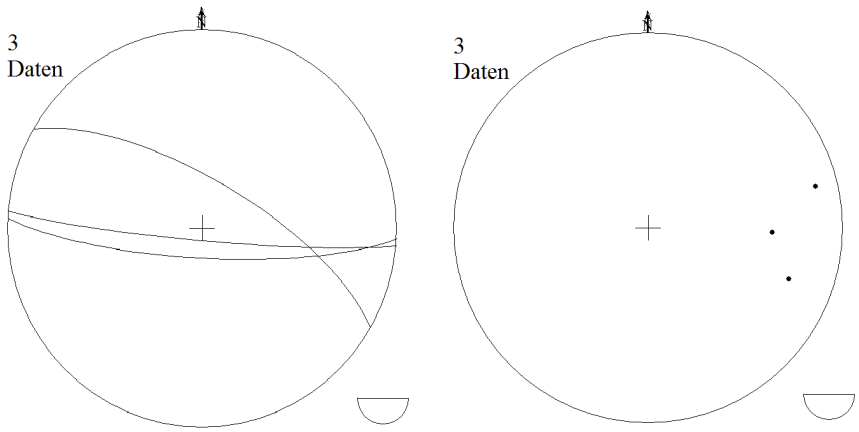

Fig. 24 left: Lambert projection (equal-area projection) of host rock 1 samples (according to the classification described in chapter 3.1). right: stereographic projection (globular projection) of host rock I sample. Both projections are on the lower hemisphere.

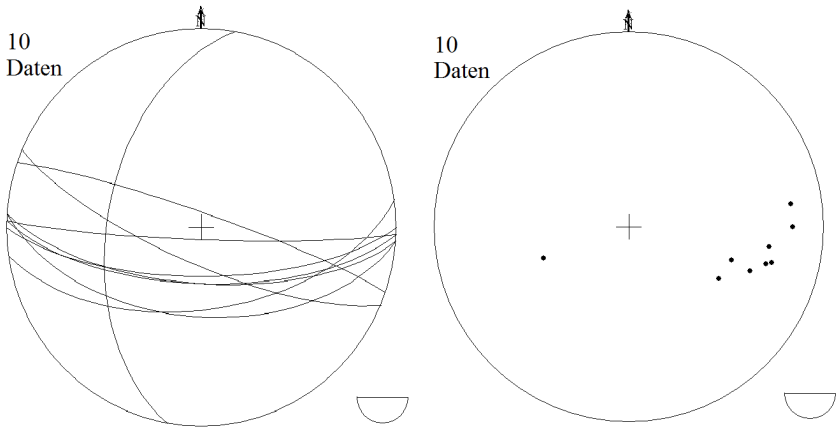

Fig. 25 left: Lambert projection (equal-area projection) of host rock II samples (according to the classification described in chapter 3.1). right: stereographic projection (globular projection) of host rock II sample. Both projections are on the lower hemisphere.

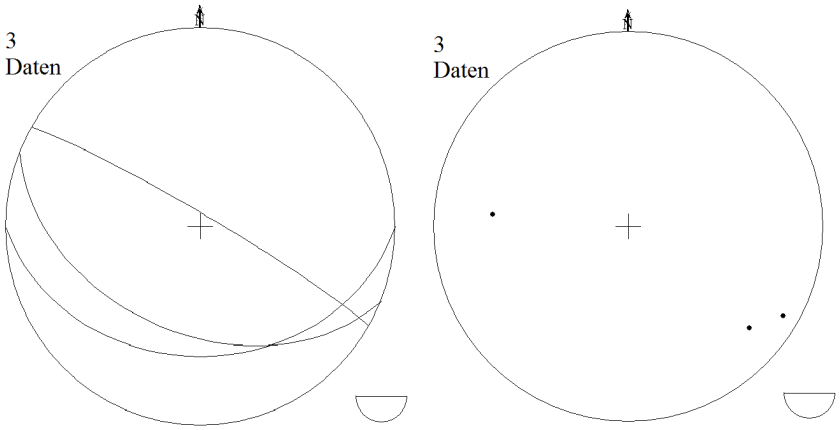

Fig. 26 left: Lambert projection (equal-area projection) of host rock III samples (according to the classification described in chapter 3.1). right: stereographic projection (globular projection) of host rock III sample. Both projections are on the lower hemisphere.

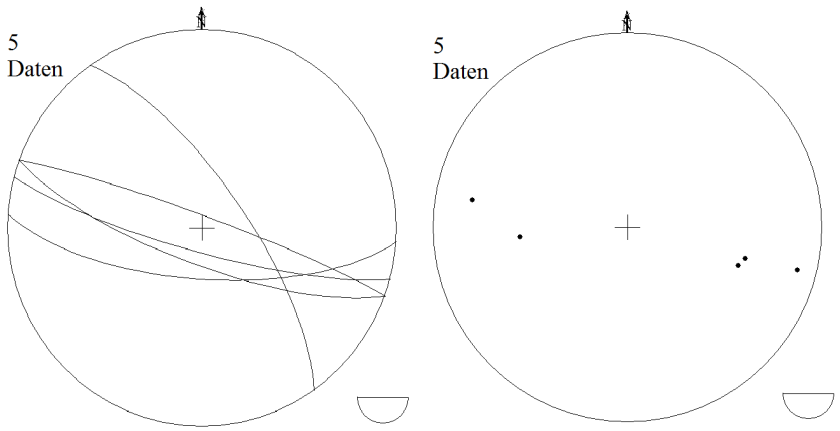

Fig. 27 left: Lambert projection (equal-area projection) of the migmatite samples (according to the classification described in chapter 3.1). right: stereographic projection (globular projection) of the migmatite sample. Both projections are on the lower hemisphere.

3.3. Microanalysis

3.3.1. Microstructures

The thin sections were investigated to distinguish between magmatic flow, submagmatic flow and solid state deformation structures. To unravel the igneous, metamorphic and structural evolution of these rocks the micro-tectonic analyses is essential *(Passchier & Trouw, 2005)*. The recrystallization of quartz is triggered by temperature and strain dependent mechanisms. At high temperatures (500° - 700°C) “grain boundary migration”, hence fore GBM, is mostly common. With lower temperatures (400-500°C) “sub-grain rotation” (SGR) is replacing GBM in importance. At temperatures between 300 and 400 degrees Celsius quartz recrystallization is active by “bulging” (BLG). Below 300°C quartz is behaving brittle. The recrystallization of feldspar is generally controlled by the same mechanisms. The temperatures of feldspar recrystallization are much higher (BLG starting at 450°C; SGR at 600°C and GBM at over 800°C). The mechanisms are explained in detail by several authors. This work is leaned on the explanation of Passchier and Trouw in Microtectonics chapter 3*(2005)*.

Tonalite I:

Magmatic structures are well preserved with just little low temperature ductile overprint. Quartz appears interstitial between large magmatic grains and has lobate boundaries suggesting GBM. Further, quartz recrystallization at lower temperatures (BLG) is also preserved but rare. The mica forms, as described in chapter 3.1, orthogonal systems with the low angle pointing W – E. In general elongation in direction of foliation (e.g. grain shapes of larger minerals) is present. Also are twin lamellas of plagioclase due to stress (Fig. 28a&c) tending to be parallel to the foliation. The feldspar is reacting brittle, in very few areas bulging was detected in feldspar (Fig. 28 a).

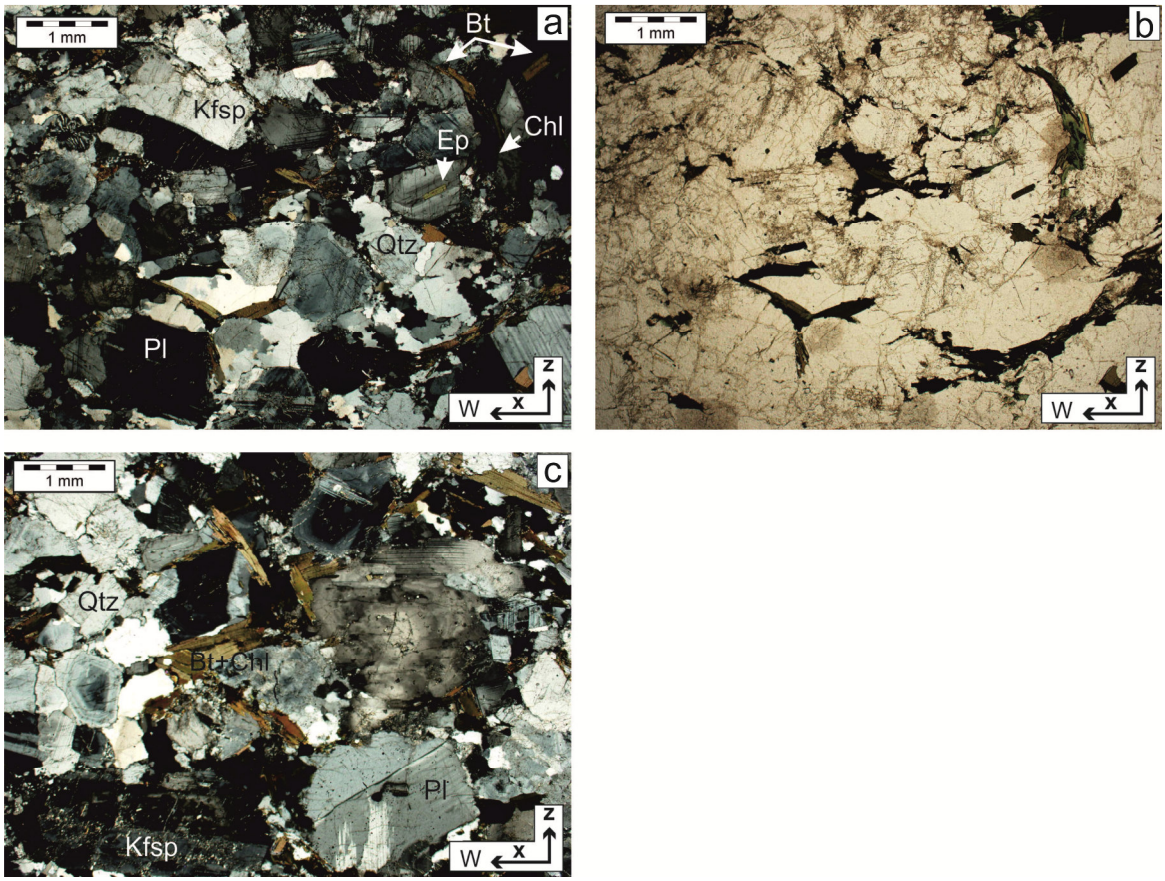

Fig. 28: photographs of IH15 – quartz recrystallizing by GBM and BLG; (a) feldspar in rare examples with bulges is in general brittle. (b) and (c) mica forming a system of orthogonal structures.

Tonalite II:

The mica is unlike in tonalite I orientated parallel to the foliation and is, therefore, the indication of the foliation in tonalite II. Quartz is elongated parallel to the foliation and recrystallizing with a core – mantle fabric in bulges (BLG) and extinguishing wavy (SGR). Isolated quartz grains exhibit GBM. The magmatic structures are preserved but low temperature flow is evident from bulging within quartz and beginning cataclasis of the rock. Other minerals are not adjusted to the foliation. The thin sections IH10, IH57 and IH68 frequently contain brittle faults forming mosaic fragments. The micro-faults between the fragments are predominantly decorated with oxide remineralisation (besides of the opaque oxides also reddish Fe-oxides). In addition the thin section IH57 also shows a carbonate vein running NW-SE in the thin section (Fig. 29).

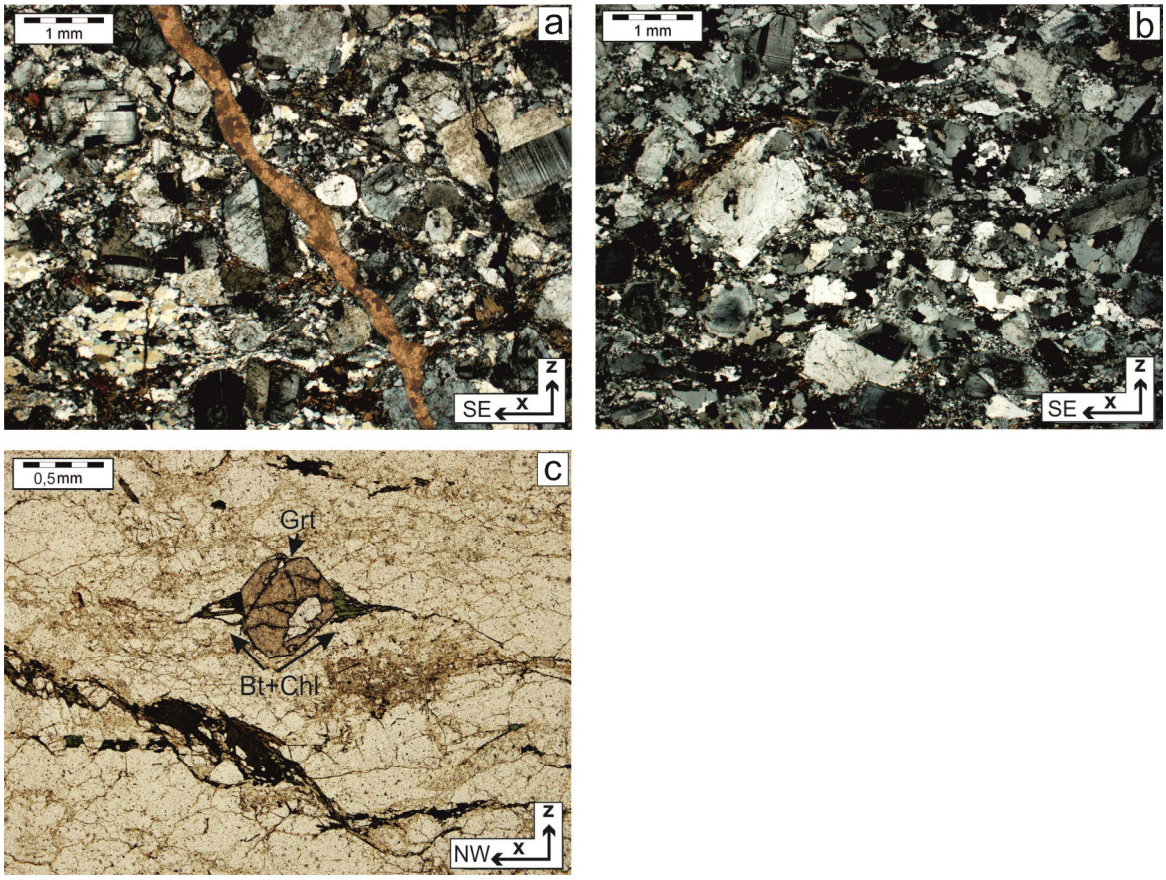

Fig. 29 (a) IH57: carbonate vein dipping NW-SE and is triggered by extension. (b) magmatic structures are still preserved coexistent with bulging (low temperature deformation) and cataclasis (c) IH90: garnet with biotit and secondary chlorite in the strain shadows parallel to the foliation. Strain shadows are symmetric and do not show any rotation of the garnet.

Tonalite III:

The main character of these tonalites is their cataclastic matrix. Other than the larger minerals, with a grain sizes larger 500 µm, the cataclastic mineral matrix, with a grain size smaller than 20 µm, have a moderate orientation subparallel to the foliation. This group contains extensional features best seen in IH35 (Fig. 30) and IH52. First one, showing extensional veins and second, micro-faults formed in an extensional regime. Domains with remaining quartz (not cataclastic) are recrystallized by BLG and SGR.

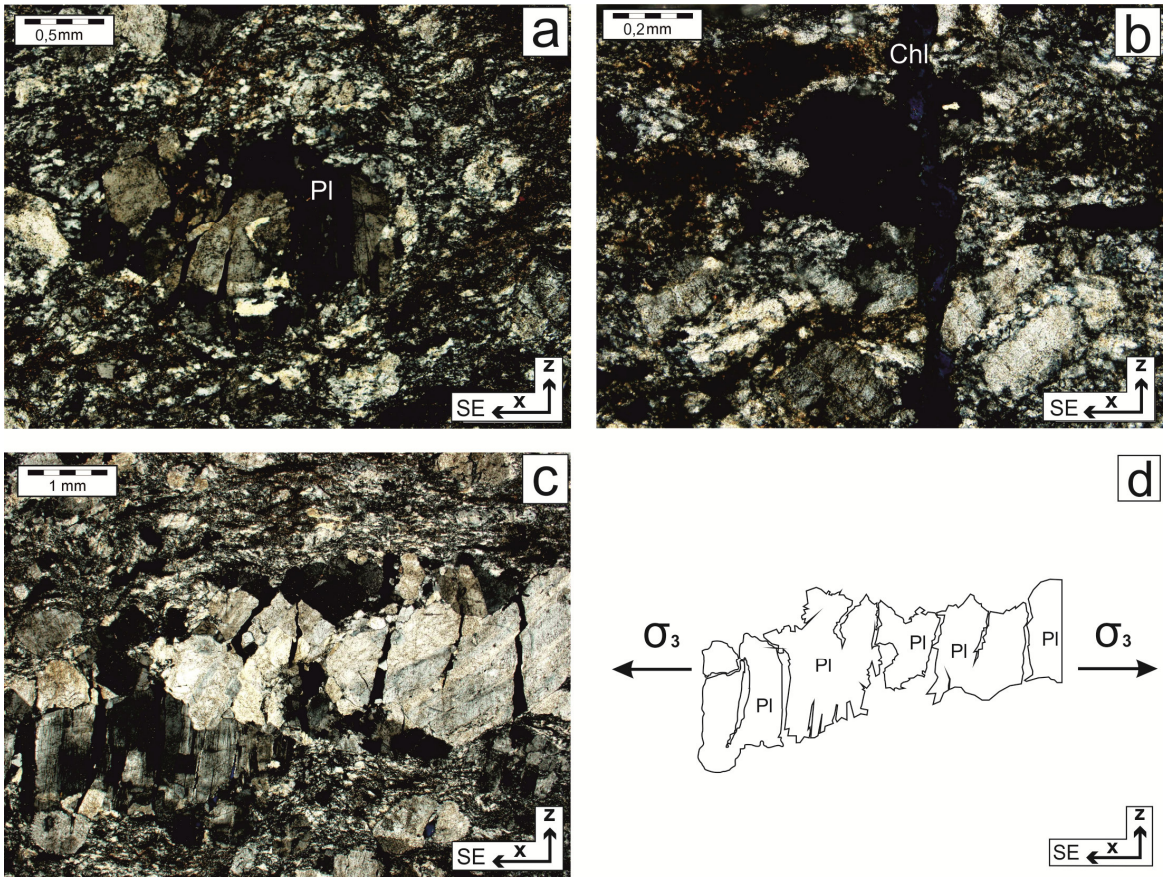

Fig. 30: (a) cataclastic texture of tonalite III. (b) extensional vein with chlorite recrystallization. (d) illustration of (c) relictic plagioclase is fragmented due to NW-SE extension.

Host rock I:

Thin sections contain frequently sericitic and numerous brittle micro faults crosscutting the direction of the foliation. The feldspar crystals are highly altered to sericite and just few crystals are still sustained as feldspar. Areas with high sericite content react incompetent and form micro folds. Within the thin section IH18 multiple shear structures with an asymmetric shape indicate a dextral displacement. Brittle faults (fractures) are conjugated diagonal to the foliation and recrystallized with either chlorite or sericite (presumably primarily feldspar). The fractures orientated NW-SE are preferably recrystallized with chlorite and the faults NE-SW with sericite (Fig. 31) (direction in thin section). The chlorite in such fractures exhibit anomalous blue interference colours *(Pichler & Schmitt-Riegraf, 1997)*. The quartz grains are elongated in direction of the foliation with a distinct recrystallization selvage. The recrystallization mechanism, therefore, is dominantly BLG and SGR.

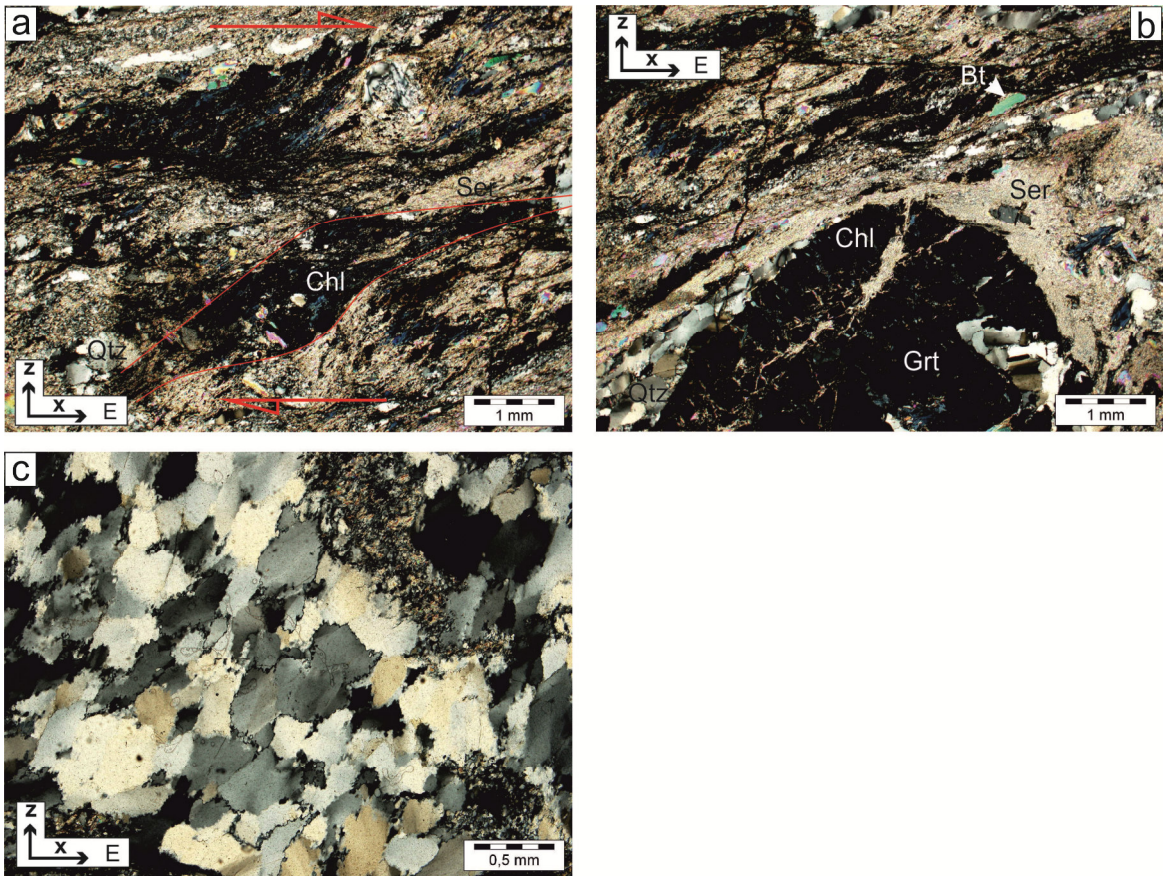

Fig. 31 (a) relictic garnet with chlorite recrystallization forming a clear evidence for top W shearing. (b) microfractures within a garnet are recrystallizing with chlorite and sericite. (c) quartz recrystallizing by BLG to a core – mantle fabric.

Host rock II:

This group share many features with host rock I, but is described as a separate group. This is in first instance because of a much weaker bulging as a quartz deformation mechanism and an incipient overprinting of a newly formed extensionary crenulations cleavage. Therefore, an extensional crenulation cleavage (ECC) is characterizing this group. The feldspar in host rock II is altered to sericite, Undestroyed and non-serecitic feldspar is very rare in host rock II. These layers of sericite react by folding to stress forming the crenulation cleavage and contain several asymmetric structures with top NW displacement (Fig. 32). Similarly is a bending of mica transversal to the layering visible. A secondary cleavage (NW-SE) is also evident by the quartz orientation. Host rock II also experienced a brittle overprint with faulting. These faults are recrystallized with oxides.

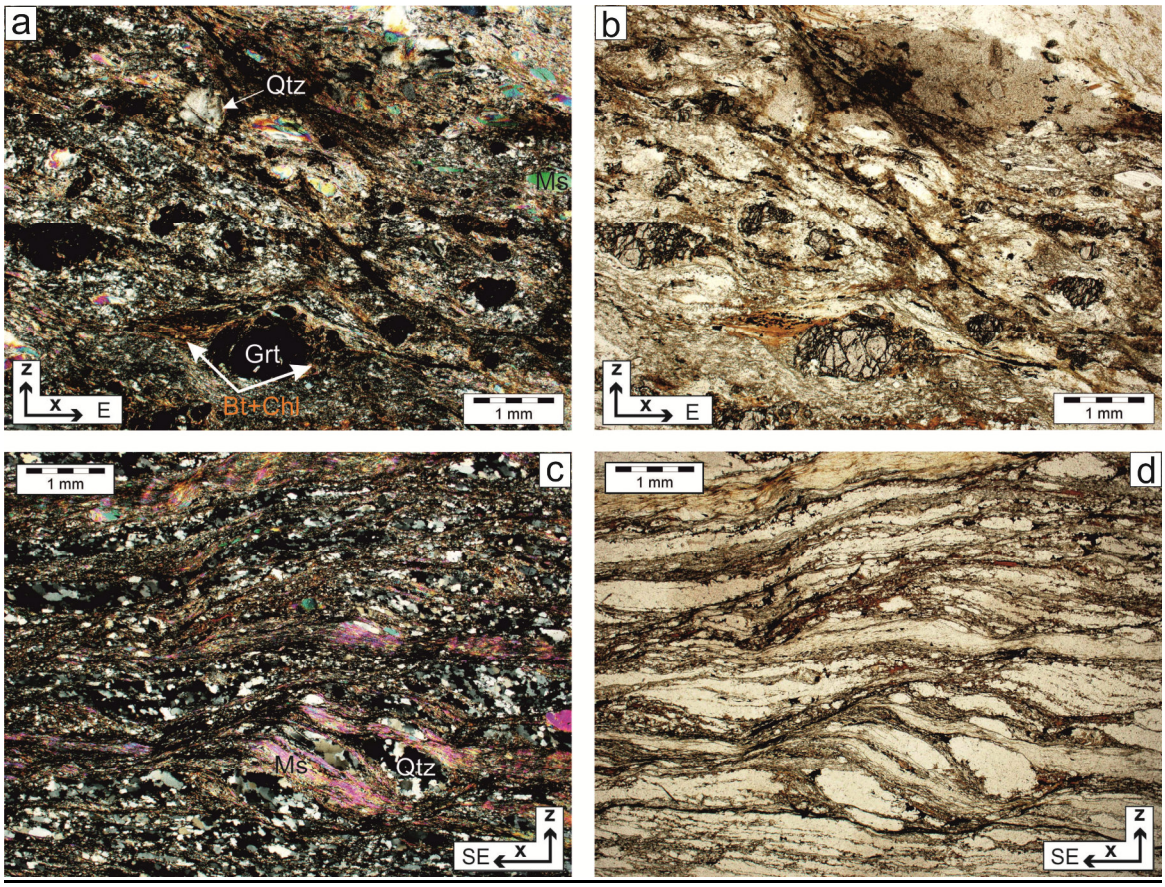

Fig. 32 (a) polarized and (b) unpolarised: garnet with strain shadow. Biotite and Chlorite in these shadows of asymmetric form indicate the top W shearing. (c) polarized and (d) unpolarised photo of ECC-fabric with the crenulation cleavage pointing NE-SW.

Host rock III:

Quartz and mica are organized in layers forming typical a mica-schist fabric. The mica is not only oriented into the direction of foliation - S plains (schistosity) - but also forming C' plains (secondary cleavage). The shear sense is also identifiable around garnet grain (e.g. IH09b). Here biotite and muscovite is growing in the stress shadows of the garnet. Thin sections of the rocks IH80 and IH81 have micro-faults and micro-folds parallel to the schistosity and a top NW offset.

Migmatite

These rocks have three distinct features. For ones, similar to host rock I & II sericitization is dominant. The minerals are almost completely disintegrated, leaving just very few primary phyllosilicates, somewhat more feldspar and quartz. The quartz is often recrystallized in layers (BLG and SGR). High temperature evidence, like shown in chapter 3.1, is rare. These rocks have a distinct low temperature shearing and cataclasis and also a high fluid participation (Fig. 33). Secondly, large grains (quartz and feldspar) remaining unaffected by sericitization and are either still remained as large crystals or are the fragments of these (brittle behaviour), in case of quartz, as mentioned, recrystallization in smaller grains. Thirdly, extensional veins are upright but varying in their orientation between dipping towards the west and the east. They are either crystallized with quart and feldspar (< 500 µm) or with oxides (<50 µm).

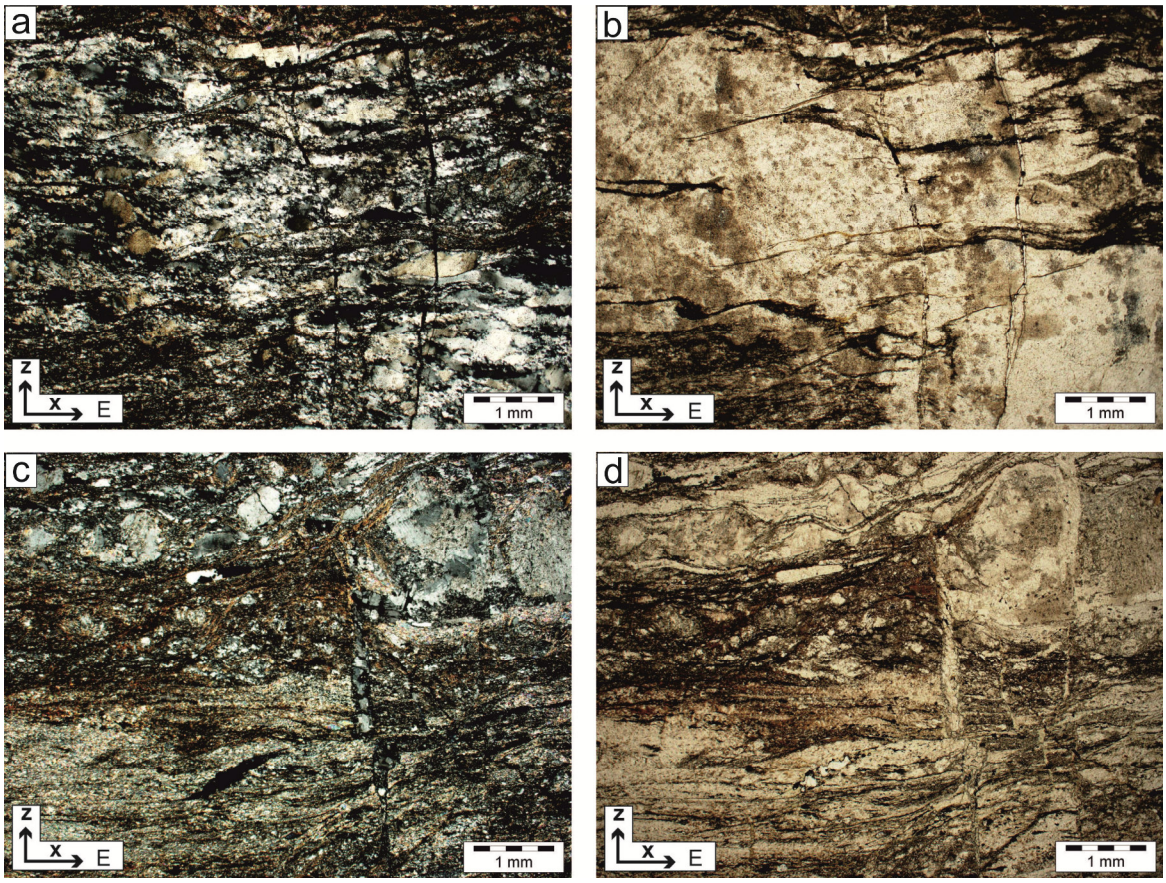

Fig. 33 (a) polarized and (b) unpolarised photo of IH 37 and (a) polarized and (b) unpolarised photo of IH38; large extensional veins are recrystallized with quartzite or feldspar, smaller veins with oxides. Veins are perpendicular to the eastwards oriented foliation. All photos show a low temperature deformation of the migmatite group.

3.3.2. Quartz textures (LPO Plots)

The quartz texture was analysed in detail with an optical imaging system described by Wilson *(2007).* The lattice preferred orientation (LPO) of the quartz c-axis was determined with an algorithm using the grayscale of the crystals in different angles. The data acquisition was done by a G50-Fabric Analyser and Investigator G50 v5.9 *(further description see Wilson, et al., 2007).* The statistical evaluation of the data was done with Fabric v.8. The resulting contour plots allow an estimation of the active gliding systems during the deformation. Hence, an interpretation of temperature, differential stress, strain and strain rate is possible. At higher differential stress it is common, that several slip systems are active at the once *(Passchier & Trouw, 2005)*. This is mainly due to the compensation of the displacement within the lattice structure. With cumulating offset in the lattice structure the intragranular stress outreaches the bounding forces and activates additional slip systems. Typical slip systems for low temperatures are basal <a> (300°C - 450°C) and rhomb <a> (450°C - 550°C) slipping. With higher temperature (>500°C) there is a continuous increase of prism <a> slipping. These temperatures differ depending on the author. A comparison was made by TOY et al. *(2008)*. In course of the investigations 14 thin sections (Table 1) were used to analyse quartz c-axis. The thin sections IH05 and IH11 (bout located on the southern rim of the intrusion) exhibit a coaxial orientation distribution of the c-axes. The other samples are all distributed non-coaxial. The divergence of the quartz c-axes from the direction of schistocity is substantial (≥ 10 degrees) within eight thin sections. Another thin section (IH80) has an angle of 9 degrees. The remaining plots show low angle offsets between zero and six degrees. Along the profil Oplotnica – Lovrenc from the five LPO plots three are indicating a sinistral shear. The two in the very south of the profile are plotting as *type I Lister crossed girdle* with very weak displacement. The LPO plots of the Ribnica na Pohorju profile are plotting both sinistral and dextral. Here the sample of the host rock (IH18) is sinistral. The samples of the tonalite close to the contact are dextral but change polarity to sinistral with distance from the contact. The quartz c-axes of IH68 plot with a greater distribution.

Table 1: list of the 14 thin sections used to determine the active glide systems by quartz c-axis analyses. Additional results of the investigation are the divergence (β) of the c-axes from the direction of foliation (pointing in west direction in a stereographic projection). The active glide systems printed in bold face indicate the maxima within the distribution.

sample-ID	classification	active glide systems			β(beta)	temperature
IH05	tonalite II		**rhomb <a>**	basal <a>	4°	350-450°C
IH11	tonalite I		**rhomb <a>**	basal <a>	3°	>400°
IH18	host rock I		rhomb <a>	**basal <a>**	42°	300-400°C
IH24b	host rock II	**prism <a>**	rhomb <a>	basal <a>	6°	>400°C
IH29	host rock II	**prism <a>**	rhomb <a>		0°	>400°C
IH31b	migmatite	**prism <a>**	rhomb <a>	basal <a>	12°	>400°C
IH45	tonalite III		rhomb <a>	**basal <a>**	36°	300-400°C
IH46	migmatite	**prism <a>**	rhomb <a>	basal <a>	15°	>400°C
IH47	migmatite	**prism <a>**	rhomb <a>	basal <a>	10°	>400°C
IH49	host rock II	**prism <a>**	rhomb <a>	basal <a>	1°	>400°C
IH68	tonalite II		rhomb <a>	**basal <a>**	4°	300-400°C
IH80	host rock III	prism <a>	**rhomb <a>**	basal <a>	9°	350-450°C
IH81	host rock III	prism <a>	**rhomb <a>**	basal <a>	17°	350-450°C
IH87	tonalite I	**prism <a>**	rhomb <a>	basal <a>	24°	>450°C

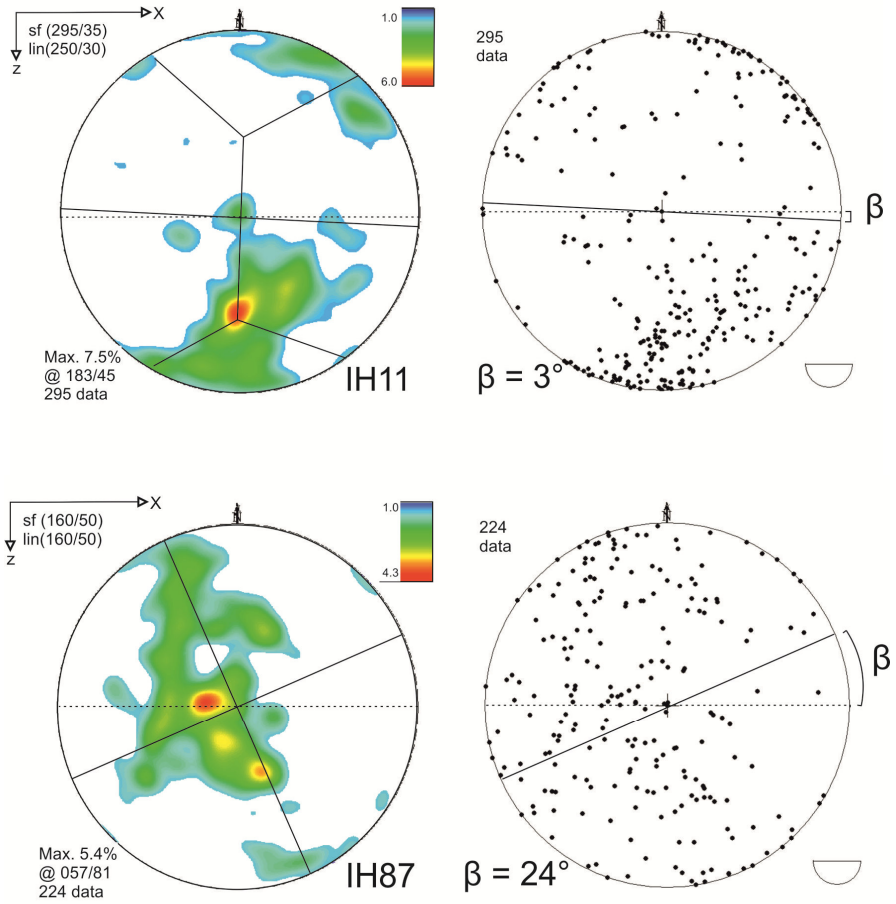

Fig. 34 Lambert projection (equal-area projection) of lattice preferred orientation of quartz c-axes on the lower hemisphere; upper sample: IH11 – tonalite I; lower sample IH87 – tonalite I: orientation of the samples in the top left corner left: contour line plots right: orientation data of the measured quartz crystals. The offset between the schistosity and the preferred orientation of the quart c-axes is given by β.

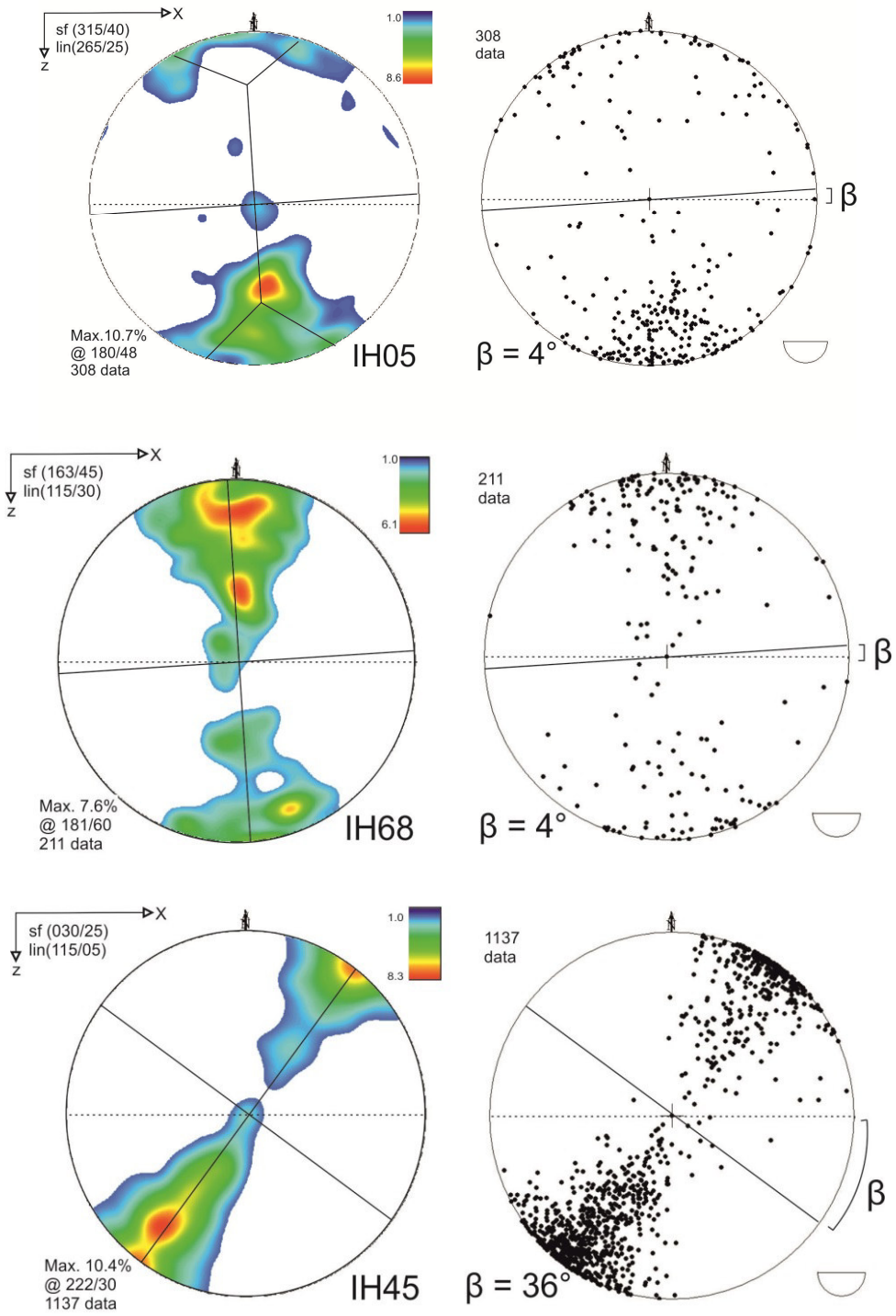

Fig. 35 Lambert projection (equal-area projection) of lattice preferred orientation of quartz c-axes on the lower hemisphere; upper sample: IH05 – tonalite II; middle sample: IH68 – tonalite II; lower sample: IH45 – tonalite III; orientation of the samples in the top left corner left: contour line plots right: orientation data of the measured quartz crystals. The offset between the schistosity and the preferred orientation of the quart c-axes is given by β.

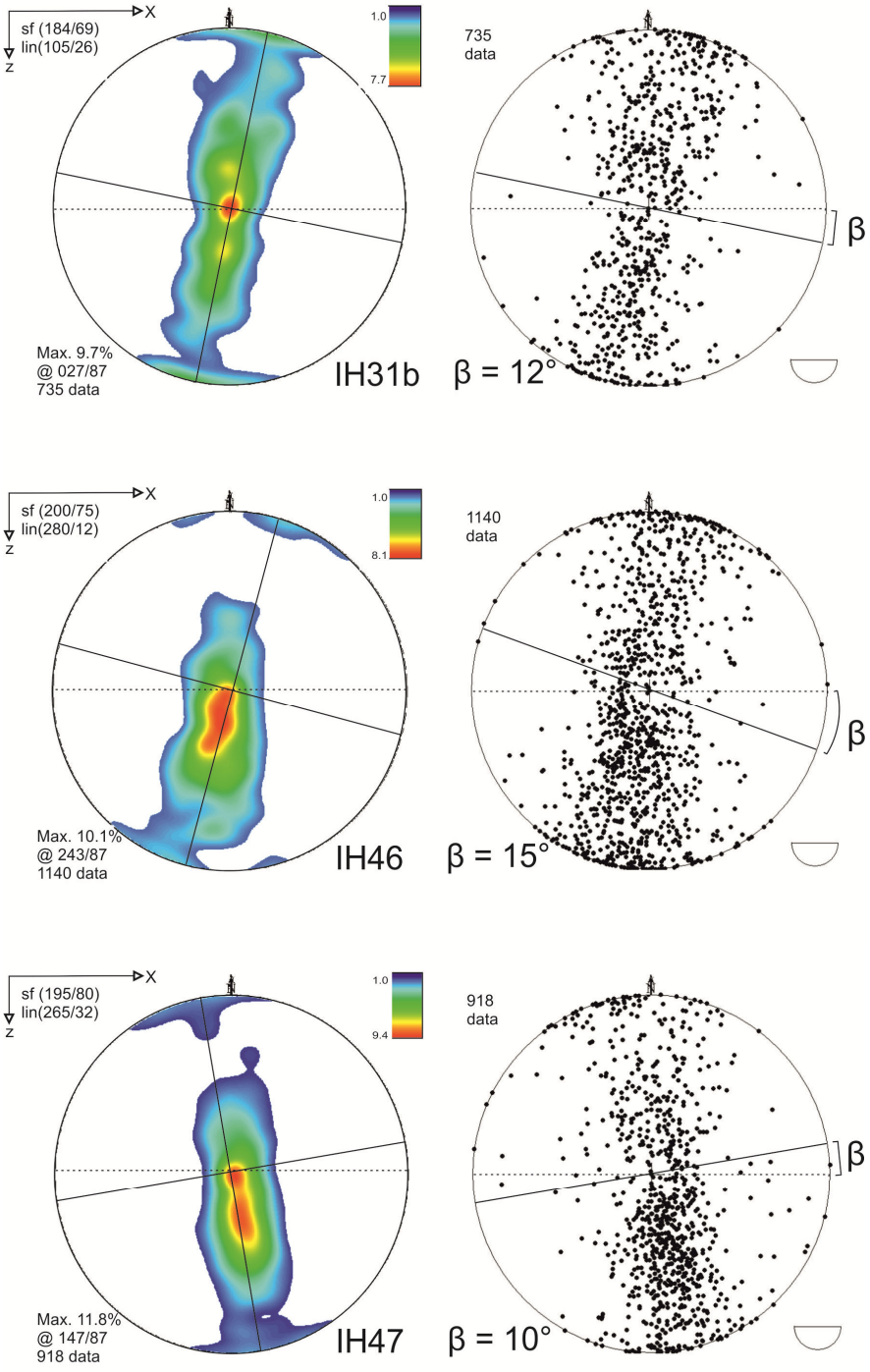

Fig. 36 Lambert projection (equal-area projection) of lattice preferred orientation of quartz c-axes on the lower hemisphere; upper sample: IH31b – migmatite; middle sample: IH46 – migmatite; lower sample: IH47 – migmatite; orientation of the samples in the top left corner left: contour line plots right: orientation data of the measured quartz crystals. The offset between the schistosity and the preferred orientation of the quart c-axes is given by β.

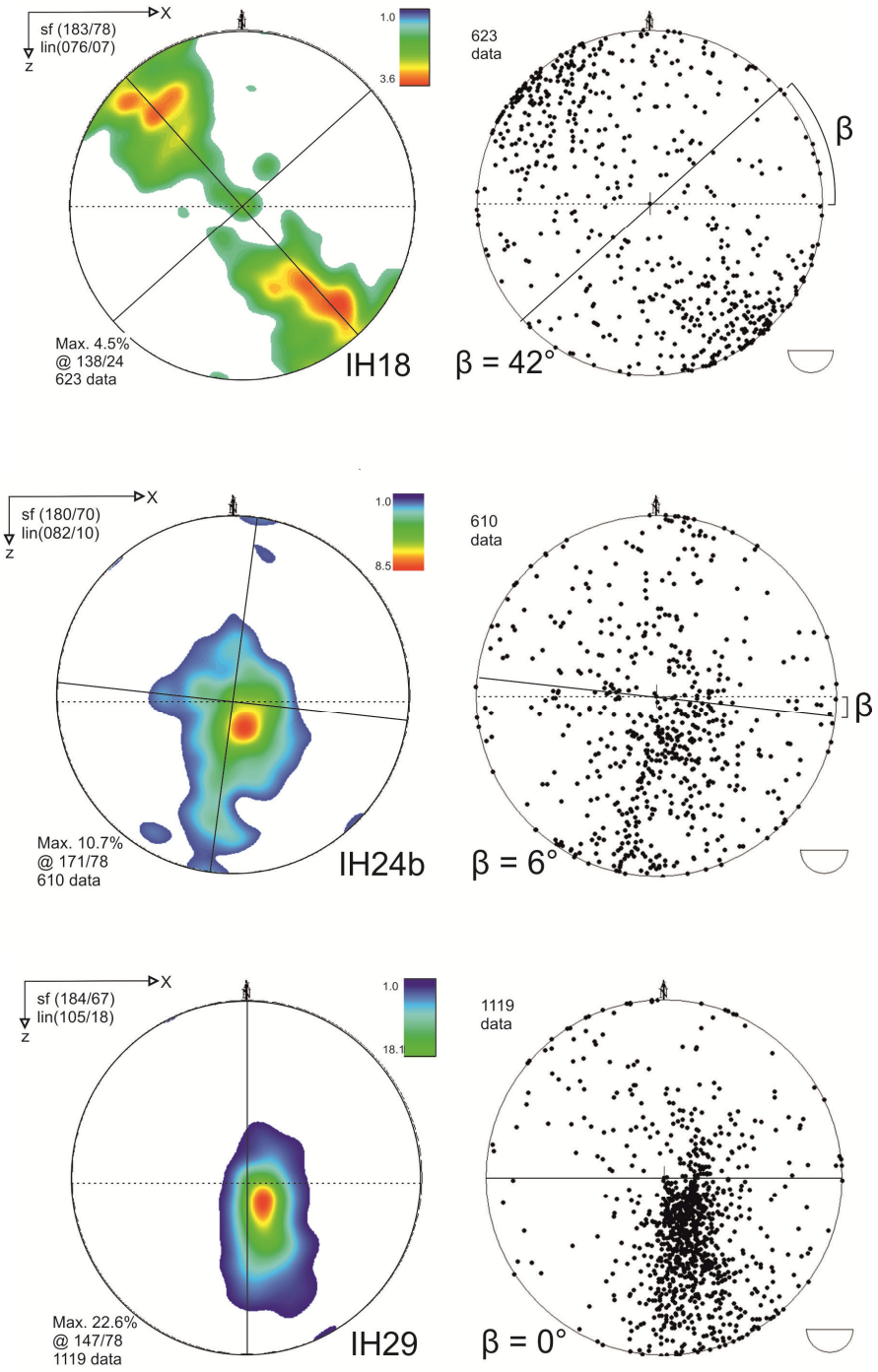

Fig. 37 Lambert projection (equal-area projection) of lattice preferred orientation of quartz c-axes on the lower hemisphere; upper sample: IH18 – host rock I; middle sample: IH24b – host rock II; lower sample: IH29 – host rock II; orientation of the samples in the top left corner left: contour line plots right: orientation data of the measured quartz crystals. The offset between the schistosity and the preferred orientation of the quart c-axes is given by β.

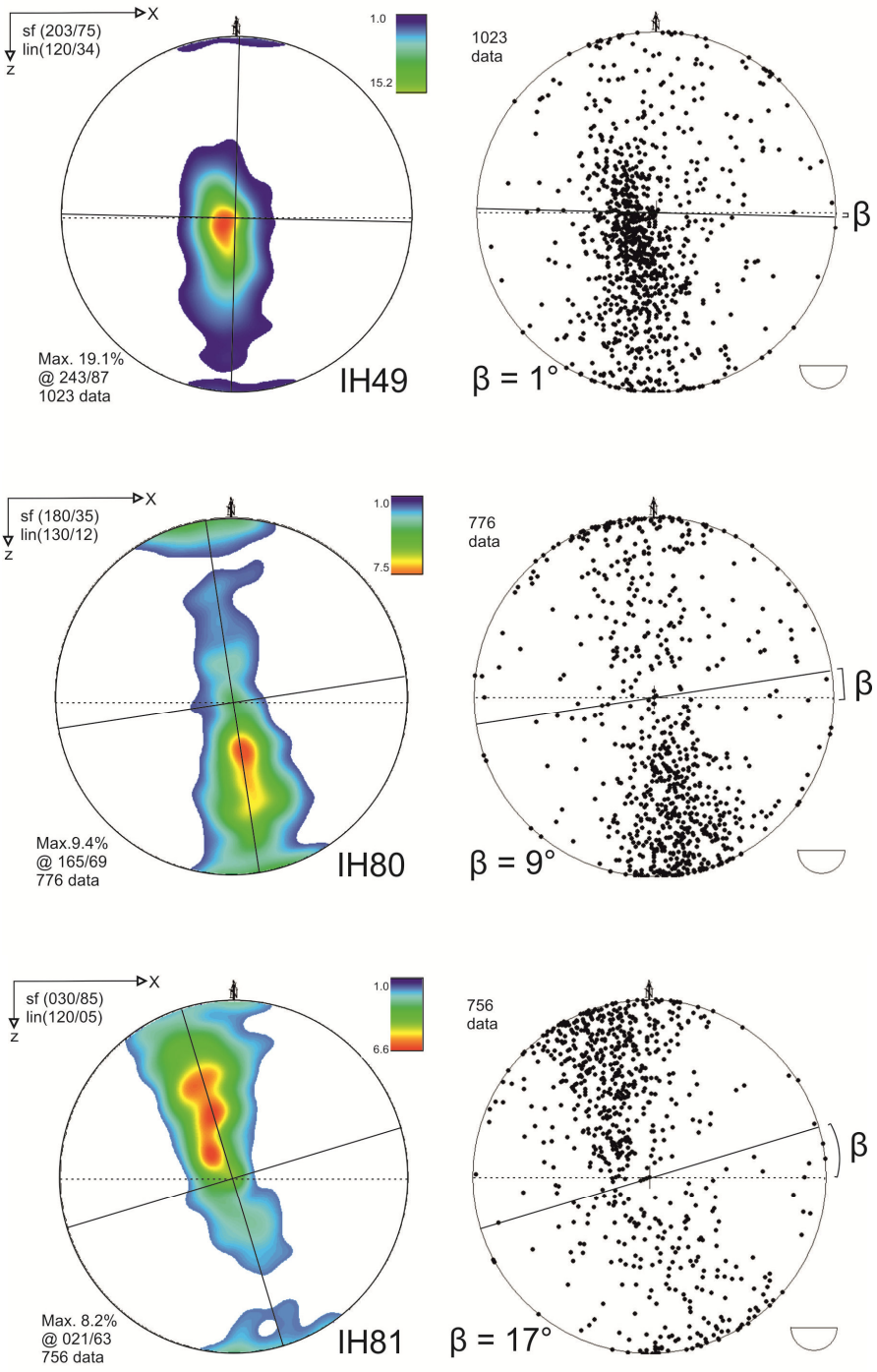

Fig. 38 Lambert projection (equal-area projection) of lattice preferred orientation of quartz c-axes on the lower hemisphere; upper sample: IH49 – host rock II; middle sample: IH80 – host rock III; lower sample: IH81 – host rock III; orientation of the samples in the top left corner left: contour line plots right: orientation data of the measured quartz crystals. The offset between the schistosity and the preferred orientation of the quart c-axes is given by β.

4. Anisotropy of magnetic susceptibility (AMS)

The technical and theoretical aspects reported in this chapter are for the most part assembled and summarized from The Magnetic Anisotropy of Rocks *(Tarling & Hrouda, 1993)*.

4.1. Theory

The magnetic susceptibility describes the permanent or non-permanent effect of an external magnetic field on certain materials. The change in direction and intensity of this physical property is also called as the anomaly of magnetic susceptibility, abbreviated as AMS. Volume magnetic susceptibility can be measured as the deviation from the bulk susceptibility (K_1, K_2 and K_3) - giving a tensor with direction and a dimension or length. In geology numerous data can be verified and encouraged with AMS. The AMS principal directions may unravel geological uncertainties or rock properties such as directions from sediment, flow-directions from magma, finite-strain directions from tectonized rocks and stress-directions from low-strain, low temperature, neotectonic environments, paleomagnetic field research and many more *(Borradaile & Henry, 1997)*. Here, the technique is used for detection of strain direction on a magmatic body. Every mineral within a rock reacts differently to magnetization. Therefore, the sum of oriented magnetic grains determines the total or bulk susceptibility (K_m) and the principle AMS directions (K_1, K_2 and K_3). Hence, we have to distinguish five different forms of magnetization (Fig. 39); these with a preferred magnetic orientation when the applied magnetic field is extinguished (remanent magnetization) and such without a preferred magnetic orientation when no additional field is applied (induced magnetization). Ferromagnetic

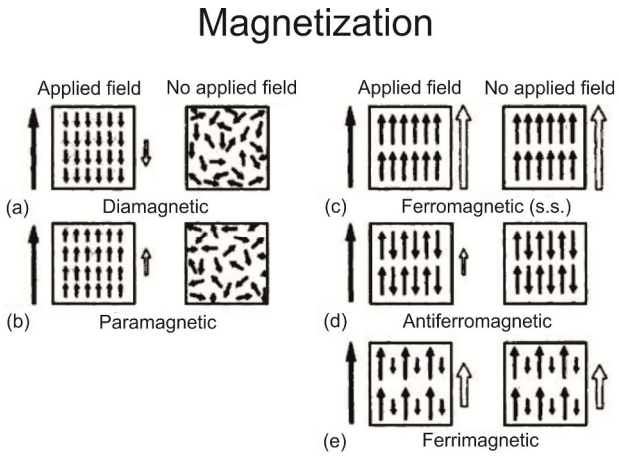

Fig. 39 Forms of magnetization, *(Hrouda & Lanza, 1989)*

(s.s.), antiferromagnetic and ferrimagnetic minerals are all of remanent kind and diamagnetic and paramagnetic minerals of induced kind. An easy way to determine the mineral responsible for magnetization is the Curie temperature measurement. The Curie temperature is the specific temperature of a mineral (or certain material) where a loss of magnetization is occurring (Table 2).

Table 2: Curie temperature of selected ferromagnetic (s.l.) minerals. The table was published in 'The Magnetic Anisotropy of Rocks' *(Tarling & Hrouda, 1993).* The 'easy' direction is describing the direction of magnetization recording to the crystal planes. The relationship between direction of the magnetization and the expansion of a mineral has a relevant impact on the interpretation.

Mineral	Composition	Curie temperature (°C)	'Easy' direction
Magnetite	α-Fe_3O_4	575	<111>*
Maghaemite	γ-Fe_2O_3	(350**) / 645	<111>
Haematite	α-Fe_2O_3	680	Basal
Goethite	-FeOOH	120-130	
Pyrrhotite (mono)	$FeS_{1.14}$	320	Basal

*The 'easy' direction in magnetite is <100> at temperatures < 130K.

**common recrystallization temperature

The most common method for magnetic susceptibility analysis is using alternating magnetic fields with low field amplitudes (low-field susceptibility) *(Borradaile & Henry, 1997)*. Especially the low field AMS proves to be particularly useful for studying the flow of igneous rocks, of both volcanic and plutonic kind *(Ferré, et al., 2004)*. Similar to the principal strain directions ($\sigma_1 > \sigma_2 > \sigma_3$) the principal susceptibility directions form an ellipsoid. A given AMS ellipsoid can be described as either oblate (K1=K2>K3) or prolate (K1>K2=K3). This formula may vary from author to author – the program used to determine magnetic foliation and lineation in this thesis is using K1/K2>K2/K3 for prolate shape and K1/K2<K2/K3 for oblate shape. These form factors also correlate with the relative position of the stereographic pole plots of K_1, K_2 and K_3 (also called K_{max}, K_{int} and K_{min}) (Fig. 40). In general, an oblate shape occurs from a magmatic foliation and a prolate shape indicates a tectonic overprint *(Tarling & Hrouda, 1993)*. According to Borradaile et al. *(1997),* the correspondence between the principle susceptibility directions and the principle strain directions is valid with the exceptions:

(a) where the AMS of a secondary fabric fails to overprint a primary fabric, (b) in rocks that produce inverse anisotropy and (c) where the fabric accumulation was noncoaxial.

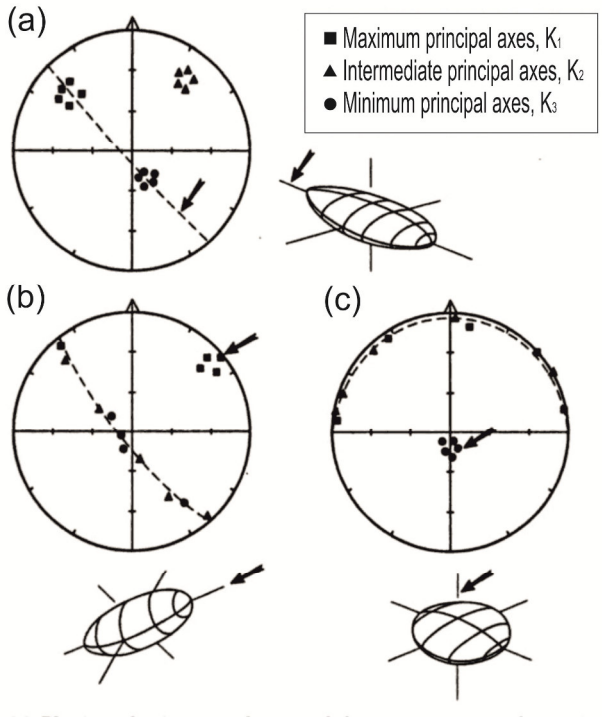

Fig. 40: stereographic projection (globular projection) of AMS directions on the lower hemisphere. The figure was published by Tarling and Hrounda *(1993)* (a) triaxial deformation with three distinctly seperated groups (K1>K2=1>K3). (b) prolate ellipsoids have well grouped K1 and K2 and K3 along a gridle 90° from K1 (K1>K2=K3). (c) oblate ellipsoids have well grouped K3 and K1 and K2 along a gridle 90° from K3 (K1=K2>K3).

4.2. Sampling

The samples were taken oriented from both host rock and the Pohorje pluton, although the focus of the susceptibility analysis was on the igneous body. The AMS analysis was carried out on three sites for the host rock and 16 sites for the pluton (Table 3). The samples were drilled and cut to cylinders with 20 mm diameter and 20 mm height.

Table 3 List of the samples used for susceptibility analysis. In general, 4 subsamples (cylinders) were taken from every oriented hand-sample.

Sight	**Rock'Type**	**Coordinates**		**field orientation**	
		Latitude (N)	*Longitude (E)*	*Dip'Direction*	*Dip'Angle*
IH02	tonalite	46°25.198'	015°26.366'	320	40
IH13	tonalite	46°25.389'	015°25.942'	258	80
IH17	micaschist	46°24.524'	015°30.716'	127	45
IH26	tonalite	46°31.581'	015°16.029'	338	21
IH34	quartzolite	46°31.625'	015°16.056'	125	70
IH43	tonalite	46°31.363'	015°15.819'	246	54
IH53	tonalite	46°31.554'	015°16.021'	151	88
IH59	tonalite	46°31.515'	015°16.009'	40	68
IH60	tonalite	46°31.163'	015°15.541'	10	79
IH61	tonalite	46°30.972'	015°15.370'	130	30
IH63*	tonalite	46°31.035'	015°15.511'	215	70
IH66	tonalite	46°31.067'	015°15.314'	220	89
IH67	tonalite	46°31.067'	015°15.314'	35	70
IH72**	micaschist	46°34.122'	015°10.061'	170	23
IH76	sandstone	46°33.912'	015°09.295'	225	36
IH82	tonalite	46°30.807'	015°20.443'	225	80
IH85	tonalite	46°29.881'	015°19.876'	125	85
IH88*	tonalite	46°28.164'	015°21.939'	140	55
IH89	tonalite	46°27.570'	015°22.875'	352	53

*site with three samples

**site with one sample

4.3. Susceptibility measurements

Besides the sample preparation, which was made at the Institute of Earth Sciences (University of Graz), the procedures of the susceptibility measurement were made at the Paleomagnetic Laboratory of the Montan Universität Leoben, situated in Gams bei Frohnleiten. All measurements were made under the supervision of R. Scholger. The samples were analysed with the AGICO MFK1-FA Multi-Funktion Kappabridge and processed with the computing programmes Safyr 4W and Anisoft 4.2. The susceptibility was measured in 15 orientations at a frequency of 976 Hz and with a field intensity of 200 A/m *(AGICO, 2009).*

The Km values (

Fig. 41) are spreading from a maximum of $22.855*10^{-03}$[SI] with an anisotropy factor (P) of 1.748 (measured on IH67D) to a minimum of $29.9*10^{-06}$[SI] with an anisotropy factor (P) of 1.049 (measured on IH34D). The average mean susceptibility of all samples is $5.89*10^{-03}$[SI] with a standard deviation of $5.92*10^{-03}$[SI]. The form factor or degree of anisotropy varies from a maximum of 1.907 at a Km of $13.796*10^{-03}$[SI] (measured on IH53C) to a minimum of 1.007 at a Km of $48.56*10^{-05}$[SI] (measured on IH17C).

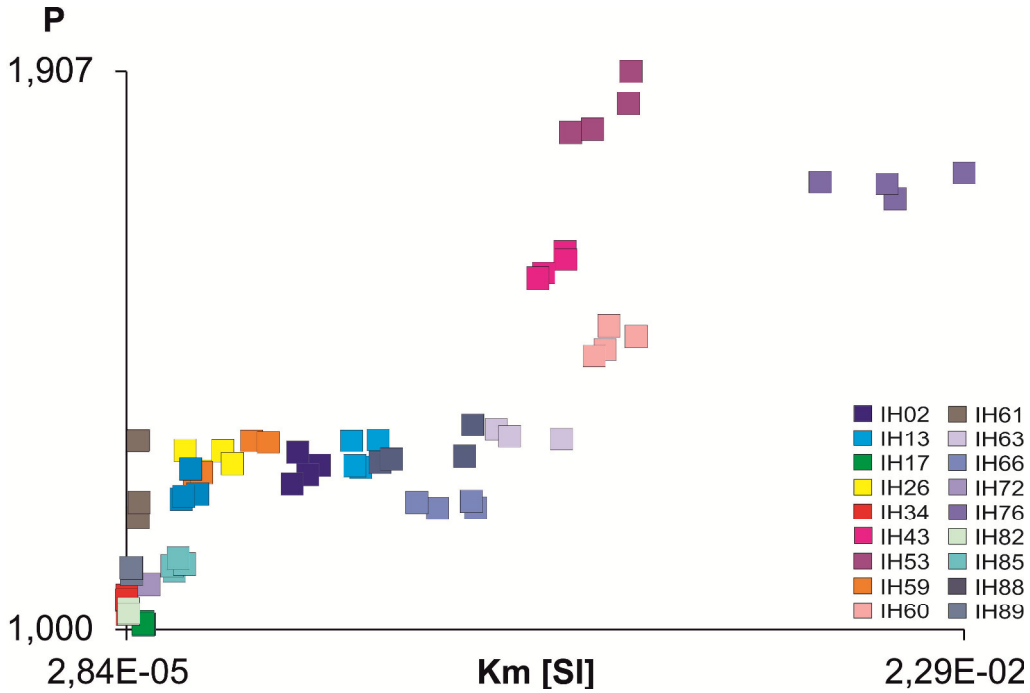

Fig. 41 Graphical output from Anisoft 4.2; P vs. Km plot of all AMS samples. The anisotropy degree P *(Nagata, 1961)* is the quotient of K1/K3 where the mean (average) susceptibility Km *(Janák, 1965)* is given by (K1+K2+K3)/3

The samples tend to have more magnetic lineation over magnetic foliation; still the distribution reaches from oblate and triaxial to prolate shape (

Fig. 42). Maximum lineation factor was measured on IH43C with a lineation value of 1.535 and a foliation value of 1.052. A maximum of foliation was measured on IH53C with a triaxial shape – with a foliation of 1.349 and a lineation of 1.414. The highest foliation ratio of oblate samples is in IH89D with a foliation of 1.216 and a lineation of 1.037. Samples with less than 8% anisotropy of lineation or foliation are all host rock samples (series of IH17, IH34, IH72 and IH76).

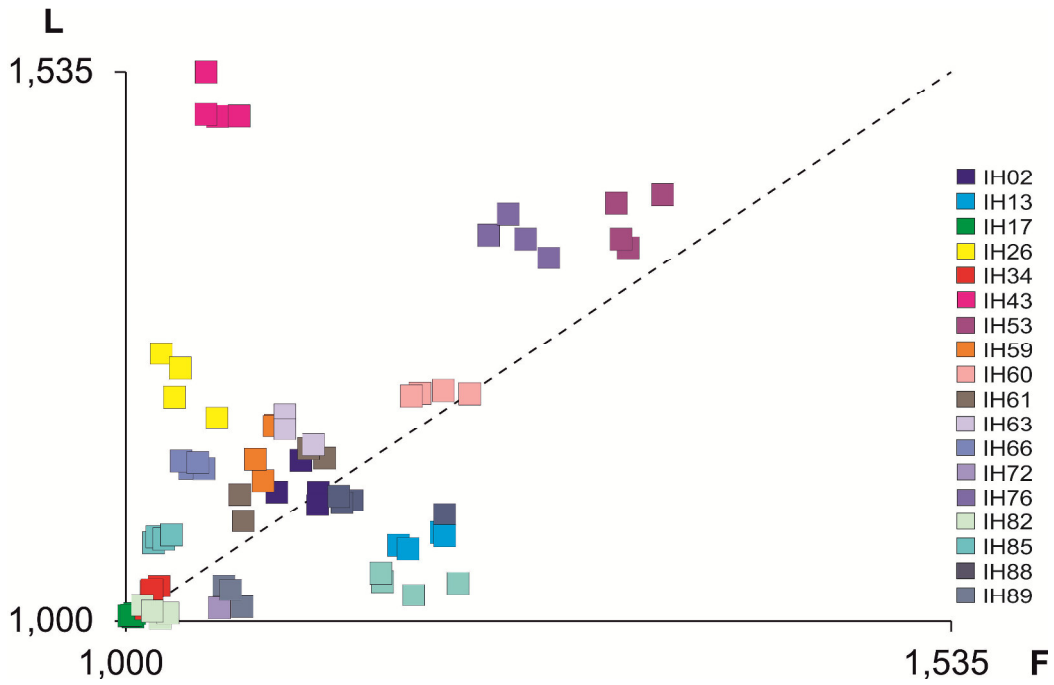

Fig. 42 Graphical output from Anisoft 4.2; L vs. F plot of all AMS samples. The Diagram compares F, the grade of magnetic foliation (K2/K3), with L, the grade of magnetic lineation (K1/K2), to distinguish the relation of K1, K2 and K3. Above the dashed line (K1/K2>K2/K3) the AMS ellipsoid is prolate, below it (K1/K2<K2/K3) the AMS ellipsoid is oblate. Along the dashed line the relation beween the maximum, intermediate and minimum susceptibility is K1/K2=K2/K3 (forming a triaxial ellipsoid).

In Fig. 43 all samples are shown on an equal-area projection on a geographically coordinated plot. The accumulated mean K1 has a declination of 123.2° and an inclination of 2.1° with confidence angles of 37.0 (dec.) and 27.2 (inc.). K2 and K3 have their mean values on a girdle with a high inclination perpendicular to K1. K2 has a declination of 27.9° and an inclination of 68.3°. The confidence angles of these are 71.0 (dec.) and 33.9 (inc.). K3 has a declination of 214.0° and an inclination 21.5°. The confidence angles are 71.0 (dec.) and 29.1 (inc.).

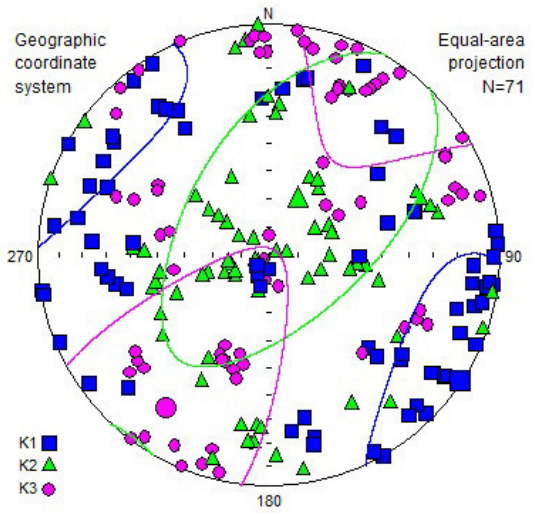

Fig. 43 Graphical output from Anisoft 4.2; Equal-area projection of all AMS analyses. The accumulated Kmax (=K1) is oriented NW and SE. Kint (=K2) and Kmin (=K3) are along a girdle oriented NE to SW. The accumulated mean directions of all three principle susceptibility directions have high variance. Therefore the data set is separated in four groups. This is described below in chapter 4.5.

4.4. Curie temperature measurements

The Curie temperature was measured with the AGICO MFK1-FA Multi-Funktion Kappabridge and analysed with Cureval 8. The samples were selected with the purpose to capture every range of field arrangement (Fig. 44). The heating progress was performed until 700°C. The cooling process was abstained.

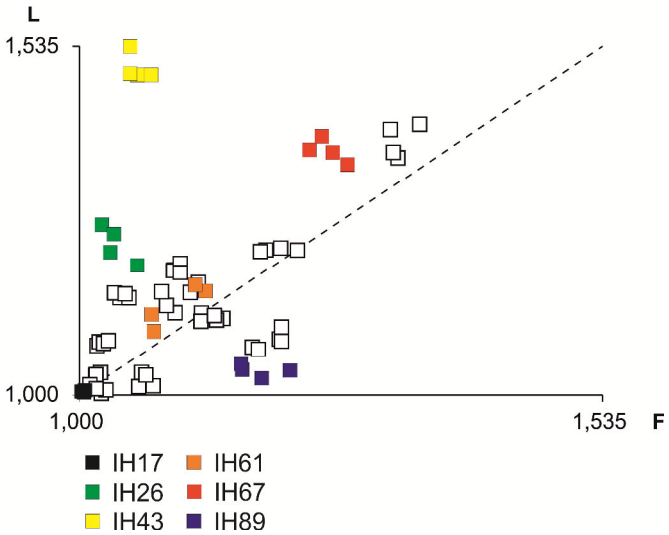

Fig. 44: modified graphical output from Anisoft 4.2; F-L Plot of all AMS samples. The 6 groups of samples in colour were used to determine Curie temperatures.

All six curie temperature samples (

Fig. 45) show a loss of ferr(o)magnetisms suggesting magnetite and subordinated haematite as main carrying minerals (see Table 2). Curie temperature is recorded between 571.2°C (start of break-down) and 588.2 (complete break-down).

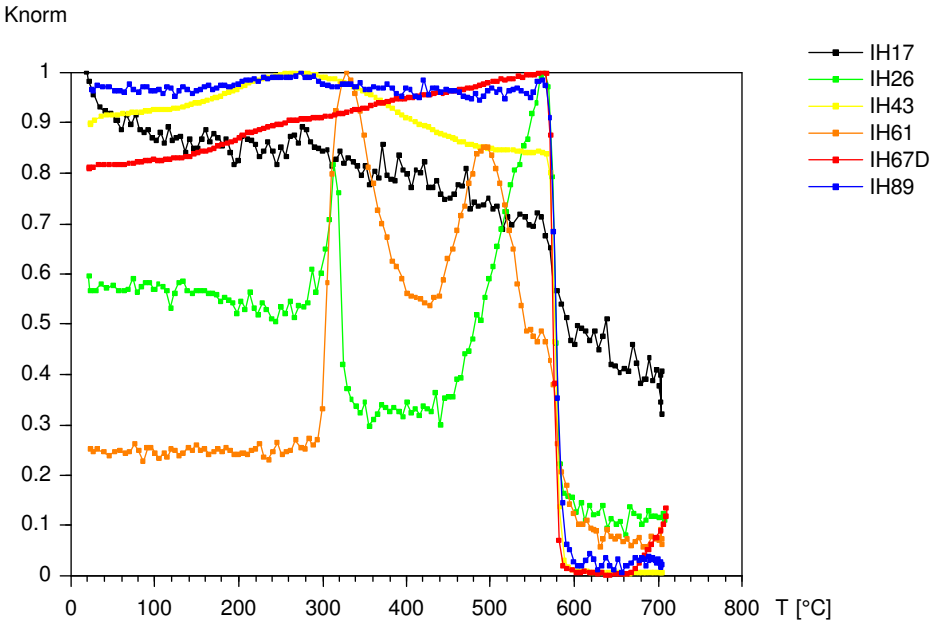

Fig. 45 Graphical output (Cureval 8) of the measured curie temperatures. The plot is normed to the maxima of each curve. All samples have a distinct break down of susceptibility at 579.7 ± 8.5. Samples IH26 and IH61 have additional transformation and break down around 300 and 500°C (see below). IH43 has a slight transformation around 300°C (approximate temperatures of reduction of goethite to its reactant)

The susceptibility is dominantly due to ferrimagnetic minerals (magnetite and haematite) and the ferrimagnetic and antiferromagnetic modification of pyrrhotite. At sample IH17 the influence of paramagnetic minerals can be detected (

Fig. 46). Other samples do not have clear evidence for para-magnetic influence. The samples IH26 and IH61 have two distinct peaks – lower peak (approximately 300°C) and higher peak (approximately at 480°C). Peaks between 250-320°C and between 370-520°C are characteristic for rocks with a mixture of monocline and hexagonal pyrrhotite (lower peak) respectively (titano-) magnetite (higher peak) *(El Bay, 2010)*. Sample IH67D has a transition to wüstite at 680°C. The sample was analysed with a flowing argon atmosphere. It is suggested that the inert condition induced by argon is responsible for the transition to wüstite.

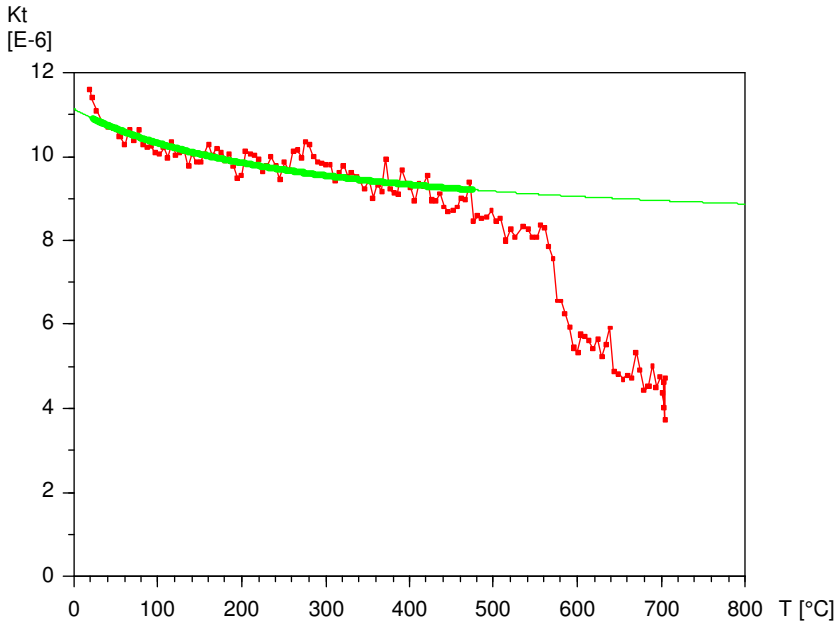

Fig. 46 Diagramm of the total susceptibility (Kt) with rising temperature. The values are purged from specimen holder susceptibility and adjusted to the bulk susceptibility of AMS analysis. The Kt path of IH17 (red) is decreasing with rising temperatures exponentially in the range between 22 and 475°C. A trend line (green) is fitted here to visualize the exponential course. Exponential decrease of Kt is due to paramagnetism. The ratio of paramagnetism in IH17 is according to Cureval 8 25.9 percent with an error of 1.7 percent. The rapid fall of Kt ending at 561°C correlates with every other sample (

Fig. 45) and suggests magnetite break-down.

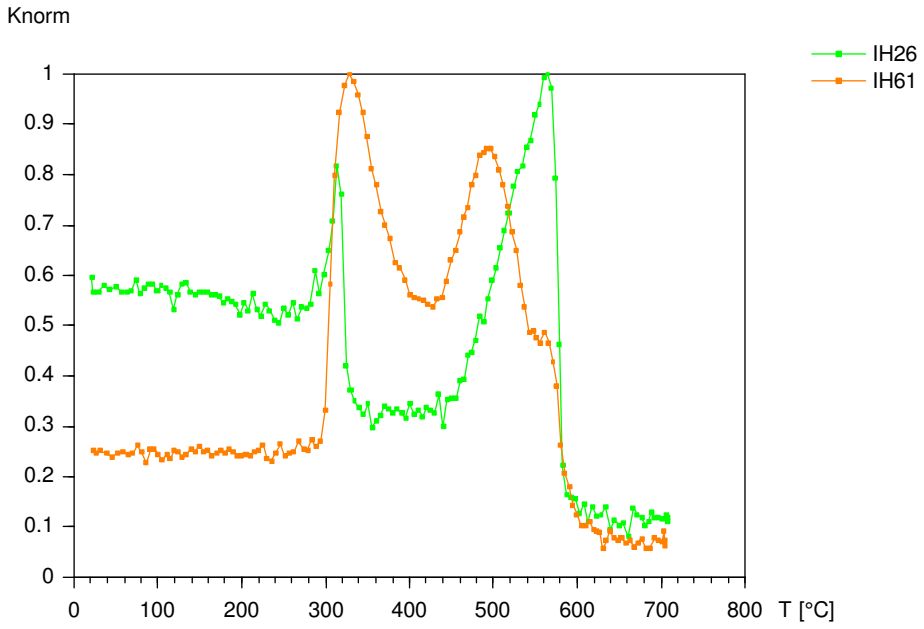

Fig. 47 showing susceptibility curve of IH26 and IH61. Diagram is normed to total susceptibility of each curve Both samples have a rise in susceptibility at approximately 300°C and 480°C

4.5. Results

According to the results and the geological position of the samples the AMS data can be categorized into four groups. The classification is named after the anisotropic (grade of magnetic foliation and magnetic lineation) character of the samples. Therefore, samples of isotropic, oblate, triaxial and prolate shape factor are grouped. The isotropic group has anisotropy (P) lower than 8% and groups the host rock samples. The oblate group samples are taken from geographically internal areas of the intrusion. Samples of the triaxial and prolate group are from the rim of the tonalite body.

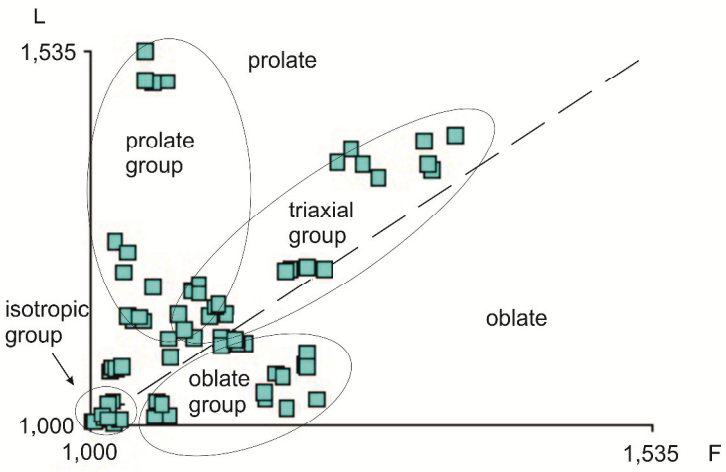

Fig.48 Graphical output from Anisoft 4.2; L vs. F plot; samples show four different patterns: isotropic group of host rock samples with almost no anisotropy, prolate group with distinct magnetic lineation, triaxial group with both distinct magnetic lineation and foliation and oblate group with distinct magnetic foliation.

Isotropic group:

Samples of the isotropic group (P<8%) have low Km values. The orientation of the principal susceptibility within this group, with the exception of IH17, is pointing NW. Therefore, the subsamples of IH17 need an independent evaluation of their orientation. The accumulated K1 direction of the isotropic group (without IH17) is (284/16). K2 and K3 plot on a girdle perpendicular from K1 with accumulated mean values: K2 (180/41) and K3 (031/45). IH17 is a sample from the high-grad metamorphic unit SE of the intrusion. The orientation of the principle susceptibility directions is due to a different geological history as the low to medium grad metamorphic rocks (i.a. IH34, IH72 and IH76) on the NE rim. A table with the statistic output of this group is added to the appendix (p.79). Samples in this group are IH17, IH34, IH72 and IH76.

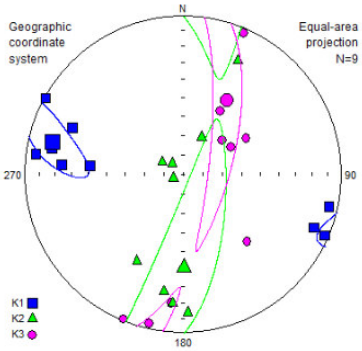

Fig. 49 Graphical output from Anisoft 4.2; Equal-area projection of the isotropic group not including IH17. K1 is almost oriented horizontal in W-direction. K2 and K3 are along a girdle perpendicular to K1.

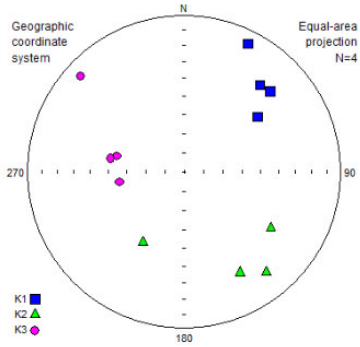

Fig. 50 Graphical output from Anisoft 4.2; Equal-area projection of IH17

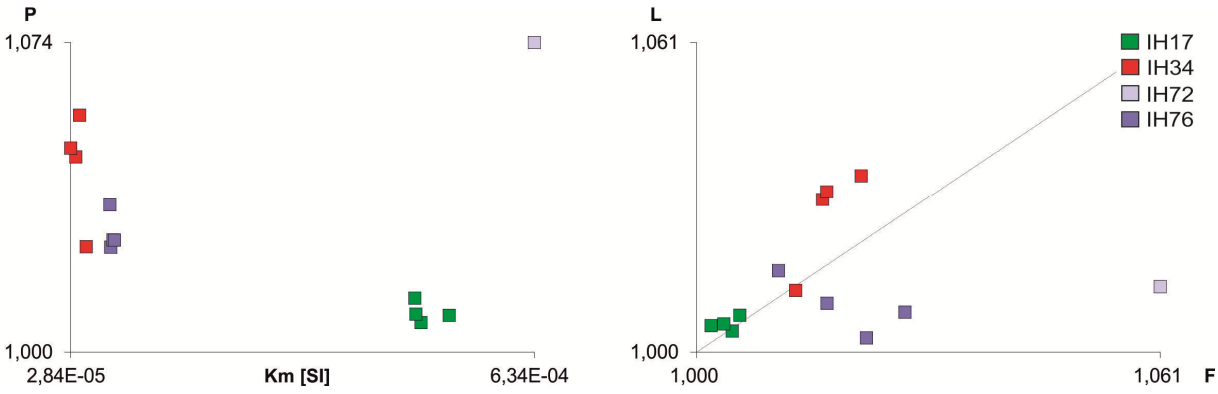

Fig. 51 Graphical output from Anisoft 4.2; P vs. Km plot (left) and F vs. L plot (right) of the isotropic group. Samples have a low anisotropy grad (<8%) and a low Km (<6,5*10^{-3}).

Oblate group:

All samples with an oblate shape parameter are from geographically interior areas of the intrusion. The accumulated mean principle susceptibilities are outstanding compared with the other groups. It is the only group with K1 not plotting in NW but in the NE direction. The accumulated mean directions are (060/12) for K1, (155/23) for K2 and (304/63) for K3. A table with the statistic output of this group is added to the appendix (p.79). Samples in this group are IH13, IH88 and IH89.

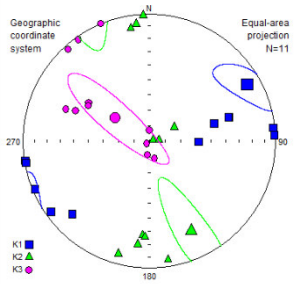

Fig. 52 Graphical output from Anisoft 4.2; Equal-area projection of the oblate group. K1 is almost oriented horizontal in NE-direction. K2 and K3 are along a girdle perpendicular to K1.

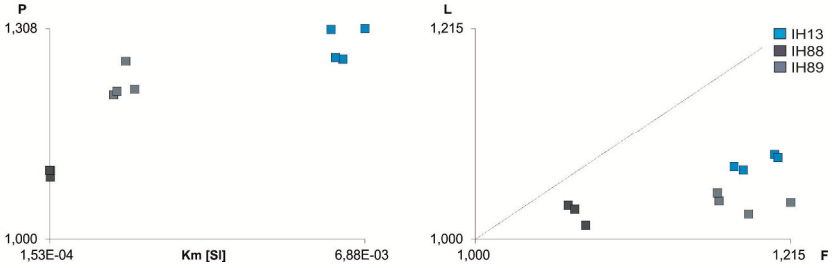

Fig. 53 Graphical output from Anisoft 4.2; P vs. Km plot (left) and F vs. L plot (right) of the oblate group.

Triaxial group:

Samples of this group have Km values reaching from 10^{-4} to 10^{-2}. The anisotropy is distinct with a relatively same ration of magnetic lineation and magnetic foliation. Principle susceptibility directions of the triaxial group are not forming a girdle but are perpendicular to each other. While K1 is horizontal in the NW-SE direction (330/11), K2 is vertical (125/78) and K3 is horizontal in the NE-SW direction (239/05). A table with the statistic output of this group is added to the appendix (p.80). Samples in this group are IH02, IH60, IH61 and IH85.

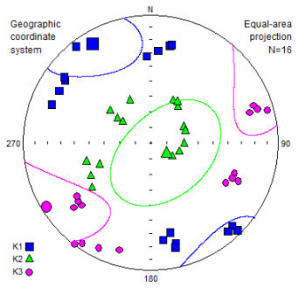

Fig. 54 Graphical output from Anisoft 4.2; Equal-area projection of the triaxial group. K1 is oriented horizontal in NW-direction. K2 is vertival and K3 is in SW-direction. Principal susceptibility directions are perpendicular to each other.

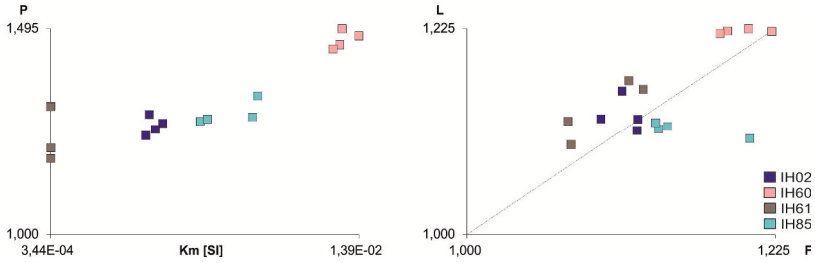

Fig. 55 Graphical output from Anisoft 4.2; P vs. Km plot (left) and F vs. L plot (right) of the triaxial group.

Prolate group:

Samples have a distinct magnetic lineation with Km values between 10^{-3} and 10^{-2}. The principle susceptibility directions are oriented similar to the anisotropic group (host rock) with a K1 orientation horizontal in SE direction (117/02) and a K2 and K3 along a girdle perpendicular to K1. Accumulated K2 plots at (012/82) and K3 at (208/08).A table with the statistic output of this group is added to the appendix (p.80). Samples in this group are IH26, IH43, IH53, IH59, IH63, IH66, IH67 and IH82.

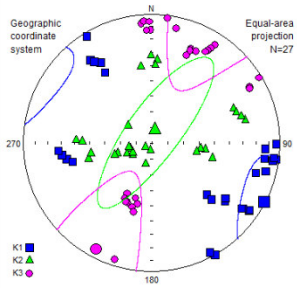

Fig. 56 Graphical output from Anisoft 4.2; Equal-area projection of the prolate group. K1 is oriented horizontal in SE-direction. K2 and K3 are along a girdle perpendicular to K1.

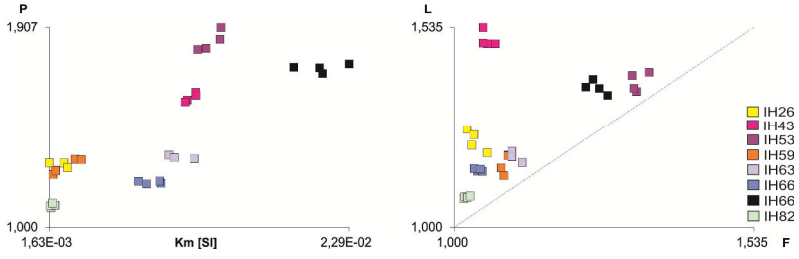

Fig. 57 Graphical output from Anisoft 4.2; P vs. Km plot (left) and F vs. L plot (right) of the prolate group.

5. Discussion

Investigations of the Pohorje intrusion and the surrounding host rocks provided evidence of different temperature and deformation stages of the pluton since its emplacement. Evidence is shown in the previous chapters for magnetic anisotrpies, for post-magmatic deformation at high to low temperatures (600-300°C) with ductile behaviour and finally solid state deformation at very low temperatures (<300°C) with cataclastic behaviour. The results show a comprehensible chronology of deformation events and correlation between the field investigations, the microscopic analyses, the lattice preferred orientation of quartz c-axes and the magnetic fabric within the research area.

5.1. Magmatic state deformation

Magmatic foliation and early cooling deformation is mainly evident in tonalite I. Minerals are crystallized without distinct orientation and grain size can be up to mm scale crystals. Myrmekite in tonalite I and II and ptygmatic folds in the migmatites are further high temperature relicts. Phyllosilicates show a shape preferred orientation and form an orthogonal pattern. This suggests subvertical flattening of the pluton and alignement of the phyllosilicates during this phase. Magmatic texture is also present in tonalite II, III and the migmatites, but these are subsequently overprinted by solid state textures. AMS data from the internal domains of the intrusion plot oblate magnetic ellipsoids with K_3 being almost vertical, K_1 horizontal in NE-SW and K_2 in NW-SE direction. This was observed at sites with rocks suggested as tonalite I and therefore, reinforces flattening during the crystallization.

5.2. Solid state deformation

Post-magmatic structures can be observed in all the studied samples, although the deformation mechanisms vary from group to group (tonalite I to III, host rock I to III and the migmatite group). Ductile solid state deformation at high temperatures (600°-450°C) and low temperatures (450°-300°C) can be distinguished in the samples by both deformation mechanisms and quartz c-axes orientation. The latter also documents non-coaxial deformation during this deformation stage.

Deformation at 600 to 450°C:

High temperature deformation is evident in tonalite I, in segregated grain aggregates of quartz within tonalite II and the migmatite group. Dynamic recrystallization due to GBM of quartz is not overprinted by low temperature recrystallization. Feldspar is recrystallizing (bulging) with a core-mantle microstructure. Quartz LPO of internal parts of the pluton suggest a slight top W shearing in the west and top E shearing in the east. The angle beta at these sites is very low (4°). Orientation maxima at prism <a> indicate temperatures above 450°C at the last recrystallization phase. Migmatite and tonalite III LPO plots along the northern rim of the pluton have beta dip angles indicating top E shear. The preservation of the earlier formed magmatic texture in tonalite I suggest no effect of the ongoing deformation (see below) in the internal domains. In tonalite II the phyllosilicates are reoriented parallel to the foliation. Phyllosilicates in the strain shadow of garnet are symmetrically grown implying pure shear.

Deformation at 450 to 300°C:

Low temperature ductile structures can be observed in various groups. Samples of the host rock are overprinted by deformation later than the emplacement of the intrusion but still have texture of previous nappe stacking related to Eoalpine evolution of the Austroalpine nappe complex and probably previous deformation along the Periadriatic lineament. Post-magmatic structures are conducted by secondary mineralization of fluid rich sericite and chlorite and oxides in tonalite III, migmatites as well as in host rock I-III and include shear indicators. Examples are given by relicts of feldspar bound by sericite strain shadows indicating top NW shearing (host rock I), oxide veins forming

shear bands with top NW shearing (host rock III) and asymmetric strain shadows around garnet grains showing W- directed shearing (host rock II). This pattern also fits the LPO and AMS data. Quartz LPO plots of host rock III are verging towards NW. The magnetic fabric of the host rock (isotropic group) has the accumulated mean susceptibility in NW to W direction. Samples grouped to the AMS groups triaxial and prolate show a gradual rotation towards the host rock magnetic fabric. Although this could have also happened during cataclastic deformation described below.

Deformation below 300°C:

Cataclastic deformation is evident along several faults within and around the pluton with a general NW-SE strike as well as the cataclastic disaggregation of tonalite III. On microscale extensional crenulation cleavage in samples from the northern rim of the pluton (host rock II) indicates NW-directed normal faulting. This is further evident by vertical micro fractures upright perpendicular to W-E, NW-SE respectively (tonalite II and III, the migmatite group and host rock I-III). Plagioclase grains (tonalite III) are fractured by extensional cracks with quartz precipitation between the fragments. Open fractures and veins are filled by quartz, chlorite, oxides or carbonate implying high fluid mobility also at low temperatures (below 300°C). Chlorite is also filling NE-SW trending joints (tonalite, JS2).

Reassembling the magnetic fabric, a reorientation of the magnetic susceptibility maxima can be detected. The interior domains of the pluton have an oblate – therefore magmatic – shape factor with NE-SW maxima. Towards the external parts the shape factor changes to triaxial – suggesting a tectonic reorientation – with NNW-SSE maxima. Finally, in the outermost parts of the pluton the shape factor is prolate – and therefore tectonically re-oriented – with NW-SE maxima. The host rock maxima point W-E. This pattern fits the analysis of the micro structure. Internal parts capture the magmatic and early post magmatic evolution of the intrusion. During this stage the intrusion was flattened and exhumed – overlying rocks were displaced towards W and E. External parts on the other hand, are affected by NW-SE oriented dextral displacement of the host rock within the regional tectonic regime related to the Periadriatic Lineament.

5.3. Deformation path

According to Fodor et al. *(2008),* crystallization age and cooling rate of the Pohorje intrusion are well known. The crystallization age is dated as Early Miocene (18.64 ± 0.11Ma) with a cooling below the zircon fission track system closure temperature (ca. 200°C) within 3 Million years *(Fodor, et al., 2008)*. The structural analyses within this thesis also suggest a rapid exhumation of the intrusion with the following stages:

- The unroofing of the tonalite conducted by W-E normal faulting led to flattening within the body. Contemporaneous E-W- directed elongation is assumed to be related to N-S shortening along the Periadriatic Fault.
- In the late phase of the exhumation the deformation is due to NW-SE shearing.
- Cataclasis and normal faulting is due to NW-SE extension.

5.4. Models

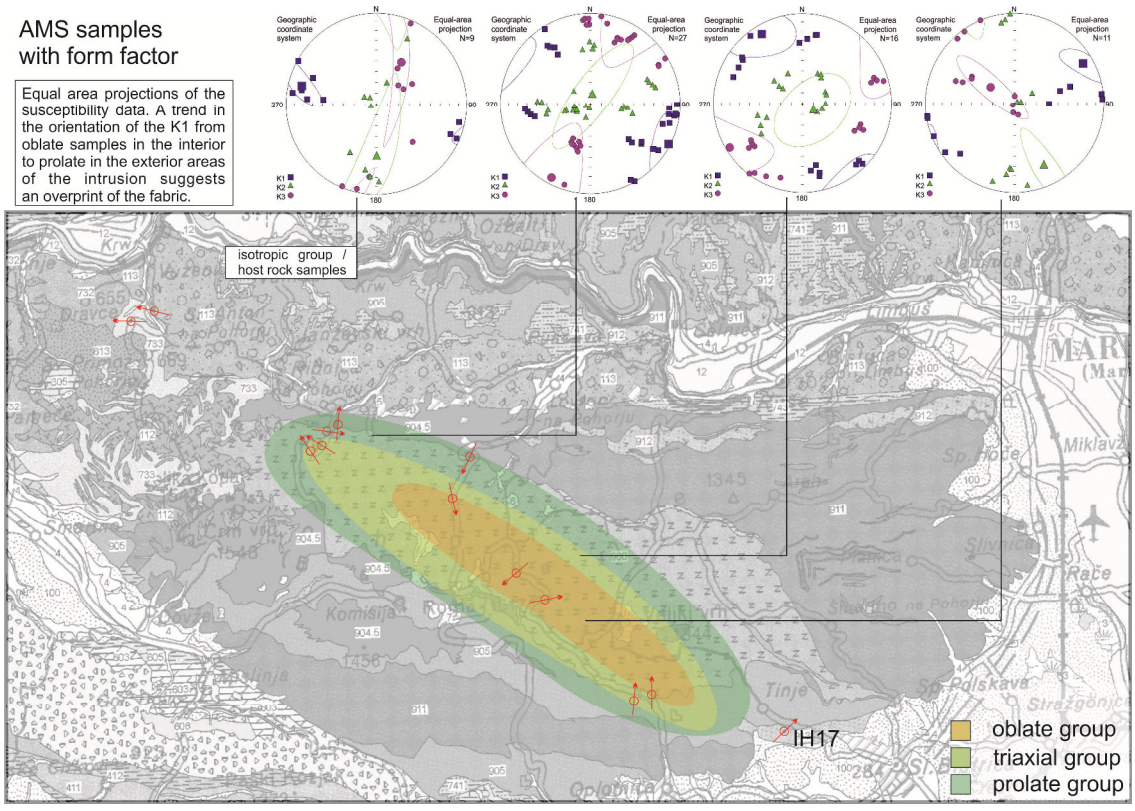

Fig. 58 Edited geological map of the Pohorje mountain range with magnetic fabric data. The magnetic data suggests a zoning of the oblate, triaxal and the prolate group. Therefore oblate sample are found in the area marked yellow, triaxial samples in area marked light green and prolate samples in the area marked dark green. (Geological map by W.Poltnig, 2007)

6. Conclusion

Based on the field work, microstructural analysis, distribution of the quartz c-axes and the magnetic fabric several stages of the deformation can be distinguished. Magmatic fabric is still existent in the internal areas of the Pohorje intrusion. The intrusion was rapidly exhumed with flattening of the tonalite body. During the late stage of exhumation the external parts of the pluton were influenced by the regional tectonic regime by ductile deformation with NW-directed shearing. The host rock has a fabric with pre-existing shear sense pointing also towards NW. A contact areole within several tens of meters from adjacent to the intrusion altered the host rock. Late NW-SE extension led to normal faulting in the northern part of the Pohorje pluton.

7. Abbreviations Index

Deformation mechanisms:	BLG	bulging
	GBM	grain boundary migration
	SGR	subgrain rotation
Geophysics:	F	magnetic foliation (K2/K3)
	Km	mean magnetic susceptibility (K1+K2+K3)/3
	L	magnetic lineation (K1/K2)
	P	anisotropy degree (K1/K3)
	Pj	corrected anisotropy degree (Jelinek, 1981, 79)
	T	shape parameter (Tarling & Hrouda, 1993)
	U	shape parameter (AGICO, 2009)
Mineral names:	Bt	Biotite
	Chl	Chlorite
	Czo	Clinozoisite
	Ep	Epidote
	Fe-Ox	Fe-oxide (Iron oxide)
	Grt	Garnet
	Kfsp	K-feldspar / Alkali Feldspar
	Ms	Muscovite
	Ox	Oxide
	Pl	Plagioclase
	Qtz	Quartz
	Ser	Sericite
Others:	AMS	Anisotropy of magnetic susceptibility
	Lin	dip-direction of lineation
	LPO	lattice preferred orientation
	Ma	million ages (absolute age)
	My	million years (duration)
	Sf	dip-direction of schistosity/foliation

8. Figures Index

9. References:

AGICO, 2009. *MFK1-FA / CS4 / CSL User's Guide,* Brno: Advanced Geoscience Instruments Co.

AGICO, 2014. *Agico - advanced geoscience instruments company.* [Online]
Available at: http://www.agico.com/
[Zugriff am 22 04 2014].

Bauer, F. K., 1980. *Kleine Geologie der Ostalpen.* Wien: Springer-Verlag.

Bellieni, G. et al., 1991. Geochemical and isotopic evidence for crystal fractionation, AFC and crustal anatexis in the genesis of the Rensen Plutonic Complex (Eastern Alps, Italy). *Chemical Geology 92*, pp. 21-43.

Berger, A. & Stünitz, H., 1996. Deformation mechanisms and reaction of hornblende: examples from the Bergell tonalite (Central Alps). *Tectonophysics 257*, pp. 149-174.

Borradaile, G. J. & Henry, B., 1997. Tectonic applications of magnetic susceptibility and its anisotropy. *Earth Science Reviews 42*, pp. 49-93.

Borradaile, G. J. & Jackson, M., 2010. Structural geology, petrofabrics and magnetic fabrics (AMS, AARM, AIRM). *Journal of Structural Geology*, pp. 1519-1551.

Borsi, S., Del Moro, A., Sassi, F. P. & Zirpolo, G., 1973. Metamorphic evolution of the Austridic Rocks to the south of the Tauern Window (Eastern Alps): radiometric and geo-petrologic data. *Mem. Soc. geol. ital. 12*, pp. 549-571.

Davies, H. J. & von Blanckenburg, F., 1995. Slab breakoff: A model of lithosphere detachment and its test in the magmatism and deformation of collisional orogens. *Earth and Planetary Science Letters 129*, pp. 85-102.

El Bay, R., 2010. *Crustal deformation in southern Tibet and the Higher Himalayan Crystalline –a palaeomagnetic approach,* Tübingen : Geowissenschaftlichen Fakultät der Eberhard-Karls-Universität .

Exner, C., 1976. Die geologische Position der Magmatite des periadriatischen Lineamentes. *Verh. Geol. B.-A.*, pp. 3-64.

Ferré, E. C., Martin-Hernandez, M., Teyssier, C. & Jackson, M., 2004. Paramagnetic and ferromagnetic anisotropy of magnetic susceptibility in migmatites: Measurements in high and low fields and kinematic implications. *Geophys. J. Int.*, pp. 1119-1129.

Fodor, L. et al., 2008. Miocene emplacement and rapid coolng of the Pohorje pluton at the Alpine-Pannonian-Dinaridic junction, Slovenia. *Swiss J. Geosci.*, pp. 255-271.

Fodor, L. et al., 1998. Miocene-Pliocene tectonic evolution of the Slovenian Periadriatic fault: Implications for Alpine-Carpathian extrusion models. *Tectonics Vol.17, Issue 5*, 10, pp. 690-709.

Gasser, D. et al., 2009. *Geology of Styria: An overview,* Graz: Mitteilung des naturwissenschaftlichen Vereines für Steiermark.

Götzinger, M. & Wagreich, M., 2006. *Der geologische Aufbau der Steiermark – ein Überblick,* Wien: Unisersity of Vienna.

Gratzer, R. & Koller, F., 1993. *Variszische und alpidische Intrusionen entlang der Periadriatischen Naht - ein geochemischer Vergleich,* Wien: Abh.Geol.B.-A..

Hoinkes, G. et al., 1999. Alpine metamorphism in the Eastern Alps, 79. *Schweiz. Mineral. Petrogr. Mitt.*, pp. 155-181.

Hrouda, F. & Lanza, R., 1989. Magnetic fabric in the Biella and Traversella stocks (Periadriatic Line): implications for the mode of emplacement. *Physics of the Earth and Planetary Interiors, 56*, pp. 337-348.

http://alpengeologie.org/, 2013. s.l.: s.n.

http://en.wikipedia.org/wiki/File:General_map_of_slovenia.svg, 2014. s.l.: s.n.

http://www.austrianmap.at/amap/index.php?SKN=1&XPX=637&YPX=492, 2014. s.l.: s.n.

Janák, F., 1965. Determination of anisotropy of magneic susceptibility of rocks.. *Stud. Geoph. Geod. 9*, pp. 290-301.

Janák, M. et al., 2006. Ultrahigh-pressure metamorphism and exhumation of garnet peridotite in Pohorje, Eastern Alps. *J. metamorphic Geol.*, pp. 19-31.

Jelinek, V., 1981, 79. Characterization of the magnetic fabric of rocks. *Tectonophysics*, pp. 63-67.

Ježek, J. & Hrouda, F., 2007. SUSIE: A program for inverse strain estimation from magnetic susceptibility. *Computers & Geosciences*, pp. 749-759.

Kázmér, M. et al., 1996. Late Miocene paleageography of Slovenia and the Southern Alps: A palinpastic approach.. *Amann, G. (Ed.). Tektonik-Strukturgeologie-Kristallingeologie. Facultas-Universitätsverlag, Salzburg*, pp. 212-214.

Krenn, K., Fritz, H., Biermeier, C. & Scholger, R., 2003. Oligocene Rensen Pluton (Eastern Alps, South Tyrol): Magma emplacement and structures during plate convergence. *Mitteilung der Österreichischen Geologischen Gesellschaft 94*, August, pp. 9-26.

Kuhlemann, j., Scholz, T. & Frisch, W., 2003. Postcollisional stress field changes in Eastern Carinthia (Austria). *Mitt. Österr. Geol. Ges. 94*, pp. 55-61.

Márton, E., Trajanova, M., Zupančič, N. & Jelen, B., 2006. Formation, uplift and tectonic integration of a Periadriatic intrusive complex (Pohorje, Slovenia) as reflected in magnetic parameters and palaeomagnetic directions. *Geophys. J. Int.*, pp. 1148-1159.

Miller, C. & Konzett, J., 2005. Comment on "First evidence for ultrahigh-pressure metamorphism of the eclogites in Pohorje, Slovenia: Tracing deep continental subduction in the eastern Alps" by Marian Janák et al.. *Tectonics vol. 24*, pp. 1-6.

Müller, W., Mancktelow, N. S. & Meier, M., 2000. Rb-Sr microchrons of synkinematic mica in mylonites: an example from the DAV fault of the Eastern Alps. *Earth and Planetary Science Letters 180*, pp. 385-397.

Nagata, T., 1961. Rock Magnetism. In: 2nd Hrsg. Tokyo: Maruzen, p. 350.

Neubauer, F., Genser, J. & Handler, R., 1999. The Eastern Alps: Result of a two-stage collision process. *Mitt. Österr. Geol. Ges 92*, pp. 117-134.

Okrusch, M. & Matthes, S., 2005. *Mineralogie - Eine Einführung in die spezielle Mineralogie, Petrologie und Lagerstättenkunde.* 7.Edition Hrsg. Heidelberg: Srpinger-Verlag Berlin.

Ortner, H., Reiter, F. & Brandner, R., 2006. Kinematics of the Inntal shear zone–sub-Tauern ramp fault system and the interpretation of the TRANSALP seismic section, Eastern Alps, Austria. *Tectonophysics*, pp. 241-258.

Pamić, J., Balen, D. & Herak, M., 2002. Origin and geodynamic evolution of Late Paleogene magmatic associations along the Periadriatic-Sava-Vadar magmatic belt. *Geodinamica Acta*, pp. 209-231.

Pamić, J. & Palinkaš, L., 2000. Petrology and geochemestry of Paleogene tonalites from the easternmost parts of the Periadritic Zone. *Mineralogy and Petrology 70*, pp. 121-141.

Passchier, C. W. & Trouw, R. A., 2005. *Microtectonics.* 2nd Edition ed. Heidelberg: Springer-Verlag Berlin.

Pennacchioni, G. et al., 2006. Brittle-ductile-brittle deformation during cooling of tonalite (Adamello, Southern Italian Alps). *Tectonophysics 427*, pp. 171-197.

Pfiffner, A. O., 2009. *Geologie der Alpen.* 1st edition Hrsg. Germany: Haupt Berne .

Pichler, H. & Schmitt-Riegraf, C., 1997. Rock-forming Minerals in Thin Section. In: 2nd ed. London: Chapman and Hall, p. 116.

Rosenberg, C. L. & Stünitz, H., 2003. Deformation and recrystallization of plagioclase along a temperature gradient: an example from the Bergell tonalite. *Journal of Structural Geology 25*, pp. 389-408.

Sachsenhofer, R. F., Dunkl, I., Hasenhüttl, C. & Jelen, B., 1998. Miocene thermal history of the southwestern margin of the Styrian Basin: vitrinite reflectance and fission-track data from the Pohorje/Kozjak area (Slovenia). *Tectonophysics 297*, pp. 17-29.

Sachsenhofer, R. F., Dunkl, I., Hasenhüttl, C. & Jelen, B., 1998. Miocene thermal history of the southwestern margin of the Styrian Basin:vitrinite reflectance and fission-track data from the Pohorje/Kozjak area (Slovenia). *Tectonophysics 297*, pp. 17-29.

Scharbert, S., 1975. Radiometrische Altersdaten von Intrusivgesteinen im Raum Eisenkappel (Karawanken, Kärnten). *Verh. Geol. B.-A.*, pp. 301-304.

Schmid, S. M., Fügenschuh, B., Kissling, E. & Schuster, R., 2004. Tectonic map and overall architecture of the Alpine orogen. In: *Eclogae geol. Helv. 97.* Basel: Birkhäuser Verlag, pp. 93-117.

Schuster, R. et al., 2004. *EXPLANATORY NOTES TO THE MAP: METAMORPHIC STRUKTURE OF THE ALPS METAMORPHIC EVOLUTION OF THE EASTERN ALPS,* s.l.: Mitt.Österr.Miner.Ges..

Sprenger, W. L., 1996. *Das Periadriatische Lineament südlich der Lienzer Dolomiten.* 52 Hrsg. Wien: Geologische Bundesanstalt.

Steeken, A., Siegesmund, S. & Heinrichs, T., 2000. The emplacement of the Rieserferner Pluton (Eastern Alps, Tyrol): constraints from field observations, magnetic fabrics and microstructures. *Journal of Structural Geology 22*, pp. 1855-1873.

Stipp, M., Stünitz, H., Heilbronner, R. & Schmid, S. M., 2002. The eastern Tonale fault zone: a 'natural laboratory' for crystal plastic deformation of quartz over a temperature range from 250 to 700°C. *Journal of Structural Geology 24*, pp. 1861-1884.

Tarling, D. H. & Hrouda, F., 1993. *The Magnetic Anisotropy of Rocks.* First Edition ed. Great Britain: Chapman & Hall.

Tollmann, A., 1977. *Geologie von Österreich.* Band 1 Hrsg. Vienna: Deuticke.

Toy, V. A., Pior, D. J. & Norris, R. J., 2008. Quartz fabrics in the Alpine Fault mylonites: Influence of pre-existing preferred orientations on fabric developement during progressive uplift.. *Journal of Structural Geology,* Issue 30, pp. 602-621.

von Blanckenburg, F., Früh-Green, G., Diethelm, K. & Stille, P., 1992. Nd-, Sr-, O-isotopic and chemical evidence for a two-stage contamination history of mantle magma in the Central-Alpine Bergell intrusion. *Contributions to Mineralogy and Petrology Volume 110*, pp. 33-45.

Wilson, C. J., Russell-Head, D. S., Kunze, K. & Viola, G., 2007. The analysis of quartz c-axis fabrics using a modified optical microscope. *Journal of Microscopy,* Issue 227, pp. 30-41.

Winkler, A. et al., 1997. The magnetic anisotropy of rocks: principles, techniques and geodynamic applications in the Italian peninsula. *Annali di Geofisica*, June, pp. 729-740.

Wölfler, A., Kurz, W., Fritz, H. & Stüwe, K., 2011. Lateral extrusions in the Eastern Alps revisited: Refining the model by thermochronological, sedimentary, and seismic data. *Tectonics, Vol. 30*, pp. 1-15.

Žurga, J., 1926. Age of the granite of the Pohorje Mts. (in Croatian). *Geograf. vest. II*, pp. 35-37.

Appendix

A1.Sample Index:

Sample	Rock'Type	Coordinates		Foliation		Lineation	
		Latitude (N)	*Longitude (E)*	*Dip'Direction*	*Dip'Angle*	*Dip'Direction*	*Dip'Angle*
IH04	tonalite	46°25.519'	015°25.103'	315	40	265	25
IH05	tonalite	46°25.519'	015°25.103'	216	32	268	20
IH06	aplite	46°25.519'	015°25.103'	205	30	275	10
IH09	paragneiss	46°24.230'	015°26.582'	202	45	275	20
IH10	tonalite	46°24.991'	015°26.427'	176	37	261	02
IH11	tonalite	46°25.324'	015°26.257'	295	35	250	30
IH15a	tonalite	46°25.405'	015°25.920	325	40	255	15
IH16	pyroxenite	46°24.524'	015°30.942'	125	65	052	02
IH17	pyroxenite	46°24.524'	015°30.716'	127	45	180	28
IH18	micaschist	46°31.695'	015°16.078'	183	78	076	07
IH19	micaschist	46°31.670'	015°16.079'	030	70	110	15
IH20	micaschist	46°31.656'	015°16.063'	185	85	092	25
IH21b	migmatite	46°31.625'	015°16.056'	125	60	060	20
IH23	micaschist	46°31.601'	015°16.053'	184	53	110	23
IH24a	micaschist	46°31.601'	015°16.053'	180	70	082	10
IH24b	micaschist	46°31.601'	015°16.053'	180	70	082	10
IH25	tonalite	46°31.581'	015°16.029'	203	65	294	20
IH27	micaschist	46°31.582'	015°16.036'	182	67	108	32
IH28	micaschist	46°31.582'	015°16.036'	172	56	098	18
IH29	micaschist	46°31.560'	015°16.020'	184	67	105	18
IH30	tonalite	46°31.572'	015°16.022'	230	80	168	50
IH31b	migmatite	46°31.572'	015°16.022'	184	69	105	26
IH32	gneiss	46°31.625'	015°16.056'	019	84	104	16
IH35	migmatite	46°31.625'	015°16.056'	123	65	118	28
IH36	micaschist	46°31.625'	015°16.056'	182	85	090	10
IH37	migmatite	46°31.625'	015°16.056'	020	85	104	06
IH38	aplite	46°31.625'	015°16.056'	055	72	109	28
IH40	micaschist	46°31.601'	015°16.053'	173	70	098	27
IH43	tonalite	46°31.363'	015°15.819'			148	45
IH44	tonalite	46°31.568'	015°16.026'	004	44	275	06
IH45	tonalite	46°31.568'	015°16.026'	030	25	115	05
IH46	migmatite	46°31.568'	015°16.026'	200	75	280	12
IH47	migmatite	46°31.568'	015°16.026'	195	80	265	32
IH48	migmatite	46°31.568'	015°16.026'	215	85	118	30
IH49	gneiss	46°31.568'	015°16.026'	203	75	120	34
IH51	migmatite	46°31.568'	015°16.026'	198	70	115	25
IH52	tonalite	46°31.568'	015°16.026'	290	80	295	05
IH55	tonalite	46°31.554'	015°16.021'	280	75	205	22

IH57	tonalite	46°31.554'	015°16.021'	195	85	110	35
IH64	tonalite	46°31.067'	015°15.314'	135	65		
IH65	tonalite	46°31.067'	015°15.314'	035	85	130	12
IH68	tonalite	46°31.143'	015°15.376'	163	45	115	30
IH70	tonalite	46°29.978'	015°15.563'	180	55		
IH75a		46°34.137'	015°09.897'	000	20	050	15
IH77	serpentinite	46°31.255'	015°21.919'	020	35	090	10
IH78	gneiss	46°31.255'	015°21.919'	335	35	075	10
IH79	gneiss	46°31.203'	015°21.531'	280	50	250	40
IH80	gneiss	46°30.779'	015°20.531'	180	35	130	12
IH81	gneiss	46°30.888'	015°20.319'	030	85	120	05
IH83	tonalite	46°28.313'	015°20.097'	140	35	090	25
IH87	tonalite	46°28.518'	015°21.001'	160	45		
IH90	tonalite	46°26.319'	015°23.805'	240	50	292	35

A2.Joint set plots

Lambert projection (equal-area projection) on the lower hemisphere of the conjugated joint sets (JS1, JS2 and JS3) from the southern boundary of the Pohorje mountain range.

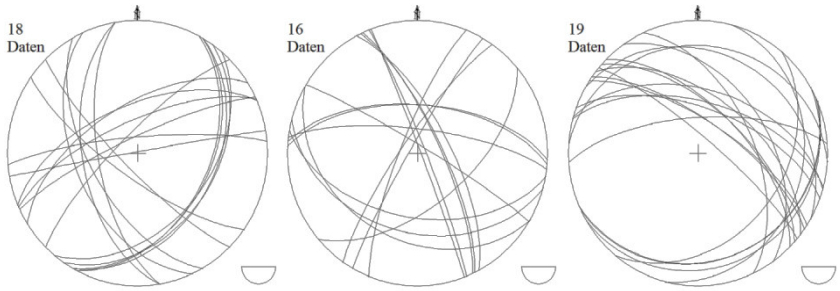

Lambert projection (equal-area projection) on the lower hemisphere of the conjugated joint sets (JS1, JS2 and JS3) from the northern boundary of the Pohorje mountain range.

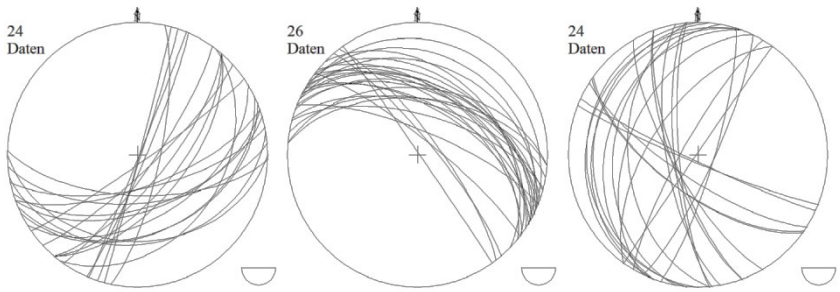

A3.Tables of mineral content:

Table 4 Mineral content of Tonalite I

Sample	Rock'Type	Mineralogy																		
		Qtz	*Plg*	*Kfsp*	*Grt*	*Ms*	*Bt*	*Chl*	*ChlB*	*Serz*	*Epd*	*Zoi*	*Kzoi*	*Myr*	*Ore*	*Gph*	*Cbt*	*Px*	*Zr*	*Ti*	*Rt*
IH11	tonalite	x	x	x			x	x			x	x		x					x		
IH15a	tonalite	x	x	x			x	x	x		x			x					x		
IH83	tonalite	x	x	x			x	x			x		x	x	x						x
IH87	tonalite	x	x	x			x	x			x		x	x	x						

Table 5 Mineral content of Tonalite II

Sample	Rock'Type	Mineralogy																		
		Qtz	*Plg*	*Kfsp*	*Grt*	*Ms*	*Bt*	*Chl*	*ChlB*	*Serz*	*Epd*	*Zoi*	*Kzoi*	*Myr*	*Ore*	*Gph*	*Cbt*	*Px*	*Zr*	*Ti*	*Rt*
IH04	tonalite	x	x				x	x			x		x	x				x			
IH05	tonalite	x	x	x			x	x		x			x	x							
IH06	aplite	x	x				x	x					x	x					x		
IH10	tonalite	x	x	x	x	x	x						x						x		
IH57	tonalite	x	x	x			x	x		x			x				x		x		
IH65	tonalite	x	x	x			x	x					x		x		x		x		
IH68	tonalite	x	x	x			x	x			x			x	x					x	x
IH90	tonalite	x	x	x	x		x	x			x	x		x	x						

Table 6 Mineral content of Tonalite III

Sample	Rock'Type	Mineralogy																		
		Qtz	*Plg*	*Kfsp*	*Grt*	*Ms*	*Bt*	*Chl*	*ChlB*	*Serz*	*Epd*	*Zoi*	*Kzoi*	*Myr*	*Ore*	*Gph*	*Cbt*	*Px*	*Zr*	*Ti*	*Rt*
IH25	tonalite	x	x	x			x		x										x		
IH35	migmatite	x	x	x			x		x			x									
IH43	tonalite	x	x	x			x	x		x			x		x						
IH44	tonalite	x	x	x			x	x													
IH45	tonalite	x	x	x			x		x			x									
IH52	tonalite	x	x	x			x			x		x			x				x	x	x
IH55	tonalite	x	x	x			x	x		x	?	x			x						

Table 7 Mineral content of Host Rock I

Sample	Rock'Type	Mineralogy																		
		Qtz	*Plg*	*Kfsp*	*Grt*	*Ms*	*Bt*	*Chl*	*ChlB*	*Serz*	*Epd*	*Zoi*	*Kzoi*	*Myr*	*Ore*	*Gph*	*Cbt*	*Px*	*Zr*	*Ti*	*Rt*
IH18	micaschist	x	x	x	x		x		x	x					x	x					
IH19	micaschist	x		x		x							x								
IH20	micaschist	x	x	x	x	x			x	x			x								

Table 8 Mineral content of Host Rock II

Sample	Rock'Type	Mineralogy																		
		Qtz	*Plg*	*Kfsp*	*Grt*	*Ms*	*Bt*	*Chl*	*ChlB*	*Serz*	*Epd*	*Zoi*	*Kzoi*	*Myr*	*Ore*	*Gph*	*Cbt*	*Px*	*Zr*	*Ti*	*Rt*
IH23	micaschist	x	x	x	x	x	x						x								
IH24a	micaschist	x	x	x	x	x	x						x								
IH24b	micaschist	x	x	x	x	x	x						x								
IH27	micaschist	x	x			x	x			x											

IH28	micaschist	x					x			x											
IH29	micaschist	x					x			x											
IH32	gneiss	x		x	x	x				x	x								x		
IH36	micaschist																				
IH49	gneiss	x	x	x		x	x			x											
IH79	gneiss	x	x		x	x	x	x				x									

Table 9 Mineral content of Host Rock III

Sample	**Rock'Type**	**Mineralogy**																			
		Qtz	*Plg*	*Kfsp*	*Grt*	*Ms*	*Bt*	*Chl*	*ChlB*	*Serz*	*Epd*	*Zoi*	*Kzoi*	*Myr*	*Ore*	*Gph*	*Cbt*	*Px*	*Zr*	*Ti*	*Rt*
IH09	paragneiss	x		x	x	x	x					x							x		
IH80	gneiss	x	x	x	x	x	x	x		x					x				x		x
IH81	gneiss	x	x	x		x	x			x					x	x					

Table 10 Mineral content of Migmatite

Sample	**Rock'Type**	**Mineralogy**																			
		Qtz	*Plg*	*Kfsp*	*Grt*	*Ms*	*Bt*	*Chl*	*ChlB*	*Serz*	*Epd*	*Zoi*	*Kzoi*	*Myr*	*Ore*	*Gph*	*Cbt*	*Px*	*Zr*	*Ti*	*Rt*
IH31b	migmatite	x		x			x			x		x									
IH37	migmatite	x		x			x			x						x					
IH38	aplite	x		x	x		x			x											
IH46	migmatite	x		x			x			x											
IH47	migmatite	x		x					x	x											

A4.Fault Activity by Wölfler et at.

Table 11 Geochronological Data on Fault Activity in the Eastern Alps *(Wölfler, et al., 2011)*.

Age, Age range (Ma)	Area	Method	Authors
~ 22	northeastern Tauern Window; activity of the Katschberg normal fault	Ar-Ar, white mica	Liu et al. (2001)
35-28	SEMP, northeastern Tauern Window	Ar-Ar, white mica	Urbanek et al. (2002)
26.7 ±1.2; 21.5±0.8; 19.4±4.0; 16.9±0.6	Central Tauern Window	Rb-Sr, biotite/white mica	Glodny et al. (2008)
21±2.0; 18.3±2.6; 17.8±1.8	Brenner normal fault	Rb-Sr, white mica	Glodny et al. (2008)
19.8±0.4	southwestern Tauern Window	Rb-Sr, white mica	Glodny et al. (2008)
31-28	southern Tauern Window	Rb-Sr, white mica	Glodny et al. (2008)
25.3±2.9; 20.7±2.3	Mölltal fault	Rb-Sr, white mica	Glodny et al. (2008)
20-15	western Tauern Window	Rb-Sr, white mica	von Blanckenburg et al. (1989)
21±2.0	western Tauern Window	Rb-Sr, white mica	Satir and Morteani (1982)
19-17	western Tauern Window	Rb-Sr, microsampling, mylonite	Schneider et al. (2007)
~29	Jaufen-Passeir fault	Rb-Sr, white mica	Müller et al. (2000)
33-30	southwestern Tauern Window	Rb-Sr, white mica	Müller et al. (2000)
21-17	Jaufen-Passeir fault	Rb-Sr, microsampling, mylonite	Müller et al. (2001)
32-29	Guidicarie fault	Rb-Sr, microsampling, mylonite	Müller et al. (2001)
33-30	DAV	Rb-Sr, white mica; Rb-Sr, microsampling, mylonite	Müller et al. (2000; 2001)
22-20	Periadriatic fault system	Ar-Ar, white mica	Müller et al. (2001)
~31	southwestern Tauern Window	Rb-Sr, white mica	Satir (1975)
31-28	southern Tauern Window	Rb-Sr, white mica	Inger and Cliff (1994)
29.5±0.5	southern Tauern Window	Rb-Sr, multimineral	Gleissner et al. (2007)
35-28	southern Tauern Window	K-Ar, white mica	Lambert (1970)
27.3±0.8; 25.5±0.3	southeastern Tauern Window	Rb-Sr, microsampling	Cliff and Meffan-Main (2003)
32-28; 18-13	Periadriatic fault system	K-Ar, Ar-Ar, white mica	Läufer et al. (1997)
32-30; 23-22	shear zone to the southeast of the Tauern Window (Kreuzeck Group)	K-Ar, Ar-Ar, clay minerals	Kralik et al. (1987)

A5.Statistic Data Output of the AMS groups:

Table 12 Jelinek statistics of the isotropic group calculated by Anisoft 4.2.

N=13	mean	Average	stand. deviation
Km	N/A	2,37E-04	2,37E-04
L	1,015	1,014	0,011
F	1,001	1,017	0,015
P	1,016	1,031	0,021
Pj	1,018	1,032	0,022
T	-0,877	0,042	0,399
U	-0,877	0,036	0,399

	mean	declination	inclination	conf. angel dec.	conf. angel inc.
K1	1,01	282,6	13,2	32,2	12,7
K2	0,995	14	5,7	82,3	10,8
K3	0,994	126,7	75,6	82,3	29,3

Table 13 Jelinek statistics of the oblate group calculated by Anisoft 4.2.

N=11	mean	Average	stand. deviation
Km	N/A	3,01E-03	2,01E-03
L	1,058	1,049	0,025
F	1,067	1,155	0,058
P	1,13	1,213	0,081
Pj	1,13	1,224	0,084
T	0,071	0,499	0,154
U	0,041	0,463	0,162

	mean	declination	inclination	conf. angel dec.	conf. angel inc.
K1	1,06	59,7	12,1	22,2	9,8
K2	1,002	155	23,3	42,8	9,3
K3	0,938	304,4	63,4	44,5	9,7

Table 14 Jelinek statistics of the triaxial group calculated by Anisoft 4.2.

N=16	mean	Average	stand. deviation
Km	N/A	6,67E-03	4,90E-03
L	1,104	1,151	0,047
F	1,063	1,143	0,046
P	1,174	1,318	0,098
Pj	1,176	1,319	0,098
T	-0,239	-0,03	0,132
U	-0,277	-0,097	0,131

	mean	declination	inclination	conf. angel dec.	conf. angel inc.
K1	1,088	329,5	11,1	29,5	20,9
K2	0,985	124,6	77,8	41,1	27,1
K3	0,927	238,6	5	42	19,1

Table 15 Jelinek statistics of the prolate group calculated by Anisoft 4.2.

N=27	mean	Average	stand. deviation
Km	N/A	1,00E-02	6,17E-03
L	1,207	1,29	0,13
F	1,051	1,133	0,11
P	1,268	1,467	0,244
Pj	1,285	1,485	0,246
T	-0,584	-0,4	0,263
U	-0,622	-0,472	0,227

	mean	declination	inclination	conf. angel dec.	conf. angel inc.
K1	1,146	117,4	2,2	24,4	17
K2	0,95	12,1	81,7	60,7	16,6
K3	0,904	207,7	8	60,4	20,5

A6. Geological map with sample locations

The following three figures are modified geological maps (Poltnig, W., 2007) with

1. sampling sites (all samples),
2. the position of AMS samples and
3. the position LPO samples.

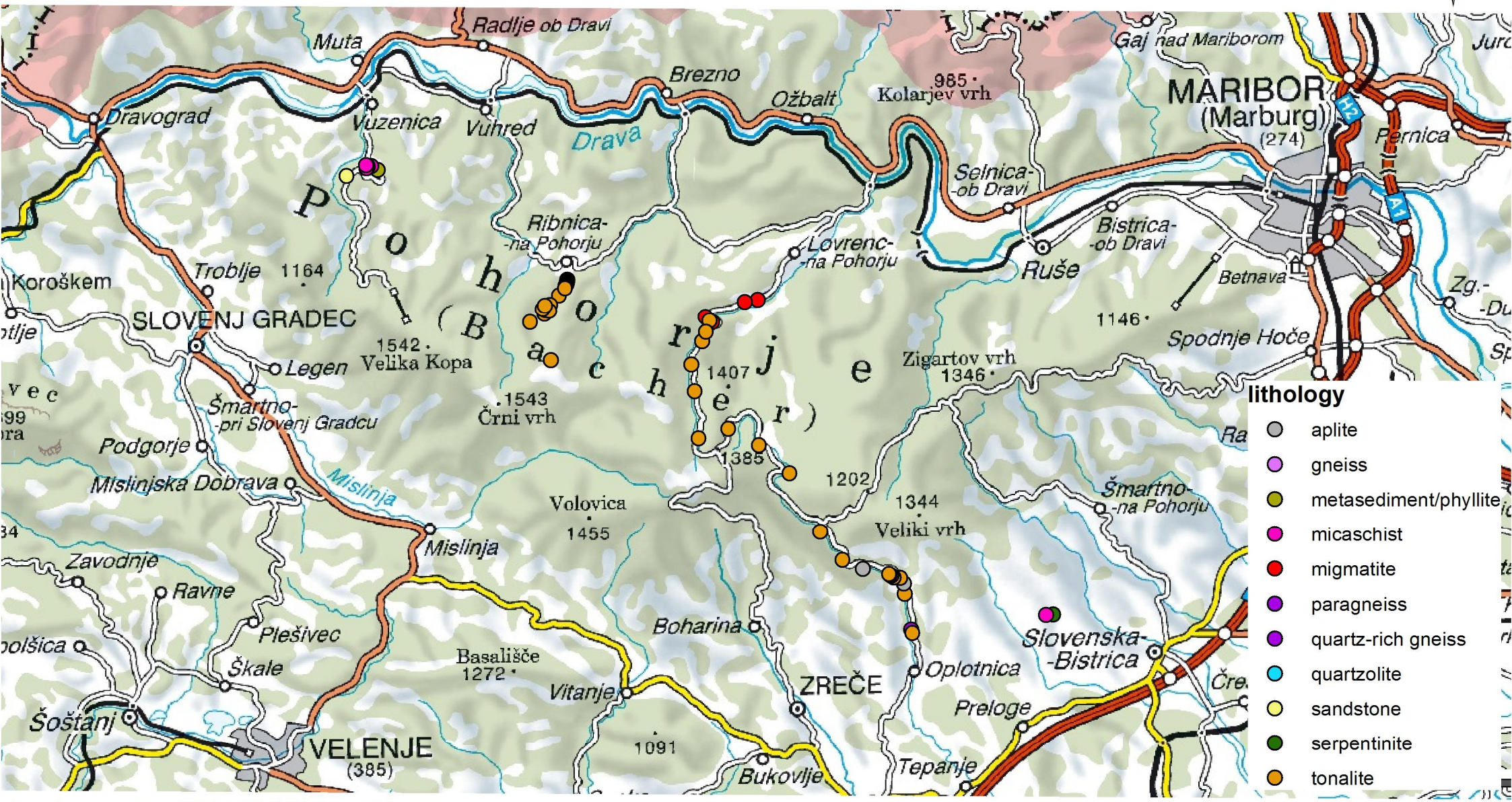

Koordinatensystem: WGS 1984 UTM Zone 33N
Projektion: Transverse Mercator
Datum: WGS 1984
False Easting: 500.000.0000
False Northing: 0.0000
Central Meridian: 15.0000
Scale Factor: 0.9996

0 3.75 7.5 15 Kilometer

Geological map (Poltnig W., 2007) with location of AMS plots; Lambert projection on the lower hemisphere, K3 projected as great circles and K1 as directions on K3 plains

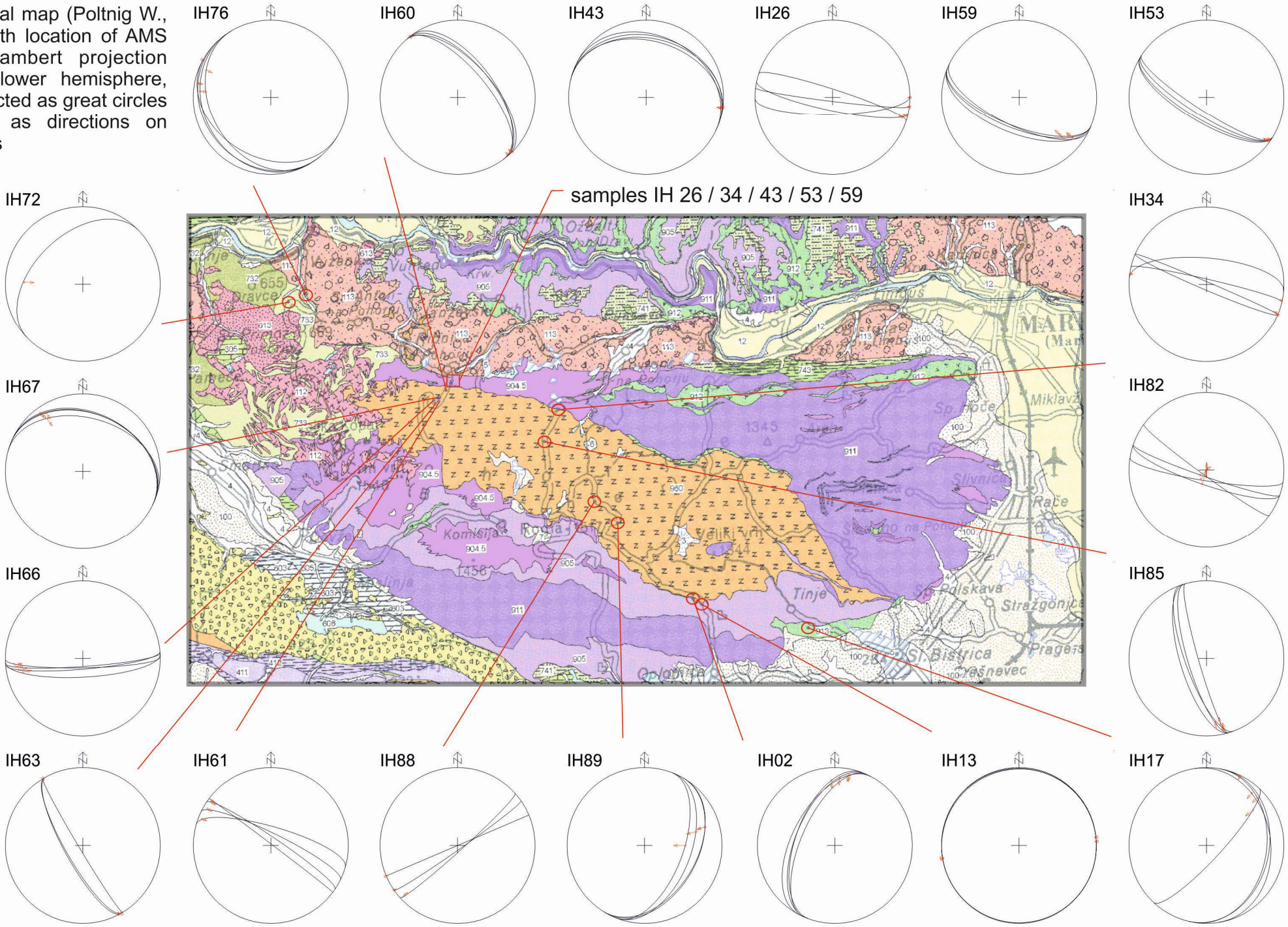

geological map (Poltnig W.,2007) with LPO plot of the Qtz c-axes

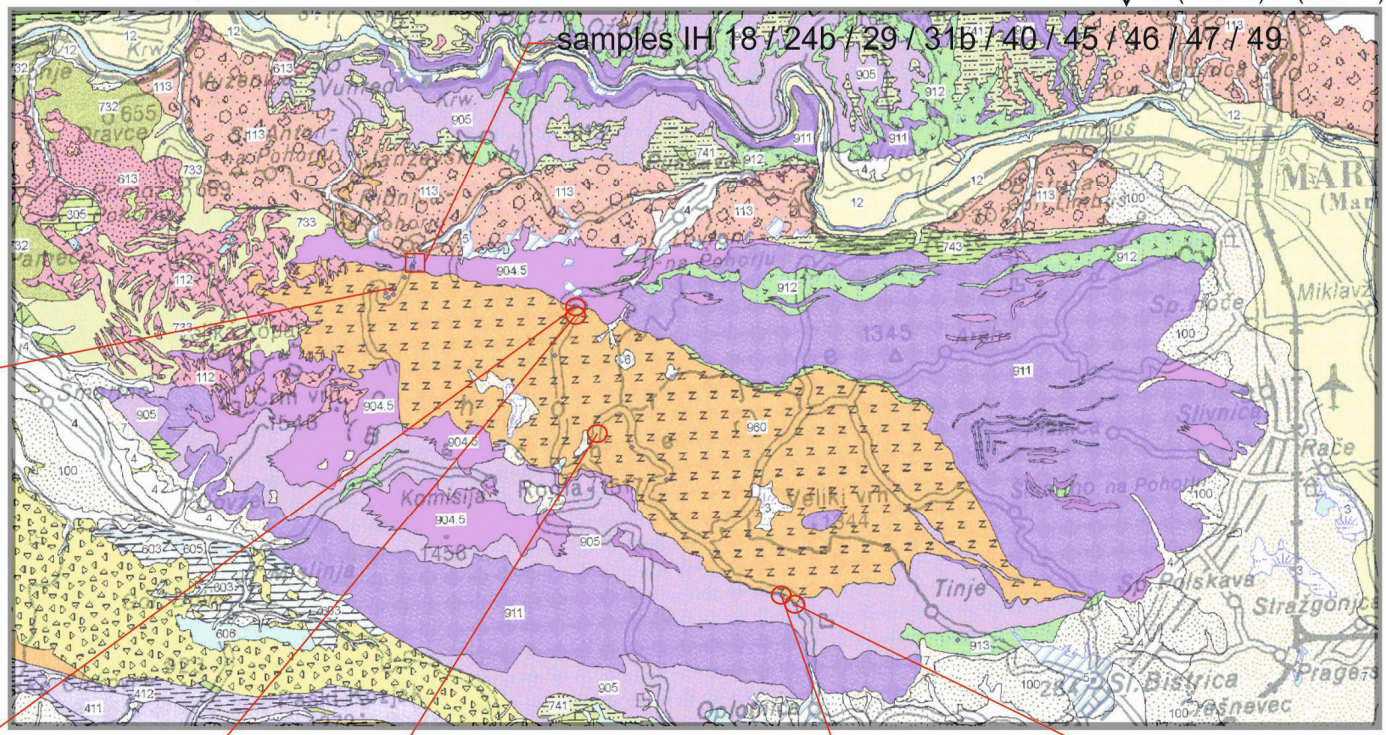

IH18

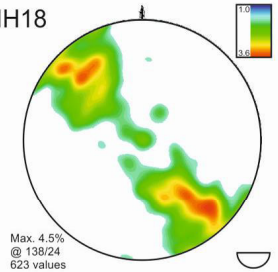

sf (183/78) lin(076/07)

IH24b

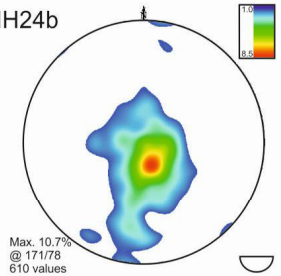

sf (180/70) lin(082/10)

IH29

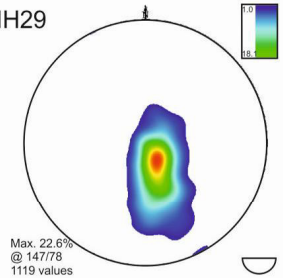

sf (184/67) lin(105/18)

IH31b

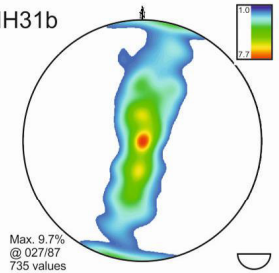

sf (184/69) lin(105/26)

IH40

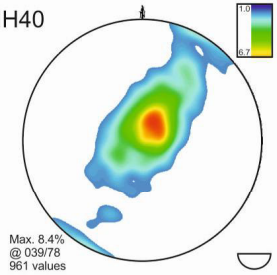

sf (173/70) lin(098/27)

IH45

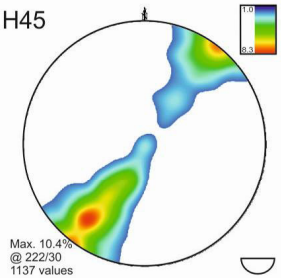

sf (030/25) lin(115/05)

IH46

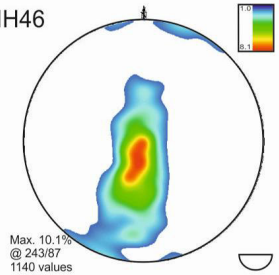

sf (200/75) lin(280/12)

IH47

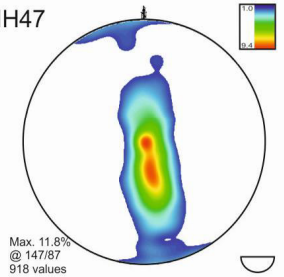

sf (195/80) lin(265/32)

IH68

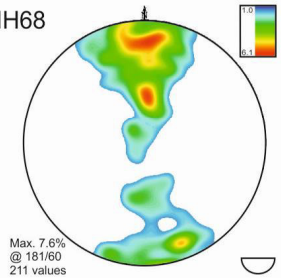

sf (163/45) lin(115/30)

IH80

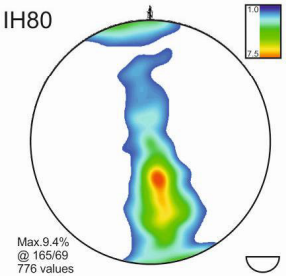

sf (180/35) lin(130/12)

IH81

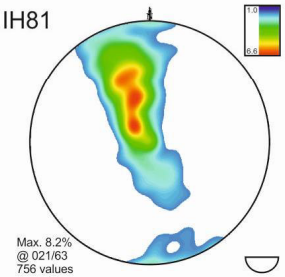

sf (030/85) lin(120/05)

IH87

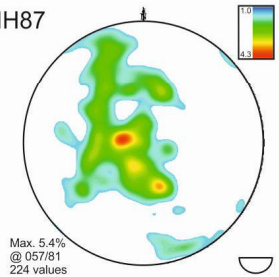

sf (160/50) lin(160/50)

IH05

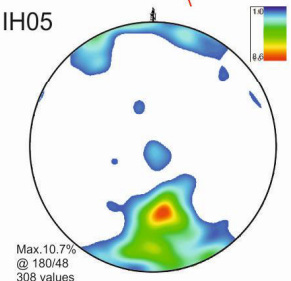

sf (315/40) lin(265/25)

IH11

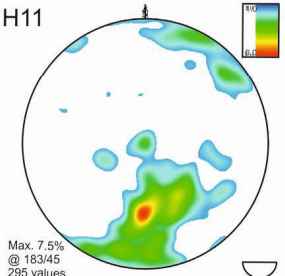

sf (295/35) lin(250/30)

IH49

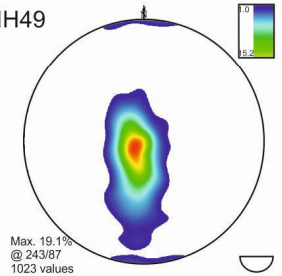

sf (203/75) lin(120/34)